TECHNISCHE UNIVERSITÄT
KAISERSLAUTERN

Department of Mathematics

Master's thesis

Fiber based Lagrangian Modeling and Numerical Simulation of Skeletal Muscle Tissue

Steffen Plunder

supervised by

Prof. Dr. Bernd Simeon

October 2018

Contents

Preface 3

Notations 5

Chapter 1. Classical Field Theory, Hyperelasticity and Constraints 7

§1. A Quick Recall of the Euler-Lagrange Equations in Classical Mechanics 9

§2. The Euler-Lagrange Equations for Classical Fields 9

§3. Non-conservative Euler-Lagrange Equations 18

§4. Equations of Hyperelasticity 20

§5. Example: One Dimensional Hyperelasticity 26

§6. Constraints in Classical Field Theory 29

Chapter 2. Physiology and Models of Skeletal Muscle Tissue 35

§1. Physiology of Skeletal Muscles 36

§2. Control of the Cross-Bridge Cycle 46

§3. Mathematical Models for Muscle Contraction 49

§4. A Popular Method: The Distributed Moment Approximation 54

§5. Hyperelastic Models for Skeletal Muscle Tissue 57

Chapter 3. A Lagrangian Perspective on Cross-Bridge Theory 63

§1. Coupling between Hyperelasticity and Cross-Bridge Theory 65

§2. The Liouville Equation for Cross-Bridges 70

§3. Averaging in Cross-Bridge Theories 73

§4. Non-conservative two state model 74

Chapter 4. Numerical Methods for Nonlinear Hyperelasticity and Cross-Bridge Models 75
§1. Nonlinear Finite Elements for Static Hyperelasticity 76
§2. FEniCS – A Magic Finite Element Framework 86
§3. Numerical Results for Static Hyperelasticity with Constraints 90
§4. Time Integration Methods 93

Conclusion 103

Acknowledgments 105

Appendix A. Differential Calculus on Banach Spaces 107

Appendix B. Tools from Differential Geometry 109
§1. Tangent Vectors as Velocities 109
§2. Tensors and Two-Point Tensors 109

Appendix. Bibliography 113

Preface

> The fools who write the textbooks of advanced mathematics – and they are mostly clever fools – seldom take the trouble to show you how easy the easy calculations are. On the contrary, they seem to desire to impress you with their tremendous cleverness by going about it in the most difficult way.
>
> Silvanus Thompson, [**Tho98**, Prolog]

In the spirit of the quote, I must admit that I wrote this master's thesis to "impress others with my tremendous cleverness by going about it in the most difficult way". In some sense, one could say that it is the main purpose of a master's thesis to show (off) knowledge and competence. But without doubt, I do not present the easiest way to model and simulate muscles. I try to present the most elegant way to look at the equations. Explaining the most elegant way as easy as possible is always a challenge.

The first topic of this thesis is classical field theory in Chapter 1, which I first discovered on page 275 in the book "Mathematical foundations of Elasticity" by Jerrold E. Marsden and Thomas J. R. Hughes [**MH83**, section 5.4]. Classical field theory can handle electromagnetism, general relativity and continuum mechanics with ease and still features highlights like Noether's theorem and more. However, at least to my knowledge, it is not included in the usual education for mathematicians with interest in physics. The rather detailed introduction in this thesis is more a mathematical hobby than a reasonable effort. Nevertheless, we will use the Lagrangian formulation of hyperelasticity extensively in Chapter 3.

As a complement to all this abstract nonsense, Chapter 2 is about the physiology of skeletal muscles and completely non-mathematical in the first half. Physiology is still a field with many open questions and uncertainties. For me, physiology is far more difficult than mathematics. Most symmetries and nice structures are gone, but in some way order arises from molecular chaos. After a gallery of muscle images, we also introduce mathematical models for the cellular contraction mechanism. In the last section of the chapter we also discuss common multi-scale methods for skeletal muscle tissue.

In Chapter 3, we forget about all nasty non-conservative, stochastic parts of the muscle contraction mechanism and derive a simple form of a common skeletal muscle model as a constrained Lagrangian system. In this way, we see which assumptions are hidden behind common multi-scale models for muscle contraction in more detail. From this perspective, the cellular model is just a variation of the Liouville equation.

Finally, we discuss some numerical methods for skeletal multi-scale models in Chapter 4. We use the finite element framework FEniCS for our simulations. The static case is already well covered by classical theory, but still requires a combination of many different numerical methods. The dynamic setting carries many numerical pitfalls and we were not able to overcome all of them. The final simulation in Chapter 4 is a time dependent simulation of the nonlinear partial differential equations of a quasi-incompressible hyperelastic material which is coupled to a collection of transport equations. This might sound quite impressive, but the reader should be warned that we did not perform a careful convergence analysis for the complete model.

Therefore, I cannot stress enough, that all simulations in this thesis are nothing more than simulations of Donald Duck's arm muscles, which are fictional muscles and not obligated to any laws of physics or physiology.

Notations

In some equations, we use gray color to put non-essential details into the background, for example

$$\sum_{i,j=1}^{3} \frac{\mathrm{d}}{\mathrm{d}X^i} \frac{\partial \mathcal{L}}{\partial\, \mathrm{D}_i \varphi^j}[w^j].$$

The upper super-index from φ^j denotes the j-th coordinate of φ. If the super-index denotes a power, it should be clear from the context. As usual, super-indices are used for covariant coordinates and sub-indices represent contravariant parts. We do not use the Einstein summation convention.

The expression above can also be read without the gray objects and then represents the coordinate-free version of the same term, i.e.

$$\frac{\mathrm{d}}{\mathrm{d}X} \frac{\partial \mathcal{L}}{\partial\, \mathrm{D}\varphi}[\omega].$$

We will often neglect the evaluation at certain point,

Differential Geometry. We use bold letters to denote elements of linear spaces, such as tangential or co-tangential vectors or tensors. An exception are variations η or ξ.

$\mathcal{M}, \mathcal{N}$		smooth manifolds
$T_p\mathcal{M}$		tangent space of $\mathcal{M}$ at $p \in \mathcal{M}$
$T\mathcal{M}$	$= \coprod_{p\in\mathcal{M}} T_p\mathcal{M}$	tangent bundle of $\mathcal{M}$
$\mathrm{D}f$	$: T\mathcal{M} \to T\mathcal{N}$	differential of a smooth function f
d		Cartan derivative (or exterior derivative)

Continuum Mechanics. Following [**MH83**], we use upper-case variables for objects in material space and lower-case variables denote spatial objects.

$\mathcal{B}$		manifold of (fixed) material points
$\mathcal{S}$		manifold for spatial points
φ	$: \mathcal{B} \to \mathcal{S}$	configuration
X	$\in \mathcal{B}$	material point
x	$= \varphi(X)$	spatial point
$\boldsymbol{F}$	$= T\varphi : T\mathcal{B} \to T\mathcal{S}$	deformation gradient
$\boldsymbol{C}$	$= \boldsymbol{F}^T \boldsymbol{F}$	deformation tensor (or right Cauchy-Green tensor)
$\mathcal{L}$		Lagrangian density
$\mathcal{W}$		stored strain energy density
$\boldsymbol{P}$	$= \dfrac{\partial \mathcal{W}}{\partial \boldsymbol{F}}$	first Piola-Kirchhoff stress tensor
$\boldsymbol{S}$	$= \boldsymbol{F}^{-T} \boldsymbol{P}$	second Piola-Kirchhoff stress tensor
$\boldsymbol{\sigma}$		spatial stress tensor
$\boldsymbol{\tau}$		traction
$\boldsymbol{b}$		external body force field

Chapter 1

Classical Field Theory, Hyperelasticity and Constraints

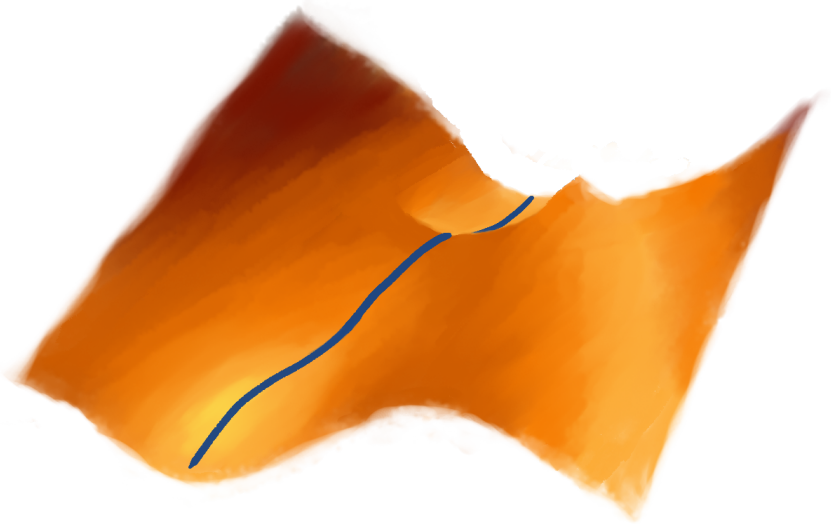

This chapter introduces the Euler-Lagrange equations of classical fields, discusses hyperelasticity from an field theoretical perspective and finally extends these equations to include constraints. In this way we can model incompressibility and couple a micro-scale model (for the contraction of skeletal muscle cells) with a macro-scale model for hyperelastic solids.

A complete introduction to elasticity is of course not possible, we only want to focus on specific *mathematical* aspects of hyperelasticity. Many theorems from classical mechanics are also true for classical fields. This perspective yields a direct – but abstract – approach to hyperelasticity. For example, we can apply Noether's theorems to rediscover the conservation laws of hyperelasticity as consequences of symmetry. From a numerical perspective, the Euler-Lagrange equations and their discrete counterparts are the starting point for the development of variational integrators. Another feature of classical field theory is that time is "just another" space dimension.

For a proper introduction to elasticity, we refer to [**MH83**], [**TN04**] or [**Cia94**].

We follow [**CH17**, chapter 5] and [**MH83**, section 5.4], but most Theorems are presented in a less general and simplified version. For sake of simplicity, the theorems and proofs are stated in Cartesian coordinates, but we use the language from differential geometry.

To summarize the essential points of this chapter:

- A *field* φ maps a material point X and a time t onto the current spatial position $x = \varphi(X, t)$.
- Hamilton's principle asserts that physical fields are stationary points of the action functional
$$S(\varphi) = \iint \mathcal{L}(\varphi, \dot{\varphi}, \mathrm{D}\varphi)\,\mathrm{d}X\,\mathrm{d}t.$$
- The corresponding Euler-Lagrange equation is
$$\frac{\partial \mathcal{L}}{\partial \varphi} - \frac{\mathrm{d}}{\mathrm{d}t}\frac{\partial \mathcal{L}}{\partial \dot{\varphi}} - \sum_i \frac{\mathrm{d}}{\mathrm{d}X^i}\frac{\partial \mathcal{L}}{\partial\, \mathrm{D}_i\varphi} = 0.$$
- The weak formulation of the Euler-Lagrange equation is
$$\iint \frac{\partial \mathcal{L}}{\partial \varphi}[\eta] + \frac{\partial \mathcal{L}}{\partial\, \mathrm{D}\varphi}[\mathrm{D}\eta] - \rho\ddot{\varphi}\cdot\eta\,\mathrm{d}X\,\mathrm{d}t = 0,$$
which has to hold for all variations η.

My contributions: This chapter contains only classical results. Nonetheless, there is not a lot of literature, where hyperelasticity is derived as a special case of classical field theory. In particular, the treatment of Neumann boundary conditions by application of the Lagrange d'Alembert principle was not found in any of the used literature, but this is due to my limited knowledge of the relevant literature in classical field theory. (The approach in [**MH83**] is not compatible with the more general theory in [**CH17**]. On

the other hand [**CH17**] does not treat non-conservative boundary conditions for fields at all.)

1. A Quick Recall of the Euler-Lagrange Equations in Classical Mechanics

To fix the notation, we shortly recall the principle idea of Lagrangian mechanics.

The kinematics of a physical system can be represented by a finite dimensional manifold $\mathcal{M}$, which is called the configuration space. The dynamics of the system are determined by a Lagrangian function $L = E_{\text{kin}} - E_{\text{pot}}$, which is the difference between kinetic and potential energy.

Hamilton's principle asserts that physical *trajectories*

$$q : [0, T] \to \mathcal{M}$$

are stationary points of the action functional

$$S(q) = \int_0^T L(q(t), \dot{q}(t))\, \mathrm{d}t.$$

Under certain assumptions, stationary points are exactly the solutions of the Euler-Lagrange equations

$$\frac{\partial L}{\partial q}(q, \dot{q}) - \frac{\mathrm{d}}{\mathrm{d}t}\frac{\partial L}{\partial \dot{q}}(q, \dot{q}) = 0.$$

In many cases, these equations boil down to Newton's second law. Hamilton's principle is a useful starting point to derive equations of motions for many different physical systems.

If we do not allow an infinite dimensional configuration space $\mathcal{M}$, this framework is restricted to systems with finitely many degrees of freedom, which excludes important systems from continuum mechanics, e.g. fluids and solids.

2. The Euler-Lagrange Equations for Classical Fields

A *field* in the context of *classical field theory* is a smooth map

$$\varphi : \mathcal{D} \to \mathcal{S}$$

from a source manifold $\mathcal{D}$ (possibly with boundary) to a target manifold $\mathcal{S}$.

For simplicity, we will always assume $\mathcal{S} = \mathbb{R}^m$.

The principle idea of classical field theory is to replace trajectories by fields. Intuitively, we might think of trajectories as the motion of finitely many

particles, whereas fields can represent the dynamics of an infinite collection of particles.

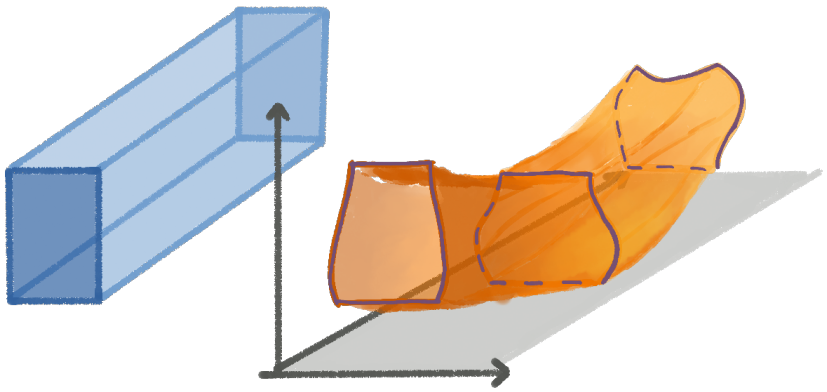

Figure 1. The abstract space $\mathcal{D} = \mathcal{B} \times [0, T]$ on the left hand side and of the current deformations of the body $\varphi(\mathcal{B}, t)$ in the spatial space $\mathcal{S} = \mathbb{R}^2$ at different times t on the right.

Remark 1.1 (Space-Time)**.** The source manifold can have the form

$$\mathcal{D} = \mathcal{B} \times [0, T] \,,$$

where $\mathcal{B}$ denotes a compact manifold of space-like coordinates (possibly with boundary). Therefore, the definition of fields includes already the dynamic case as well. For relativistic theories, this factorization is not always possible. But within this thesis, we will always assume the source manifold to be either $\mathcal{B}$ or $\mathcal{B} \times [0, T]$.

Remark 1.2 (Interpretation of fields in elasticity)**.** In elasticity, a point $X \in \mathcal{B}$ is called a *material point* and the corresponding value of the *deformation* field $x = \varphi(X)$ or $x = \varphi(X, t)$ is called a *spatial point*. The material space does encode the geometry of the solid, but it is per se a purely abstract space. Spatial coordinates describe the world how we perceive it, and thus a spatial point described the actual positions of the solid's atoms. This situations is visualized in Figure 1.

Following the classical path, our next step is the definition of the Lagrangian. In classical mechanics, the Lagrangian is defined on the tangent space $T\mathcal{M}$. For classical field theory, the appropriate domain is a jet bundle

[**EEMnLRR96**]. In simplified terms, we want to build a space where two functions are equal, if their first k derivatives are equal. We are mostly interested in the case $k = 1$, although the case $k = 2$ has one small application in this thesis as well.

Remark 1.3 (Working definition of jets)**.** It is intuitive to think of the k-jet of a field φ at point p as the k-order Taylor polynomial. Thus, $j^k_p(\varphi)$ carries the data

$$j^k_p(\varphi) \approx \Big(\varphi(p), \mathrm{D}\varphi(p), \ldots, \mathrm{D}^k\varphi(p)\Big).$$

A function $\mathcal{L} : \mathrm{Jet}^k(\mathbb{R}^n, \mathbb{R}^m) \to \mathbb{R}$ is a function which depends only on the first k derivatives of φ.

For a Lagrangian $\mathcal{L}(\varphi, \mathrm{D}\varphi)$, the concept of jets allows us to define terms like

$$\frac{\partial \mathcal{L}}{\partial \varphi} \quad \text{and} \quad \frac{\partial \mathcal{L}}{\partial\, \mathrm{D}\varphi},$$

where φ and $\mathrm{D}\varphi$ are considered to be independent during the differentiation. This is easy in coordinates, we might just write $\mathcal{L}(\varphi, \boldsymbol{F})$ and denote the latter derivative as $\frac{\partial \mathcal{L}}{\partial \boldsymbol{F}}$. But this construction does not generalize well to the geometric setting.

For mathematical joy, we therefore want to introduce a better notion, which does generalize to the geometric setting.

Definition 1.4 (k-jets in Euclidean space, [**IL03**])**.** We say two functions $f, g \in C^\infty(\mathbb{R}^n, \mathbb{R}^m)$ have *contact of order k at a point $p \in \mathbb{R}^n$*, if their first k derivatives are all equal at the point p. Let $\sim_{p,k}$ be the associated equivalence relation.

We define the k-order jet space at $p \in \mathbb{R}^n$ as the quotient vector space

$$\mathrm{Jet}^k_p(\mathbb{R}^n, \mathbb{R}^m) := C^\infty(\mathbb{R}^n, \mathbb{R}^m) \Big/ \sim_{p,k}.$$

The k-order jet fiber-bundle is defined as the disjoint union (with canonical smooth structure)

$$\mathrm{Jet}^k(\mathbb{R}^n, \mathbb{R}^m) := \coprod_{p \in \mathbb{R}^n} \mathrm{Jet}^k_p(\mathbb{R}^n, \mathbb{R}^m).$$

The equivalence class of $f \in C^\infty(\mathbb{R}^n, \mathbb{R}^m)$ at p is called the k-jet of f at p

$$j^k_p(f) \in \mathrm{Jet}^k_p(\mathbb{R}^n, \mathbb{R}^m)$$

and it defines a smooth section

$$j^k(f) : \mathbb{R}^n \to \mathrm{Jet}^k(\mathbb{R}^n, \mathbb{R}^m).$$

Remark 1.5 (Nonlinear source manifold)**.** We can replace $\mathbb{R}^n$ by a smooth manifold $\mathcal{D}$ in Definition 1.4. Two functions $f, g : \mathcal{D} \to \mathbb{R}^m$ have a contact of order k at point $p \in \mathcal{D}$ if there exists a local chart $h : U \to \mathbb{R}^n$ at p such that the associated chart representations $f \circ h^{-1}$ and $g \circ h^{-1}$ have a contact of order k at $h(p)$.

By virtue of the chain rule, this property does not depend on the choice of the chart h.

Hamilton's Principle. Hamilton's principle states that true fields are stationary points of the action functional

$$S(\varphi) = \int_{\mathcal{D}} \mathcal{L}(j^k(\varphi)) \, \mathrm{dV},$$

where dV is fixed volume form on $\mathcal{D}$ and the *Lagrangian (density)* $\mathcal{L}$ is a smooth function on the jet bundle $\mathrm{Jet}^k(\mathcal{D}, \mathcal{S})$ over $\mathcal{D}$ [**CH17**].

In hypereleasticity, the Lagrangian is of the form

$$\mathcal{L} = \mathcal{E}_{\mathrm{kin}} - \mathcal{E}_{\mathrm{pot}},$$

where the energy densities will depend on derivatives of the field φ in time and space direction.

Dirichlet boundary and initial conditions. For space-time formulations, initial conditions are just Dirichlet boundary conditions which are imposed at the boundary $t = 0$ of the source manifold $\mathcal{D}$.

We can rewrite conditions like

$$\varphi(X, t) = \varphi_{\mathrm{D}}(X) \quad \text{for all } (X, t) \in \partial_D \mathcal{B} \times [0, T]$$

or

$$\varphi(X, 0) = \varphi_{\mathrm{init}}(X) \quad \text{for all } X \in \mathcal{B},$$

into the combined formulation

$$\varphi = \widetilde{\varphi}_{\mathrm{D}} \quad \text{on } \partial_D \mathcal{D}.$$

Since every field is supposed to satisfy the boundary conditions we impose, we will restrict Hamilton's principle to the set $\mathcal{C}$ of feasible fields

$$\mathcal{C} = \{\varphi : \mathcal{D} \to \mathcal{S} \mid \varphi \text{ is a smooth diffeomorphism and satisfies the Dirichlet boundary conditions.}\} \tag{1.1}$$

We will call the set $\mathcal{C}$ the *configuration space*.[1]

[1] This definition only coincides with [**MH83**, section 5.1] if $\mathcal{D} = \mathcal{B}$, but not in the dynamic case.

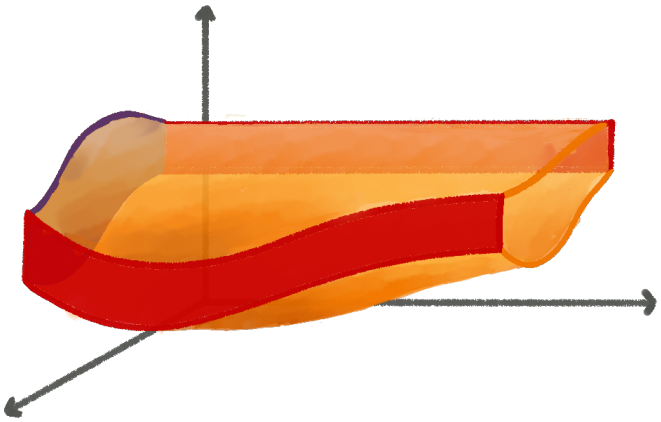

Figure 2. Dirichlet boundary conditions in space-time are a combination of initial conditions (purple on the left plane) and usual spatial Dirichlet boundary conditions (red). Time varying Dirichlet boundary conditions are also included in the current formulation.

We take for granted that the field space $\mathcal{C}$ is an infinite dimensional Banach-submanifold of $C^\infty(\mathcal{D} \to \mathcal{S})$ [**MH83**, section 4.2], this might exclude strange or non-smooth boundary and initial conditions.

First order conditions for stationary points. We will use the letter Z to denote points of the source manifold $\mathcal{D}$.

Applying the first order condition for stationary points from Theorem A.4 yields

$$\mathrm{d}S(\varphi) = 0 \in T^*_\varphi \mathcal{C},$$

where $T^*_\varphi \mathcal{C}$ denotes the dual space of the tangent space $T_\varphi \mathcal{C}$.

The next theorem enlightens the relation of tangent vectors $\eta \in T_\varphi \mathcal{C}$ and smooth variations of φ. Using this relation, we can translate the condition

$$\mathrm{d}S(\varphi)[\eta] = 0, \qquad \text{for all } \eta \in T_\varphi \mathcal{C}$$

into the the weak formulation of the Euler-Lagrange equation.

To prepare for the next theorem, we recall the definition of the bundle projection $\pi_\mathcal{S}$ for the tangent bundle $T\mathcal{S}$. This projection maps a tangent vector onto its base point. Since in our case $\mathcal{S} = \mathbb{R}^m$, this map is simply

$$\pi_\mathcal{S} : T\mathcal{S} \to \mathcal{S} : (x, v) \mapsto x.$$

Lemma 1.6 (Infinitesimal variations, cp. [**MR11**, Prop. 8.1.2])**.** *The tangent space $T_\varphi\mathcal{C}$ is the set of smooth maps $\eta : \mathcal{D} \to T\mathcal{S}$ such that*

(i) $\pi_\mathcal{S} \circ \eta = \varphi$ *and*

(ii) $\eta(Z) = 0 \quad$ *for all* $Z \in \partial_D\mathcal{D}$.

Sketch of the proof. Following the interpretation of tangent vectors as equivalence class of curves with first order contact at a common point, like in Remark B.1, then each tangent vector $\eta_\mathcal{C} \in T_\varphi\mathcal{C}$ has a representing curve

$$\gamma : (-\delta, \delta) \to \mathcal{C} : \varepsilon \mapsto \gamma(\varepsilon),$$

such that the base point is φ, i.e.

$$\gamma(0) = \varphi$$

and its equivalence class is $[\gamma] = \eta_\mathcal{C} \in T_\varphi\mathcal{C}$.

For a fixed point $Z \in \mathcal{D}$, we can define a curve in the target manifold, given by

$$\gamma(\varepsilon; Z) := \gamma(\varepsilon)(Z).$$

The equivalence class of this curve in $\mathcal{S}$ defines a tangent vector

$$\eta(Z) := [\gamma(\cdot; Z)] \in T_{\varphi(Z)}\mathcal{S}.$$

For (i), we just have to calculate the base point

$$\eta(0) = \gamma(0; Z) = \varphi(Z).$$

The second statement (ii) holds true, since the fields in $\mathcal{C}$ are prescribed at the Dirichlet boundaries. Therefore, the curves $\gamma(\cdot; Z)$ are constant and thus their derivative with respect to ε is zero. □

Theorem 1.7 (Weak formulation of the first order condition for stationary points)**.** *Let $\mathcal{L}$ be a smooth function on $\mathrm{Jet}^1(\mathcal{D}, \mathbb{R}^m)$ and assume the source manifold $\mathcal{D}$ to be a compact manifold. A smooth field $\varphi : \mathcal{D} \to \mathbb{R}^m$ is a stationary point of the corresponding action functional $S : \mathcal{C} \to \mathbb{R}$ if and only if*

$$0 = \int_\mathcal{D} \frac{\partial \mathcal{L}}{\partial \varphi}(j^1(\varphi))[\eta] + \frac{\partial \mathcal{L}}{\partial\, \mathrm{D}\varphi}(j^1(\varphi))[\mathrm{D}\eta]\, \mathrm{d}V = \mathrm{d}S(\varphi)[\eta] \tag{1.2}$$

holds for all smooth variations $\eta \in T_\varphi\mathcal{C}$.

Sketch of the proof. 1. In order to apply Theorem A.4, we need to show Gatêaux-differentiability of

$$S : \mathcal{C} \to \mathbb{R} : \varphi \mapsto \int_\mathcal{D} \mathcal{L}(j^1(\varphi))\, \mathrm{d}V.$$

This is not too hard to prove, since we can write the action functional as a composition of smooth maps.

2. For the computation of $\mathrm{d}S$ we start with the differential of the 1-jet $j^1(\varphi)$.

We do not want to go into details here, but the map j^1 evaluated at $Z \in \mathcal{D}$ is more or less

$$\mathrm{J}^k_Z(\varphi) \approx (\varphi(Z), \mathrm{D}\varphi(Z)),$$

which is clearly a linear map in φ. Thus, the differential – which is the best linear approximation – is just the map itself, i.e.

$$\mathrm{D}j^1(\varphi)[\eta] = j^1(\eta),$$

where we use Lemma 1.6 to convert $\eta \in T\mathcal{C}$ into a map $\mathcal{D} \to T\mathcal{S}$ and identify $T_{\varphi(Z)}\mathcal{S} \cong \mathbb{R}^m$, which yields a map

$$\eta : \mathcal{D} \to \mathbb{R}^m.$$

With these domains, $j^1(\eta)$ is well defined.

This implies

$$\begin{aligned} \mathrm{D}(\mathcal{L} \circ j^1)(\varphi)[\eta] &= \mathrm{D}\mathcal{L}(j^1(\varphi)) \left[\mathrm{D}j^1(\varphi)[\eta]\right] \\ &= \mathrm{D}\mathcal{L}(j^1(\varphi))[j^1(\eta)] \\ &= \frac{\partial \mathcal{L}}{\partial \varphi}[\eta] + \frac{\partial \mathcal{L}}{\partial\, \mathrm{D}\varphi}[\mathrm{D}\eta]. \end{aligned} \tag{1.3}$$

By the linearity of the integral, we get

$$\mathrm{d}S(\varphi)[\eta] = \int_{\mathcal{D}} \frac{\partial \mathcal{L}}{\partial \varphi}[\eta] + \frac{\partial \mathcal{L}}{\partial\, \mathrm{D}\varphi}[\mathrm{D}\eta]\, \mathrm{d}V.$$

□

We remark that a physicist would rewrite Equation (1.3) as

$$\delta\mathcal{L} = \frac{\partial \mathcal{L}}{\partial \varphi}\delta\varphi + \frac{\partial \mathcal{L}}{\partial\, \mathrm{D}\varphi}\delta\, \mathrm{D}\varphi.$$

Definition 1.8 (Momentum)**.** If the source manifold is of the form $\mathcal{D} = \mathcal{B} \times [0, T]$, then the *momentum* is given by

$$\boldsymbol{p} := \frac{\partial \mathcal{L}}{\partial \dot{\varphi}}.$$

Remark 1.9 (Stress, [**MH83**, chapter 5, Definition 4.4])**.** Using notations from elasticity, we define the *first Piola-Kirchhoff stress tensor* as

$$\boldsymbol{P} := -\frac{\partial \mathcal{L}}{\partial\, \mathrm{D}\varphi}.$$

From a field theoretical perspective, it is natural to use the letter 'p' to denote momentum *and* stress, since they both denote derivatives of $\mathcal{L}$ with respect to changes of the field in space respectively in time.

Remark 1.10 (Sources of Nonlinearities)**.** We can already identify the principle reasons for nonlinear terms in the weak formulation [**Wri08**, chapter 2]. To get a linear problem, we always need to ensure that the space of fields $\mathcal{C}$ is a linear vector space and the gradient of the action potential, i.e. $\mathrm{d}S(\varphi)$, is also linear with respect to the field φ.

Before we derive the strong form of the Euler-Lagrange equations, two definitions are necessary to handle the natural boundary conditions.

Definition 1.11 (Normal fields at the boundary)**.** To treat boundary conditions, we have to consider $\mathcal{D}$ as a Riemannian manifold with boundary, which allows us to define a covector field on the boundary

$$\boldsymbol{N} : \partial\mathcal{D} \to T^*\mathcal{D}\big|_{\partial\mathcal{D}},$$

such that a vector field $\boldsymbol{V} : \partial\mathcal{D} \to T\mathcal{D}$ is tangential to $\mathcal{D}$, if and only if $\boldsymbol{N}(Z)[\boldsymbol{V}(Z)] = 0$.

Definition 1.12 (Contraction)**.** For a bilinear form

$$\boldsymbol{T} : V^* \times W \to \mathbb{R}$$

and a covector

$$\boldsymbol{N} : V^* \times W$$

we define the contraction as

$$\boldsymbol{T} \cdot \boldsymbol{N} : W \to \mathbb{R} : \boldsymbol{w} \mapsto \boldsymbol{T}[\boldsymbol{N}, \boldsymbol{w}].$$

The name contraction is motivated by the equivalent definition via indices, where the sum over one pair of indices is taken

$$(\boldsymbol{T} \cdot \boldsymbol{N})_j = \sum_i T^i_j N_i.$$

For tensor fields on manifolds, the contraction is defined pointwise.

Theorem 1.13 (Euler-Lagrange equations for fields, cp. [**CH17**, Theorem 5.2])**.** *Let $\mathcal{L}$ be a smooth function on $\mathrm{Jet}^1(\mathcal{D}, \mathbb{R}^m)$, let $\mathcal{D} \subseteq \mathbb{R}^n$ be a compact Riemannian manifold (possibly with boundary) and consider the corresponding action functional $S : \mathcal{C} \to \mathbb{R}$. A smooth map $\varphi : \mathcal{D} \to \mathbb{R}^m$ is a critical point of the action under smooth variations if and only if it has finite action and is the solution of the following system of partial differential equations*

$$0 = \frac{\partial \mathcal{L}}{\partial \varphi} - \sum_i \frac{\mathrm{d}}{\mathrm{d}Z^i} \left(\frac{\partial \mathcal{L}}{\partial \, \mathrm{D}_i \varphi} \right), \tag{1.4}$$

with Dirichlet boundary conditions

$$\varphi = \varphi_D \quad \text{on } \partial_D \mathcal{D} \tag{1.5}$$

and natural boundary conditions

$$\frac{\partial \mathcal{L}}{\partial \, \mathrm{D}\varphi} \cdot \boldsymbol{N} = 0 \quad \text{on } \partial_N \mathcal{D} := \partial \mathcal{D} \setminus \partial_D \mathcal{D}. \tag{1.6}$$

Remark 1.14 (Time-Space factorization)**.** If we use $Z = (X, t)$ and consider D to be the derivative with respect to X, we get the equations

$$0 = \frac{\partial \mathcal{L}}{\partial \varphi} - \frac{\mathrm{d}}{\mathrm{d}t} \frac{\partial \mathcal{L}}{\partial \dot{\varphi}} - \sum_i \frac{\mathrm{d}}{\mathrm{d}X^i} \left(\frac{\partial \mathcal{L}}{\partial \, \mathrm{D}_i \varphi} \right).$$

Sketch of the proof. We recall that an upper index like φ^i denotes the i-th component of φ.

1. Let φ be a stationary point of S. In particular we have $\varphi \in \mathcal{C}$ which implies the Dirichlet boundary condition Equation (1.5).

We start with the weak formulation from Theorem 1.7,

$$0 = \int_{\mathcal{D}} \frac{\partial \mathcal{L}}{\partial \varphi}[\eta] + \sum_{i,j} \frac{\partial \mathcal{L}}{\partial \, \mathrm{D}_i \varphi^j} [\mathrm{D}_i \eta^j] \, \mathrm{d}V,$$

which has to hold for all variations $\eta \in T\mathcal{C}$.

We apply Stoke's Theorem to get

$$0 = \int_{\mathcal{D}} \frac{\partial \mathcal{L}}{\partial \varphi}[\eta] - \sum_{i,j} \frac{\mathrm{d}}{\mathrm{d}Z^i} \frac{\partial \mathcal{L}}{\partial \, \mathrm{D}_i \varphi^j} [\eta^j] \, \mathrm{d}V + \int_{\partial \mathcal{D}} \sum_{i,j} \frac{\partial \mathcal{L}}{\partial \, \mathrm{D}_i \varphi^j} [N_i \otimes \eta^j] \, \mathrm{d}A,$$

where $\boldsymbol{N}$ denotes a field of outward pointing normal vectors.

We skip details here. The map $\boldsymbol{N} \otimes \eta : T\mathcal{D}|_{\partial_N \mathcal{D}} \to T\mathcal{S} : \boldsymbol{V} \mapsto \boldsymbol{N}[\boldsymbol{V}] \cdot \boldsymbol{\eta}$ can be seen as a two-point tensor, just like the (deformation) gradient $\mathrm{D}\varphi$. In this way, $\frac{\partial \mathcal{L}}{\partial \, \mathrm{D}\varphi}[\boldsymbol{N} \otimes \eta]$ is well defined.

By Lemma 1.6, all variations vanish on the boundary $\partial_D \mathcal{D}$, but the variations vary freely on $\partial_N \mathcal{D}$.

Applying the Riesz-isomorphism and after separating η, we arrive at

$$0 = \int_{\mathcal{D}} \left(\frac{\partial \mathcal{L}}{\partial \varphi} - \sum_i \frac{\mathrm{d}}{\mathrm{d}Z^i} \frac{\partial \mathcal{L}}{\partial \, \mathrm{D}_i \varphi} \right) \cdot \eta \, \mathrm{d}V + \int_{\partial_N \mathcal{D}} \left(\frac{\partial \mathcal{L}}{\partial \, \mathrm{D}\varphi} \cdot \boldsymbol{N} \right) \cdot \eta \, \mathrm{d}A. \tag{1.7}$$

As usual, a special choice of the variation η proves Equation (1.4) and Equation (1.6).

2. The prove the other direction, we may repeat the same arguments in reverse. Of course this is only possible since φ is assumed to be smooth! □

Remark 1.15 (Regularity, Existence and Uniqueness)**.** Both the weak form and the strong form can be ill-posed, especially if we require too much regularity. The choice of appropriate function spaces depends on the Lagrangian $\mathcal{L}$ and is not trivial.

Remark 1.16 (Second order Euler-Lagrange equation, cp. [**CH17**, Theorem 5.2])**.** If the Lagrangian also depends on second-order derivatives of φ, the strong formulation of the Euler-Lagrange equations is

$$0 = \frac{\partial \mathcal{L}}{\partial \varphi} - \sum_i \frac{\mathrm{d}}{\mathrm{d}Z^i} \left(\frac{\partial \mathcal{L}}{\partial \, \mathrm{D}_i \varphi} \right) + \sum_{i,j} \frac{\mathrm{d}}{\mathrm{d}Z^i} \frac{\mathrm{d}}{\mathrm{d}Z^j} \left(\frac{\partial \mathcal{L}}{\partial \, \mathrm{D}_i \, \mathrm{D}_j \varphi} \right). \tag{1.8}$$

There are no new ideas needed to derive these equations, but the boundary conditions are more difficult, since Stoke's Theorem has to be used twice.

3. Non-conservative Euler-Lagrange Equations

External forces and boundary conditions break the conservation of energy for time-invariant Lagrangians, which implies that we must expand or adjust Hamilton's variational principle if we want to model external influences. In theory, these external influences also originate from other physical systems, but we do not have enough information nor the resources to include them into our model. Therefore, it is no option to include all effects of the environment exactly.

3.1. The Lagrange-d'Alembert principle. If we included all external effects into one system, the *global* variational principle would state

$$\mathrm{d}S(\varphi) + \mathrm{d}S_{\mathrm{env}}(\varphi, \varphi_{\mathrm{env}}) = 0,$$

where S_{env} represents the action of an environmental system in configuration φ_{env}.

For both forces and boundary conditions, we model the perturbation of the variational equation by some co-vectorfield

$$F : \mathcal{C} \to T^*\mathcal{C},$$

which approximates

$$F(\varphi) \approx \mathrm{d}S(\varphi, \varphi_{\text{env}}).$$

The resulting variational equation is called *Lagrange-d'Alembert principle* and reads

$$\mathrm{d}S(\varphi) + F(\varphi) = 0. \tag{1.9}$$

3.2. Forces. Forces are already co-tangential vectors in classical mechanics, although this detail is often omitted. Hence it is canonical to model a force field as a co-vector field

$$\boldsymbol{b} : \mathcal{D} \to T^*\mathcal{S}. \tag{1.10}$$

The force $\boldsymbol{b}(Z) \in T^*_\varphi(X)\mathcal{S}$ acts at the spatial position $\varphi(X)$ but it does only depend on the material point $X \in \mathcal{D}$. Forces like this are called dead loads, but other choices are also possible!

To apply the *Lagrange-d'Alembert principle* from Equation (1.9), we define $F_{\boldsymbol{b}} : \mathcal{C} \to T^*\mathcal{C}$ to be constant with respect to $\varphi \in \mathcal{C}$. The co-vector $F_{\boldsymbol{b}}(\varphi) \in T^*\mathcal{C}$ is defined as

$$F_{\boldsymbol{b}}(\varphi) : T\mathcal{C} \to \mathbb{R} : \eta \mapsto \int_{\mathcal{D}} \boldsymbol{b}(Z)[\eta(Z)] \,\mathrm{d}V(Z).$$

This term is well-defined by Lemma 1.6.

The corresponding Euler-Lagrange equations are simple, the external forces are just added to the internal forces $\frac{\partial \mathcal{L}}{\partial \varphi}$, hence

$$\frac{\partial \mathcal{L}}{\partial \varphi} + \boldsymbol{b} - \frac{\mathrm{d}}{\mathrm{d}t}\frac{\partial \mathcal{L}}{\partial \dot{\varphi}} - \sum_i \frac{\mathrm{d}}{\mathrm{d}X^i}\frac{\partial \mathcal{L}}{\partial \,\mathrm{D}_i\varphi} = 0.$$

3.3. Natural boundary conditions. The variations only vanish on those parts of the boundary $\partial\mathcal{D}$ where we impose Dirichlet boundary conditions. This leads to the *natural* boundary condition on the rest of the boundary

$$\frac{\partial \mathcal{L}}{\partial \,\mathrm{D}\varphi} \cdot \boldsymbol{N} = 0 \quad \text{on } \partial_N\mathcal{B}. \tag{1.11}$$

This is a condition to the stress tensor $\boldsymbol{P}$ (from Remark 1.9) in normal direction $\boldsymbol{N}$ (Definition 1.11).

We can prescribe the stress to be non-zero as well by defining a field

$$\boldsymbol{\tau} : \mathcal{D} \to T^*\mathcal{S} \tag{1.12}$$

Analogously to the introduction of forces, we define

$$F_\tau(\varphi) : T\mathcal{C} \to \mathbb{R} : \eta \mapsto \int_{\partial_N \mathcal{D}} \tau(Z)[\eta(Z)] \,\mathrm{d}A(Z).$$

Again, this term does not depend on the configuration φ.

The corresponding variational principle

$$\mathrm{d}S(\varphi)[\eta] + F_\tau[\eta] = 0 \quad \text{for all } \eta \in T_\varphi\mathcal{C}$$

leads to a modification of Equation (1.7) and to the term

$$0 = \int_{\partial_N \mathcal{D}} \left(\frac{\partial \mathcal{L}}{\partial \,\mathrm{D}\varphi} \cdot \boldsymbol{N} + \boldsymbol{\tau} \right) \cdot \eta \,\mathrm{d}A \quad \text{for all } \eta \in T_\varphi\mathcal{C}.$$

Therefore, the Euler-Lagrange equations stay the same, but the natural constraint (1.6) must be replaced by

$$-\frac{\partial \mathcal{L}}{\partial \,\mathrm{D}\varphi} \cdot \boldsymbol{N} = \boldsymbol{P} \cdot \boldsymbol{N} = \boldsymbol{\tau} \quad \text{on } \partial_N \mathcal{D}. \tag{1.13}$$

Remark 1.17 (Traction force potential)**.** In contrast to [**MH83**], we use Hamilton's principle for fields as starting point. If we used the Euler-Lagrange equations for the Lagrangian $L = \int_{\mathcal{B}} \mathcal{L} \,\mathrm{d}X$ to derive the equations for fields, it would be possible to add a term $\int_{\partial_N \mathcal{B}} -\mathcal{V}_\tau \,\mathrm{d}A$ to the Lagrangian to get the same variational equation with $\tau = -\,\mathrm{D}\mathcal{V}_\tau$. A similar approach is possible to include body forces.

4. Equations of Hyperelasticity

Without further ado, we can apply the general theory to derive the equations of hyperelasticity. We will also introduce the usual notations from elasticity, based on [**MH83**].

Model 1.18 (Three dimensional hyperelastic solids)**.** Let $\mathcal{B} \subset \mathbb{R}^3$ be a compact set of *material points*, let $T > 0$ denote some (irrelevant) terminal time.

A motion is described by a field

$$\varphi : \mathcal{B} \times [0, T] \to \mathbb{R}^3,$$

where $x = \varphi(X, t)$ denotes the *spatial position* of a *material point* $X \in \mathcal{B}$ at time $t \in [0, T]$. We call $\varphi(\cdot, t)$ the *deformation*, $\dot{\varphi}(\cdot, t)$ is the *velocity* and

$$\boldsymbol{F} := \mathrm{D}\varphi : T\mathcal{B} \to T\mathcal{D}$$

is called the *deformation gradient*, where D denotes only derivatives with respect to X and all dependencies on t are omitted.

The Lagrangian is given by

$$\mathcal{L}(j^1(\varphi)) = \rho_{\text{ref}}\|\dot{\varphi}\|_2^2 - \rho_{\text{ref}}\mathcal{W}(\mathrm{D}\varphi)$$

and we have to provide the initial data described in Table 1.

Material properties	
$\rho_{\text{ref}}(X)$	mass density with respect to material points
$\mathcal{W}(\mathrm{D}\varphi)$	stored energy density or strain energy
Initial deformation and velocity of the solid	
$\varphi_{\text{init}}(X)$	initial deformation
$\boldsymbol{v}_{\text{init}}(X)$	initial velocity
Dirichlet boundary conditions	
$\varphi_{\mathrm{D}}(X,t)$	Dirichlet boundary conditions on $\partial_D\mathcal{B}$
The traction	
$\boldsymbol{\tau}(X,t)$	Neumann boundary conditions on $\partial_N\mathcal{B}$
External body forces as in Equation 1.10	
$\boldsymbol{b}(X,t)$	Body forces or (dead) loads.

Table 1. Initial data for Model 1.18.

Then, according to the Lagrange-d'Alembert's principle, the equations of motion are given by

$$\mathrm{d}S(\varphi) + F_{\boldsymbol{b}} + F_{\tau} = 0. \tag{1.14}$$

Remark 1.19 (Initial conditions and non-abstract material points)**.** In practice, it is convenient to choose $\mathcal{B} \subset \mathbb{R}^3$ such that the stress free deformation is given as

$$\varphi_{\text{init}} = \mathrm{id} : \mathcal{B} \hookrightarrow \mathbb{R}^3.$$

Moreover, it is common to describe the deformation by a displacement map $u\colon \mathcal{B} \to \mathbb{R}^3$, which is related to the deformation φ via

$$\varphi = \mathrm{id} + u.$$

The displacement $u = 0$ then corresponds to the stress free deformation.

Now we simply collect all previous work, namely Theorem 1.13, Equation (1.11) and Equation (1.13). We recall the definition of the first Piola-Kirchhoff stress tensor from Remark 1.9

$$\boldsymbol{P} = -\frac{\partial \mathcal{L}}{\partial\, \mathrm{D}\varphi}.$$

Remark 1.20 (Dynamic Equations for Hyperelastic Solids)**.** In the setting of Model 1.18, the equations of motion are given by

$$0 = \boldsymbol{b} - \ddot{\varphi} - \mathrm{DIV}(\boldsymbol{P}),$$

with initial conditions

$$\varphi = \varphi_{\text{init}} \quad \text{and} \quad \dot{\varphi} = v_{\text{init}} \quad \text{at } t = 0,$$

Dirichlet boundary conditions

$$\varphi = \varphi_{\text{D}} \quad \text{on } \partial_D \mathcal{B}$$

and traction boundary conditions

$$\boldsymbol{P} \cdot \boldsymbol{N} = \boldsymbol{\tau} \quad \text{on } \partial_N \mathcal{B}.$$

Remark 1.21 (Static Equations for Hyperelastic Solids)**.** In the setting of Model 1.18, but with the source manifold defined as

$$\mathcal{D} = \mathcal{B},$$

the static equations of Hyperelastictiy are

$$0 = \boldsymbol{b} - \mathrm{DIV}(\boldsymbol{P}),$$

with Dirichlet boundary conditions

$$\varphi = \varphi_{\text{D}} \quad \text{on } \partial_D \mathcal{B}$$

and traction boundary conditions

$$\boldsymbol{P} \cdot \boldsymbol{N} = \boldsymbol{\tau} \quad \text{on } \partial_N \mathcal{B}.$$

4.1. Material laws. The Lagrangian

$$\mathcal{L} = \rho_{\text{ref}} \|\dot{\varphi}\|_2^2 - \rho \mathcal{W}(\mathrm{D}\varphi)$$

includes all information we know about the material. The choice of the strain energy is the crucial step to model realistic solids.

We shortly discuss one common material law. For an overview, we refer to [**RAS16**, section 3.3].

The principle of *material frame indifference* asserts that the strain energy of homogeneous and isotropic[2] materials does only depend on the characteristic polynomial of the *right Cauchy-Green deformation tensor*

$$\boldsymbol{C} := \mathrm{D}\varphi^T \, \mathrm{D}\varphi : T\mathcal{B} \to T\mathcal{B}.$$

The transpose is defined by the relation

$$\boldsymbol{g}(\boldsymbol{v}, \mathbf{D}\boldsymbol{\varphi}\boldsymbol{W}) = \boldsymbol{G}(\mathbf{D}\boldsymbol{\varphi}^T \boldsymbol{v}, \boldsymbol{W}),$$

[2]The material laws are invariant to rotations of the material coordinates.

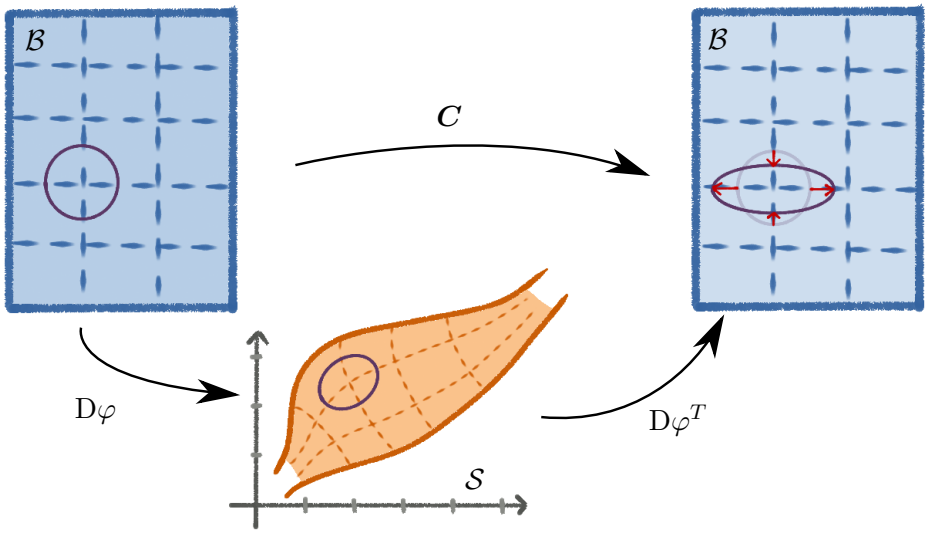

Figure 3. A unit circle in $T_X\mathcal{B}$ (left) is mapped onto an ellipse in $T_x\mathcal{S}$ (middle) under the deformation gradient $\mathrm{D}\varphi$. Without comparison to the configuration at rest, it is difficult to extract any information. But mapping it "back" into the material tangent space (right) shows how the material is stretched.

where $\boldsymbol{G}$ and $\boldsymbol{g}$ denote the Riemanniam metrics on the material space $\mathcal{B}$ and the spatial space $\mathcal{S}$.

The advantage of the right Cauchy-Green deformation tensor is illustrated in Figure 3.

Lemma 1.22 (Invariants of a symmetric linear map in three dimensions. [**MH83**, Proposition 3.5.9])**.** *Let $\boldsymbol{C} \in L(\mathbb{R}^3, \mathbb{R}^3)$ be a symmetric linear map. We define the invariants of $\boldsymbol{C}$ by*

$$I_1(\boldsymbol{C}) = \operatorname{tr} \boldsymbol{C}, \quad I_2(\boldsymbol{C}) = \frac{1}{2}\left((\operatorname{tr} \boldsymbol{C})^2 - \operatorname{tr}(\boldsymbol{C}^2)\right) \quad \text{and} \quad I_3(\boldsymbol{C}) = \det \boldsymbol{C}.$$

The invariants are related to the characteristic polynomial via

$$\det(\lambda \boldsymbol{I} - \boldsymbol{C}) = \lambda^3 - I_1\lambda^2 + I_2\lambda^1 - I_3.$$

In terms of eigenvalues of $\boldsymbol{C}$ we have

$$I_1 = \lambda_1 + \lambda_2 + \lambda_3, \quad I_2 = \lambda_1\lambda_2 + \lambda_1\lambda_3 + \lambda_2\lambda_3 \quad \text{and} \quad I_3 = \lambda_1\lambda_2\lambda_3.$$

Remark 1.23 (Mooney-Rivlin material)**.** For two parameters c_{10} and c_{01} the strain energy is given by

$$\mathcal{W}_{\text{M-R}} = c_{10}(I_1 - 3) + c_{01}(I_2 - 3).$$

This material law models the behaviour of rubber-like material.

4.2. Well-posedness. Like already noted, the theory of existence and uniqueness is non-trivial. We have not considered questions of this kind within the thesis, therefore we committed the crime of just assuming (or hoping) to stay within the area of well-posedness for our problems.

Remark 1.24 (John Ball's existence theory)**.** In the conservative case $\mathrm{d}S = 0$, it would be natural to require S, respectively the strain energy density $\mathcal{W}$, to be convex, but this is not physically reasonable. John Ball's existence theory applies for the larger class of polyconvex functions, which covers the Mooney-Rivlin material law as well. But additional assumptions on the domain, its topology and boundary conditions are not trivial [**MH83**, Chapter 6].

Remark 1.25 (Bifurcations in hyperelasticity)**.** In general we can not expect the existence of a unique solution for arbitrary boundary conditions. We shortly state an intuitive counterexample in Figure 4. Viewed as a dynamical system, many singular bifurcation points can exist. The theory for existence and uniqueness is out of the scope of this thesis, we just note that it is a complicated subject with many counterexamples for already simple systems [**MH83**, Chapter 6].

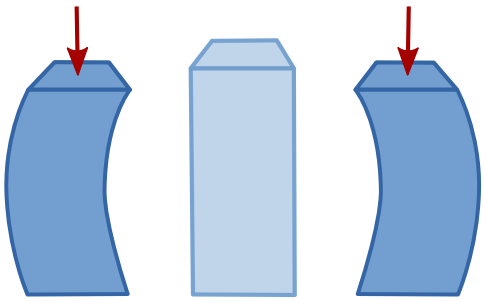

Figure 4. A force acting on the top of a bar will likely bend it into a non-unique direction.

4.3. Conservation Laws in Hyperelasticity. Emmy Noether's celebrated theorems uncovered the fundamental relation between symmetries and conserved quantities in physics.

We only state Noether's Theorem in its specialised form for hyperelasticity, taken from [**MH83**, chapter 5, example 5.6].

Theorem 1.26 (Noether's Theorem for spatial symmetries [**MH83**, chapter 5, example 5.6])**.** *Let*

$$\psi_s : \mathbb{R}^3 \to \mathbb{R}^3$$

be a flow, generated by a vector field $w : \mathbb{R}^3 \to T\mathbb{R}^3$.
If the Lagrangian $\mathcal{L}$ *is time-independent and if the pushforward of* $j^1(\varphi)$ *under* ϕ_s *leaves the Lagrangian invariant*

$$\mathcal{L}((\phi_s)_*(j^1(\varphi))) = \mathcal{L}(j^1(\varphi)),$$

then Noether's theorem states that any solution φ *of the equations of motion satisfies the conservation law*

$$\frac{\mathrm{d}}{\mathrm{d}t}\left(\frac{\partial \mathcal{L}}{\partial \dot{\varphi}} \cdot w\right) + \sum_{i,j=1}^{3} \frac{\mathrm{d}}{\mathrm{d}X^i}\left(\frac{\partial \mathcal{L}}{\partial\, \mathrm{D}_i \varphi^j} \cdot w_j\right) = 0.$$

For this (strong) formulation of the conservation laws, at least $\varphi \in C^2(\mathcal{B} \times [0,T] \to \mathbb{R}^3)$ *is required as well.*

We neglect the computations and just state the conservation laws and their corresponding symmetries.

Remark 1.27 (Conservation of Linear Momentum)**.** If the Lagrangian does not depend on point values of the configuration φ, invariance with respect to translations in space

$$x \mapsto x + s\boldsymbol{v}$$

yields the balance of (linear) momentum. If we combine the conservation laws for translations in all possible directions in space, we recover the Euler-Lagrange equations

$$\frac{\mathrm{d}}{\mathrm{d}t}\frac{\partial \mathcal{L}}{\partial \dot{\varphi}} + \mathrm{DIV}\left(\frac{\partial \mathcal{L}}{\partial\, \mathrm{D}\varphi}\right) = 0.$$

Notice that conservation of momentum holds only if no forces are present, i.e. $\frac{\partial \mathcal{L}}{\partial \varphi} = 0$.

Remark 1.28 (Conservation of Angular Momentum)**.** Similarly, rotational symmetry yields the conservation of angular momentum.

Remark 1.29 (Material symmetries)**.** In classical field theories, the material space is also equipped with a geometric structure. Therefore another class of symmetries also lead to conservation laws. These symmetries require a more general version of Noether's Theorem than stated in Theorem 1.26.

If the strain energy is isotropic, i.e. invariant with respect to all rotations in material coordinates

$$\boldsymbol{R}_{\boldsymbol{\omega}} : \mathcal{B} \to \mathcal{B} : X \mapsto \boldsymbol{R}_{\boldsymbol{\omega}} X,$$

then the second Piola-Kirchhoff stress tensor

$$\boldsymbol{S} := \boldsymbol{F}^{-1} \circ \boldsymbol{P} : T^*\mathcal{B} \to T\mathcal{B}$$

is symmetric, which means that the associated field of bilinear maps

$$\boldsymbol{F}^{-1}(X) \circ \boldsymbol{P}(X) : T^*_X\mathcal{B} \times T^*_X\mathcal{B} \to \mathbb{R}$$

are symmetric at each material point $X \in \mathcal{B}$.

Remark 1.30 (Conservation of Energy)**.** As usual, the material symmetry of time invariance

$$t \mapsto t + s$$

corresponds to the conservation of energy

$$\frac{\partial \mathcal{E}}{\partial t} + \mathrm{DIV}\left(\dot{\varphi}\frac{\partial \mathcal{L}}{\partial\, \mathrm{D}\varphi}\right) = 0,$$

with $\mathcal{E}$ denoting the total energy density

$$\mathcal{E} = \underbrace{\frac{\partial \mathcal{L}}{\partial \dot{\varphi}} \cdot \dot{\varphi}}_{2\mathcal{E}_{\mathrm{kin}}} - \mathcal{L} = \mathcal{E}_{\mathrm{kin}} + \mathcal{E}_{\mathrm{pot}}.$$

Remark 1.31 (Conservation of Mass)**.** In Model 1.18, the mass density is time-invariant and depends only on material points $X \in \mathcal{B}$, therefore conservation of mass is trivial.

5. Example: One Dimensional Hyperelasticity

To animate the theory, we discuss a model for one dimensional ropes. In Chapter 3, we use a similar approach to model a seemingly infinite collection of tiny springs.

Example 1.32 (A chain of springs)**.** To start simple, we will consider an example from classical mechanics. We model a chain of $n+1$ point masses, with a spring attached between each two consecutive point masses. In the next remark, we derive a model for a continuous rope by considering the limit $n \to \infty$.

We use the following notations for physical quantities of this system.

- m_{total} : total mass of the chain of springs.
- L_{total} : total length of the chain.
- $h = \frac{1}{n}$: length of a single spring at rest.
- $m_{\mathrm{single}} = \frac{1}{n+1} \cdot m_{\mathrm{total}} \approx h \cdot m_{total}$: single point mass.
- A: cross-section of the springs.

- E: Young's elastic modulus for the springs.
- $\kappa = \frac{E \cdot A}{h}$: stiffness of the springs.

If we ignore collisions, the kinematics of the system are described by the configuration space $(\mathbb{R}^3)^{n+1}$. Using trajectories from classical mechanics, a curve $q : [0, T] \to (\mathbb{R}^3)^{n+1}$ describes the $n + 1$ positions of the point masses. We use $\boldsymbol{q}_i \in \mathbb{R}^3$ to denote the position of the i-th point mass.

The potential energy is given by

$$E_{\text{pot}} = \sum_{i=1}^{n} \frac{E \cdot A}{2h} \left(\left\| \boldsymbol{q}_{i+1} - \boldsymbol{q}_i \right\|_2 - h \right)^2 .$$

Together with the kinetic energy

$$E_{\text{kin}} = \sum_{i=1}^{n+1} \frac{1}{2} h \cdot m_{\text{total}} \left\| \dot{\boldsymbol{q}}_i \right\|_2^2 ,$$

the dynamics are fully determined by the Euler-Lagrange equation, which are given by

$$h \cdot m_{\text{total}} \ddot{\boldsymbol{q}}_i = \kappa(\boldsymbol{q}_{i+1} - 2\boldsymbol{q}_i + \boldsymbol{q}_{i-1}) - 2\kappa \cdot h \left(\frac{\boldsymbol{r}_{i+\frac{1}{2}}}{\left\| \boldsymbol{r}_{i+\frac{1}{2}} \right\|_2} - \frac{\boldsymbol{r}_{i-\frac{1}{2}}}{\left\| \boldsymbol{r}_{i-\frac{1}{2}} \right\|_2} \right) .$$

For a large number of particles n, the dimension of the configuration tends to infinity. To overcome this issue, we can use a field to describe the motion. Therefore, we identify each mass point as an element of $\mathcal{B}_{\text{chain}} = \{0, \frac{1}{n}, \ldots, \frac{n}{n}\}$. The map

$$\varphi : \mathcal{B}_{\text{chain}} \times [0, T] \to \mathbb{R}^3$$

assigns to each *material point* $X_k = \frac{1}{k} \in \mathcal{D}_{\text{chain}}$ and each time $t \in [0, T]$ the corresponding *spatial point* in space, i.e.

$$\varphi(X_k, t) = \boldsymbol{q}_k(t) \in \mathbb{R}^3.$$

Example 1.33 (A continuous rope)**.** For a large number of springs, we might want to use an infinite collection of point masses to represent the chain of springs as a continuous rope, for example we can take $\mathcal{D}_{\text{rope}} = [0, 1] \times [0, T]$.

The interpretation of a field $\varphi : \mathcal{D}_{\text{rope}} \to \mathbb{R}^3$ remains the same! The field assigns a spatial point $x = \varphi(X, t)$ to each pair of a material point and a time $(X, t) \in \mathcal{D}_{\text{rope}}$.

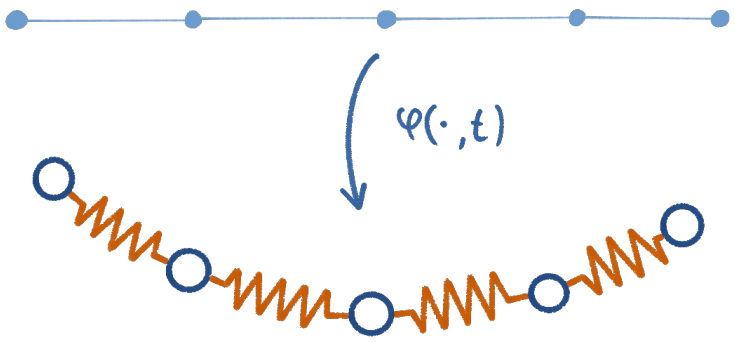

Figure 5. A field φ relates times and material point to the current spatial points in space. (The springs are only visualised as spiral springs, in our model we use Young's modulus and hence allow only uniaxial deformation.

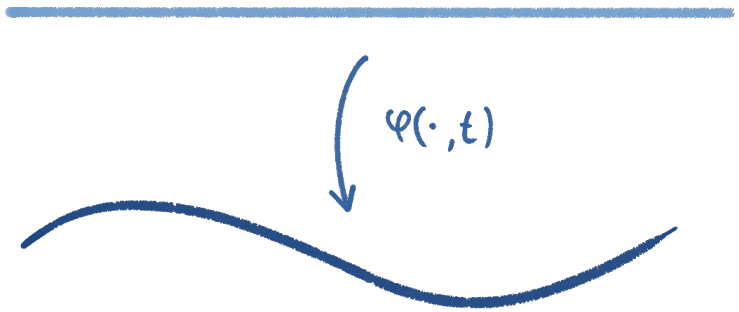

Figure 6. For ropes, the source manifold $\mathcal{D}_{\text{rope}}$ carries a non-trivial geometry. A field separates the data which do not change in time, i.e. the time domain and the source manifold from the spatial points, which can move within the target manifold.

We notice a humble difference between fields and trajectories: In the continuous chase, trajectories are maps into a infinite dimensional space, i.e. $q : [0, T] \to \mathcal{C}^\infty([0, 1] \to \mathbb{R}^3)$, whereas fields are still maps between two finite dimensional spaces.

Example 1.34 (The Lagrangian for a continuous rope)**.** We continue Example 1.32 and consider the limit $n \to \infty$.

We recall the definition of the Lagrangian of a spring and insert $h = \frac{1}{n}$ to get

$$\begin{aligned}\mathcal{L}_{\text{chain}} = &\sum_{k=0}^{n+1} h \cdot \frac{1}{2} m_{\text{total}} \left\|\dot{\varphi}(X_k, t)\right\|_2^2 \\ &- \sum_{k=1}^{n} h \cdot \frac{A \cdot E}{2} \left(\frac{\left\|\varphi(X+h,t) - \varphi(X,t)\right\|_2 - h}{h} \right)^2 .\end{aligned}$$

For the limit $n \to \infty$, we use $\sum h \approx \int \mathrm{d}X$ and the definition of the derivative to get the Lagrangian

$$L_{\text{rope}} = \int_0^1 \frac{m_{\text{total}}}{2} \left\|\dot{\varphi}(X,t)\right\|_2^2 \mathrm{d}X - \int_0^1 \frac{A \cdot E}{2} \left(\left\|\mathrm{D}_X \varphi(X,t)\right\|_2 - 1 \right)^2 \mathrm{d}X.$$

The distance between two mass points in the chain is replaced by the derivative with respect to X. This is typical for continuous models and the derivative is usually called the *deformation gradient*.

We prefer to work with a Lagrangian density with respect to time and space, hence we set

$$\begin{aligned}\mathcal{L}_{\text{rope}} &= \frac{m_{\text{density}}}{2} \left\|\dot{\varphi}\right\|_2^2 - \frac{A \cdot E}{2} \left(\left\|\mathrm{D}_X \varphi\right\|_2 - 1 \right)^2 \\ &= \mathcal{E}_{\text{kin}} - \mathcal{E}_{\text{pot}}.\end{aligned}$$

Exercise 1.35 (Classical mechanics is not a special case of field theory)**.** Why is a chain of springs (Example 1.33) not an example for classical field theory? [3]

6. Constraints in Classical Field Theory

In this section, we state the Euler-Lagrange equation of first kind for classical field theory with constraints.

The constraint is represented as

$$g(j^1(\varphi)) = 0.$$

Previous results can be reused, if we extend the target manifold by

$$\phi : \mathcal{D} \to \mathcal{S} \times \mathbb{R} : Z \mapsto (\varphi(Z), p(Z)).$$

[3] In the classical work of Walter Noll and Clifford Truesdell, the *principle of local action* was introduced to forbid non-local interactions in solids [**TN04**, section 26]. To answer the question, it might help to understand in which sense a principle of local action is included in classical field theory.

Here p represents the Lagrange multiplier corresponding to the constraint $g = 0$.

We define the *augmented Lagrangian* as

$$\widetilde{\mathcal{L}}(j^1(\phi)) = \mathcal{L}(j^1(\varphi)) - p \cdot g(j^1(\varphi)).$$

The approach of Lagrange multipliers is well-know and based on the following theorem.

Theorem 1.36 (Lagrange Multiplier Theorem for Linear Spaces, [**MR11**, Theorem 8.3.1])**.** *Let V be a Banach space and $S : V \to \mathbb{R}$ be a smooth function and $g : V \to \mathbb{R}$ a smooth constraint function with regular value 0. The constraint manifold $\mathcal{C} = g^{-1}(\{0\})$ is a submanifold of V.*
We define

$$\widetilde{S} : V \times \mathbb{R}^* \to R : (\varphi, p) \mapsto S(\varphi) - p[g(\varphi)].$$

The following are equivalent conditions on $x_0 \in \mathcal{C}$:

(i) φ is a critical point of $S|_C$ and

(ii) there is a dual vector $p \in \mathbb{R}^*$ such that (φ, p) is a critical point of $\widetilde{S}$.

A more general version of this theorem also applies if the space of feasible fields $\mathcal{C}$ is a manifold [**MR11**, Theorem 8.3.2]. This covers the case when $\mathcal{D}$ or $\mathcal{S}$ are manifolds.

The Euler-Lagrange equations (Theorem 1.13) for $\widetilde{\mathcal{L}}$ are

$$\frac{\partial \widetilde{\mathcal{L}}}{\partial \phi} - \frac{\mathrm{d}}{\mathrm{d}t}\frac{\partial \widetilde{\mathcal{L}}}{\partial \dot{\phi}} - \sum_i \frac{\mathrm{d}}{\mathrm{d}X^i}\frac{\partial \widetilde{\mathcal{L}}}{\partial \,\mathrm{D}_i\phi} = 0.$$

Since the new configuration space factorizes into $\widetilde{\mathcal{C}} = \mathcal{C} \times C^\infty(\mathcal{D}, \mathbb{R})$, we can split the derivatives into two parts

$$\frac{\partial \widetilde{\mathcal{L}}}{\partial \phi} = \left(\frac{\partial \widetilde{\mathcal{L}}}{\partial \varphi}, \frac{\partial \widetilde{\mathcal{L}}}{\partial p}\right) \in T^*\widetilde{\mathcal{C}}.$$

Hence, the Euler-Lagrange equations represent a system of two partial differential equations, which have to be satisfied by φ and p.

Inserting the definition of $\widetilde{\mathcal{L}} = \mathcal{L} - pg$ yields the equations

$$0 = \frac{\partial \mathcal{L}}{\partial \varphi} + p\frac{\partial g}{\partial \varphi} - \frac{\mathrm{d}}{\mathrm{d}t}\left(\frac{\partial \mathcal{L}}{\partial \dot{\varphi}} - p\frac{\partial g}{\partial \dot{\varphi}}\right) - \sum_i \frac{\mathrm{d}}{\mathrm{d}X^i}\left(\frac{\partial \mathcal{L}}{\partial \,\mathrm{D}_i\varphi} - p\frac{\partial g}{\partial \,\mathrm{D}_i\varphi}\right), \tag{1.15a}$$

$$0 = \frac{\partial \widetilde{\mathcal{L}}}{\partial p} = g(j^1(\varphi)). \tag{1.15b}$$

Remark 1.37 (Incompressibility)**.** For an incompressible material, the deformation field must preserve volume at each point in time, which yields a condition on the deformation gradient $\mathrm{D}\varphi = \boldsymbol{F}$, for example

$$g(j^1(\varphi)) := \det(\mathrm{D}\varphi) - 1 = 0.$$

We only have to calculate the term $\frac{\partial g}{\partial \,\mathrm{D}\varphi}$, which is the only difference to the unconstrained Euler-Lagrange equations in the momentum equation.

The determinant depends in general on the Riemannian metrics of the material space and the spatial space. Here we stay in the simplified cartesian case $\mathcal{B} \subseteq \mathcal{S} = \mathbb{R}^3$. We also denote $\boldsymbol{F} = \mathrm{D}\varphi$.

Jacobi's formula for matrices $\boldsymbol{A} \in \mathrm{GL(n)}$ reads

$$\mathrm{D}\det(\boldsymbol{A})[\delta\boldsymbol{A}] = \det(\boldsymbol{A})\,\mathrm{tr}(\boldsymbol{A}^{-1}\delta\boldsymbol{A}), \quad \text{for } \delta\boldsymbol{A} \in T_{\boldsymbol{A}}\,\mathrm{GL}(n).$$

If we use the inner product $(A, B) \mapsto \mathrm{tr}(A^T B)$, we can identify

$$\boldsymbol{P}_{\mathrm{constr}} := p\frac{\partial g}{\partial \,\mathrm{D}\varphi} = \det(\boldsymbol{F})p\boldsymbol{I}\boldsymbol{F}^{-T}. \tag{1.16}$$

For a more intuitive interpretation, we transform these terms into spatial coordinates. The Piola transformation [**Wri08**, section 3.2.4] relates the spatial Cauchy stress tensor $\boldsymbol{\sigma} : T^*\mathcal{S} \to T\mathcal{S}$ to the first Piola-Kirchhoff stress tensor $\boldsymbol{P}$. The relation is given by

$$\boldsymbol{P} = \det(\boldsymbol{F})\boldsymbol{\sigma}\boldsymbol{F}^{-T}.$$

Therefore, stress induced by the incompressibility constraint has a simple form in the spatial picture, from

$$\boldsymbol{\sigma}_{\mathrm{constr}} = p\boldsymbol{I}.$$

This stress represents a hydraulic stress induced by a pressure p. It is important to notice, that the total hydraulic pressure in the material is given by

$$p_{\mathrm{hydr}} = \mathrm{tr}(\boldsymbol{\sigma}) = p + \frac{1}{3}\,\mathrm{tr}(\boldsymbol{\sigma}_{\mathrm{unconstr}}).$$

In this way, the Lagrange multiplier can be seen as a pressure field, but it is only one term of the hydraulic pressure in the material.

Model 1.38 (Equations of incompressible hyperelastic motion.)**.** If we combine Equation (1.15) and Equation (1.16), again using the notations $\boldsymbol{P} = -\frac{\partial \mathcal{L}}{\partial \mathrm{D}\varphi}$, $\boldsymbol{b} = \frac{\partial \mathcal{L}}{\partial \varphi}$ and $\boldsymbol{G} = \frac{\partial g}{\partial \mathrm{D}\varphi}$, we get

$$\begin{aligned} \boldsymbol{b} - \ddot{\boldsymbol{\varphi}} + \mathrm{Div}(\boldsymbol{P} + p\boldsymbol{G}) &= 0, \\ g(\boldsymbol{F}) &= 0. \end{aligned}$$

In the spatial picture, the balance of linear momentum transforms into a equation which is similar to the equations of incompressible fluid flow

$$\begin{aligned} \ddot{\boldsymbol{u}} &= \boldsymbol{b} + \mathrm{div}(\sigma - p\boldsymbol{I}) \\ &= \boldsymbol{b} + \mathrm{div}(\sigma) - \mathrm{grad}(p). \end{aligned}$$

Remark 1.39 (Quasi incompressible material)**.** A formal modification of the Lagrangian allows the material to compress, but it punishes large values of the Lagrange multiplier p with an additional quadratic term in the Lagrangian.

This relaxation is very popular and allows to create numerically feasible models for incompressible materials.

The augmented Lagrangian for this relaxation is defined by

$$\widetilde{\mathcal{L}} = \mathcal{L}_{\text{hyperelastic}} - p(\det(\mathrm{D}\varphi) - 1) + \frac{p^2}{2\kappa}.$$

Here κ denotes the *Bulk modulus*, which indicates how much the material resists against compression.

Since p enters the Lagrangian in a quadratic way, it is no longer a Lagrange multiplier. But we can still use the Euler-Lagrange equations to derive a system of partial differential equations in strong form.

By adding this term, Equation (1.15a) stays unchanged and only the incompressibility condition in Equation (1.15b) changes to

$$0 = (\det(\mathrm{D}\varphi) - 1) - \frac{p}{\kappa} \quad \left(= \frac{\partial \widetilde{\mathcal{L}}}{\partial p} \right). \tag{1.17}$$

Formally, we arrive at an incompressible material for $\kappa \to \infty$. This limit can be made rigorous and is used to prove existence theorems [**MH83**, Chapter 6, Box 5.3].

For small κ, large violation of the incompressibility constraint only induces small changes in pressure. Therefore the induced stress is also small and the material behaves like an unconstrained hyperelastic material.

Like in the incompressible case, the additional equation has no time derivatives and acts like an algebraic constraint. The new term $\frac{p}{\kappa}$ reduces the differential index of the partial differential-algebraic system, since one differentiation with respect to time of Equation (1.17) yields

$$\dot{p} = \kappa \frac{\mathrm{d}}{\mathrm{d}t}(\det(\mathrm{D}\varphi)) = \kappa \operatorname{div}(\dot{\varphi}) \cdot \det(\mathrm{D}\varphi),$$

where we used [**MH83**, Chapter 1, Proposition 5.4] for the second equality. The lower case operator div represents the divergence with respect to the spatial metric $\boldsymbol{g}$.

If we use this equation, the value of $\dot{p}$ is not implicit anymore. Hence the system has differential index 1.

Chapter 2

Physiology and Models of Skeletal Muscle Tissue

> . . . everybody [in my group] is expected to be interested in the *scientific* problem, not the *mathematical* problem per se.
>
> James Sneyd, 2017

In this chapter, we describe in non-mathematical terms the basic mechanism of muscle contraction and introduce the sliding filament theory (sometimes also called Huxley's model).

We have to apologize to the experts in biology, since we mostly stick to brutally simplified vocabulary, in the hope that these are easier to grasp for mathematicians. Therefore we do not talk about A-lines, Z-lines and S1-myomeres, but use longer and less precise terms.

General introductions to the physiology of muscle contraction are given in many standart textbooks on molecular biology, for example [**AJL+14**] and [**GH06**].

An overview for skeletal muscles with an emphasis on the historic development of muscle contraction models can be found in [**Her00**].

Mathematical models for skeletal muscles are described in [**KS09**]. An excellent introduction to the mechanics of motor proteins is given in [**How01**].

My contributions: This chapter is based on the cited literature and publications. My contributions are limited to the choice of the mathematical notations.

A short summary. In a few words, skeletal muscle contraction is initiated by an electric signal from the nervous system, which causes calcium ions to enter the muscle fiber cells. In each muscle cell, actin- and myosin-filaments are aligned parallel to each other and – if not blocked by the absence of calcium – many small bridges between the actin- and myosin-filaments connect and pull the filaments alongside each other together. As a result the muscle cell shortens. After each pull, the bridges disconnect again and may bind again at another binding site.

This cycle is called the cross-bridge cycle.

Molecular motors. The conversion of chemical energy into mechanical energy is the essential function of molecular motors. In our body, most mechanical work is caused by the hydrolysis of adeonsin triphosphate (ATP), an energy rich molecule.

According to the laws of thermodynamics, the conversion of chemical energy into mechanical energy is connected to an increase of entropy, which indicates already, that all molecular motors and in particular skeletal muscle contraction is a non-conservative process.

1. Physiology of Skeletal Muscles

In this section we describe the composition of skeletal muscles at different scales and explain molecular actin-myosin motors work.

1.1. The three types of muscles tissue. Before we drift into details of skeletal muscles, we shortly want to point out their difference from the two other muscles types, which are the *cardiac muscles* of the heart and *smooth muscles*.

Cardiac muscles. Every single heart beat is the result of a complex contraction of cardiac muscle tissue. This specialized muscle has a complicated geometry, which gives rise to complex calcium waves and non-trivial propagation patterns of electric signals.

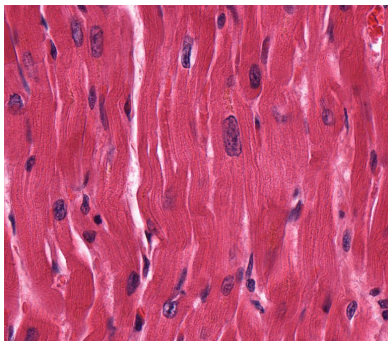

Figure 1. Muscles cells from a heart muscle. These cells are locally straightened but form together a complex network.

Smooth muscles. In contrast to straightened muscles, the contraction of smooth muscle cells is not directed. This causes the complete cell to shrink, which is useful to contract tubes or volumes. For example the arteries and veins of the circulatory system are narrowed by the contraction of the surrounding smooth muscles tissue. The iris and the lens of a human eye are also altered by the contraction of smooth muscles.

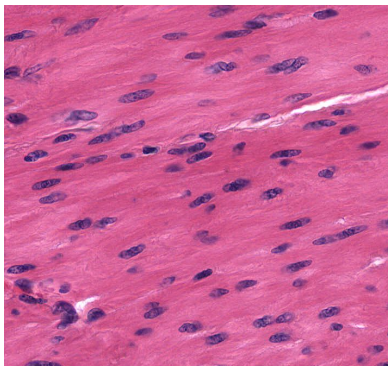

Figure 2. Smooth muscle cells do not just contract in a single direction. Instead, each cell will decrease its volume, which causes the complete muscle to shrink.

Another big difference to skeletal muscles is the ability of smooth muscles to remain in a contracted state, without consuming energy. The cross-bridges of skeletal muscles always detach after each pulling stroke, therefore a permanent contraction can only be achieved by a constant rate of pulling stokes. In contrast, the cross-bridges in smooth muscle cells stay attached after each stroke and hence, no energy, no repeated strokes are required to sustain a contraction.

Skeletal muscles. These muscle cells are also often called straightened muscle cells, since their most characteristic feature are long muscle fibers, which are all straightened into one primary direction.

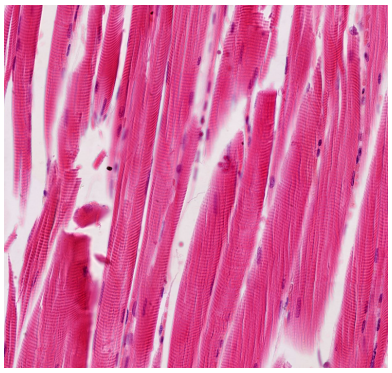

Figure 3. The fibers of skeletal muscles are parallel aligned. The purple dots are the cells nuclei.

1.2. An exploration of skeletal muscles on different scales. We want to explore some cross-sectional images of a skeletal muscle to see the different scales of skeletal muscles in a real example.

Images in this section are taken from the virtual histology laboratory[1], with kind permission from Todd Clark Brelje. We recommend a visit the virtual histology laboratory, where an interactive viewer allows to zoom into high resolution muscle images. The explanations in this section are taken from the virtual histology laboratory as well.

We start with Figure 4, where an overview of the whole muscle is given, and continue into smaller scales, until we reach the level of single sarcomeres in Figure 12. In this thesis, we will focus on the modeling of sarcomeres, which are the contractible units in skeletal muscle cells.

[1] `histologyguide.com`

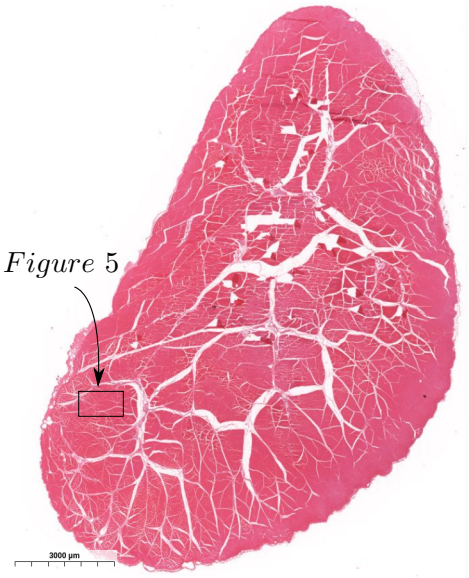

Figure 4. Cross-section of a skeletal muscle. (MHS 262 Skeletal Muscle)

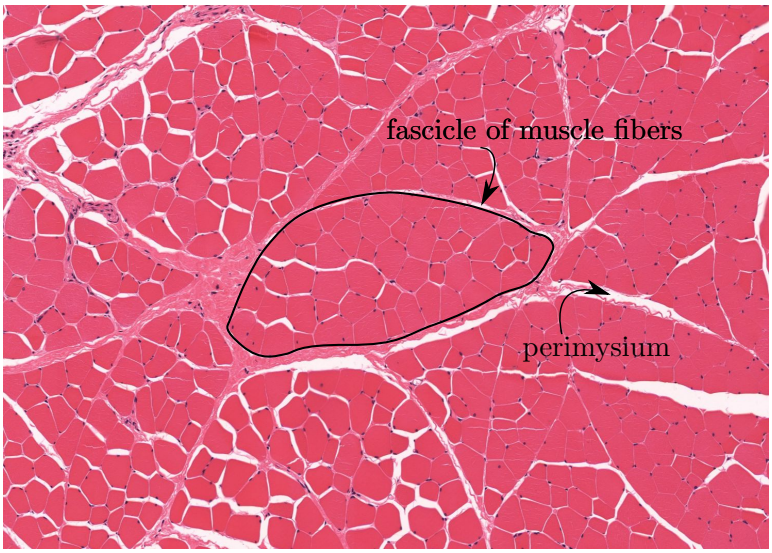

Figure 5. *Perimysium*, a connective tissue, surrounds each fascicle of the muscle fibers.

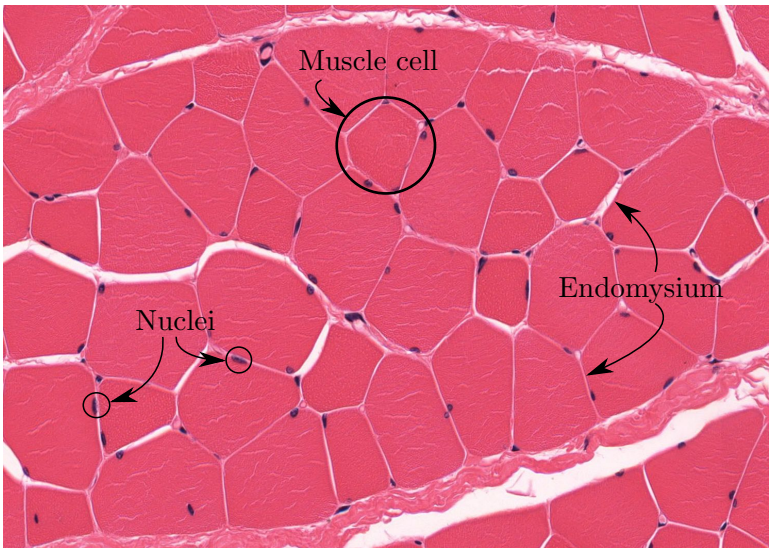

Figure 6. Individual muscle fibers are separated by *endomysium*. The area in between also contains many *nuclei* and blood supplying capillaries at the corner of muscle fibers. (MHS 262 Skeletal Muscle)

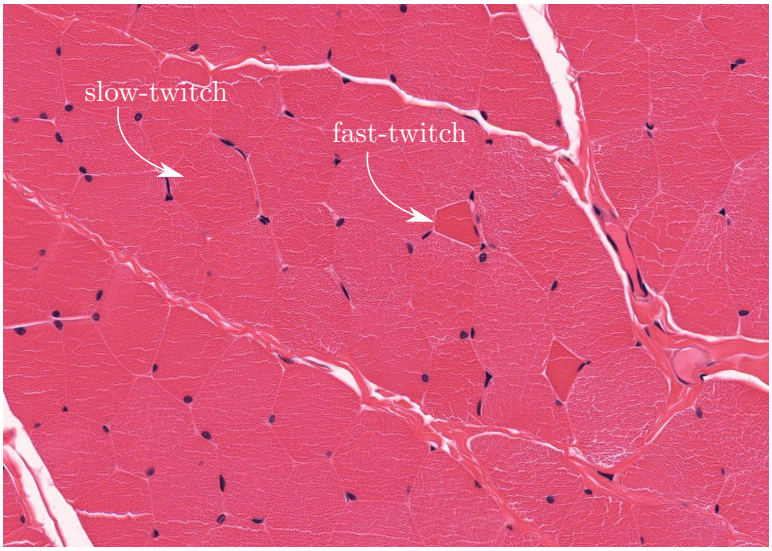

Figure 7. There are two main types of muscle fibers: slow-twitch and fast-twitch muscle fibers. The few fast-twitch muscle fibers in this image are thinner and darker than the many slow-twitch fibers. (MHS 262 Skeletal Muscle)

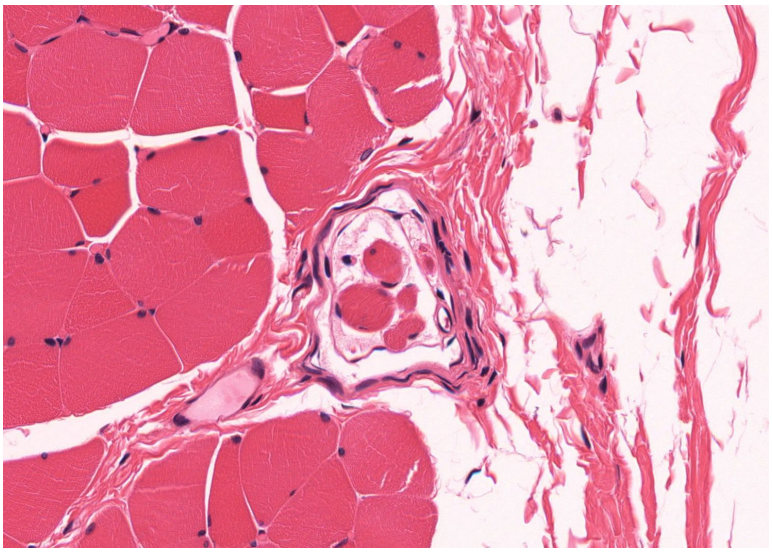

Figure 8. The curly structure in the center is a *muscle spindle*. These cells sensor the muscle contraction. (MHS 262 Skeletal Muscle)

Figure 9. Each muscle cell contains a bundle of myofibrils. These myofibrils consist out of parallely aligned *actin filaments* and *myosin filaments*. (MH 055a Skeletal Muscle)

Figure 10. A single muscle fiber from a longitudinal view. The small sarcomeres are already slightly indicated at this scale by striation around the muscle fiber.

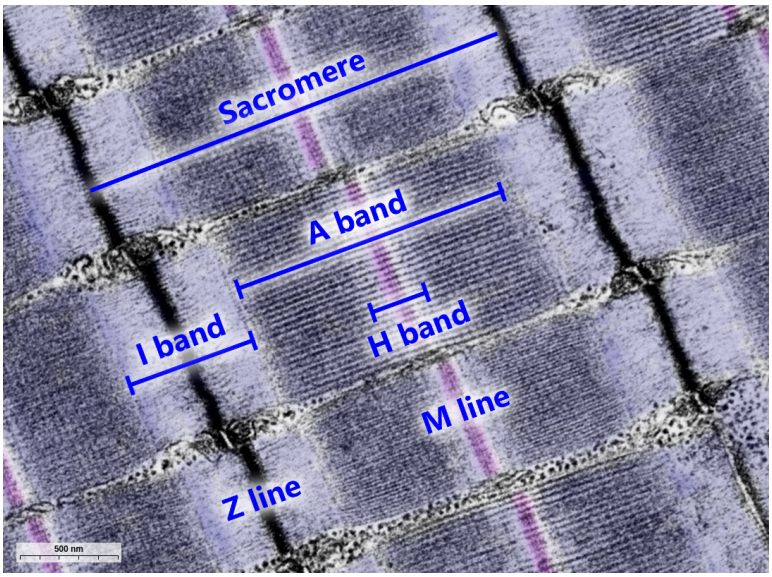

Figure 11. The smallest sub-units of skeletal muscle cells are *sarcomeres*. The myosin filaments are the black lines in the A band. The actin filaments are thinner and start from the Z line.

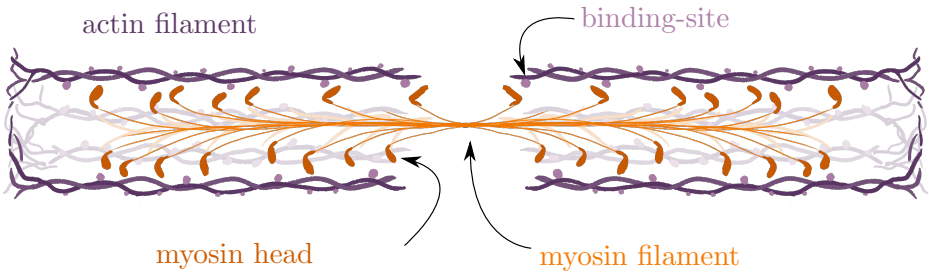

Figure 12. An idealized sketch of a single myosin filament from a sarcomere like in Figure 11.

1.3. The cross-bridge cycle. We use a common breakdown of the process into four steps, this approach can be found in [**KS09**, Section 15.1]. The cross-bridge cycle is visualized in Figure 13.

- **Chucking the myosin heads:** Unbound myosin heads can bind and hydrolyze an ATP molecule, which causes a configurational change of the myosin head. This step might be compared with the chucking of a spring, since energy is used to cause this configurational state. In this state the relaxation requires to pass an energy barrier, which causes the molecule to stay in a local equilibrium configuration.
- **Attachment:** Chucked myosin heads can bind to unblocked binding sites on the actin filament. This process is quite fast, since it allows the myosin head to change into a preferable configuration, where it is bound to the actin filament. We will usually call an attached myosin head a *cross-bridge*, since it connects the myosin filament and the actin filament.
- **Power stroke:** The attachment also causes a configurational change of the myosin head. Now, a relaxed configuration is reachable without an energy barrier in between, which induces a pulling force between the myosin filament and the actin filament.
- **Clean-up:** The mechanical work is done but the most time consuming step of the cross-bridge cycle is not done yet. The remaining ADP molecule and other left overs have to unbind from the myosin head.

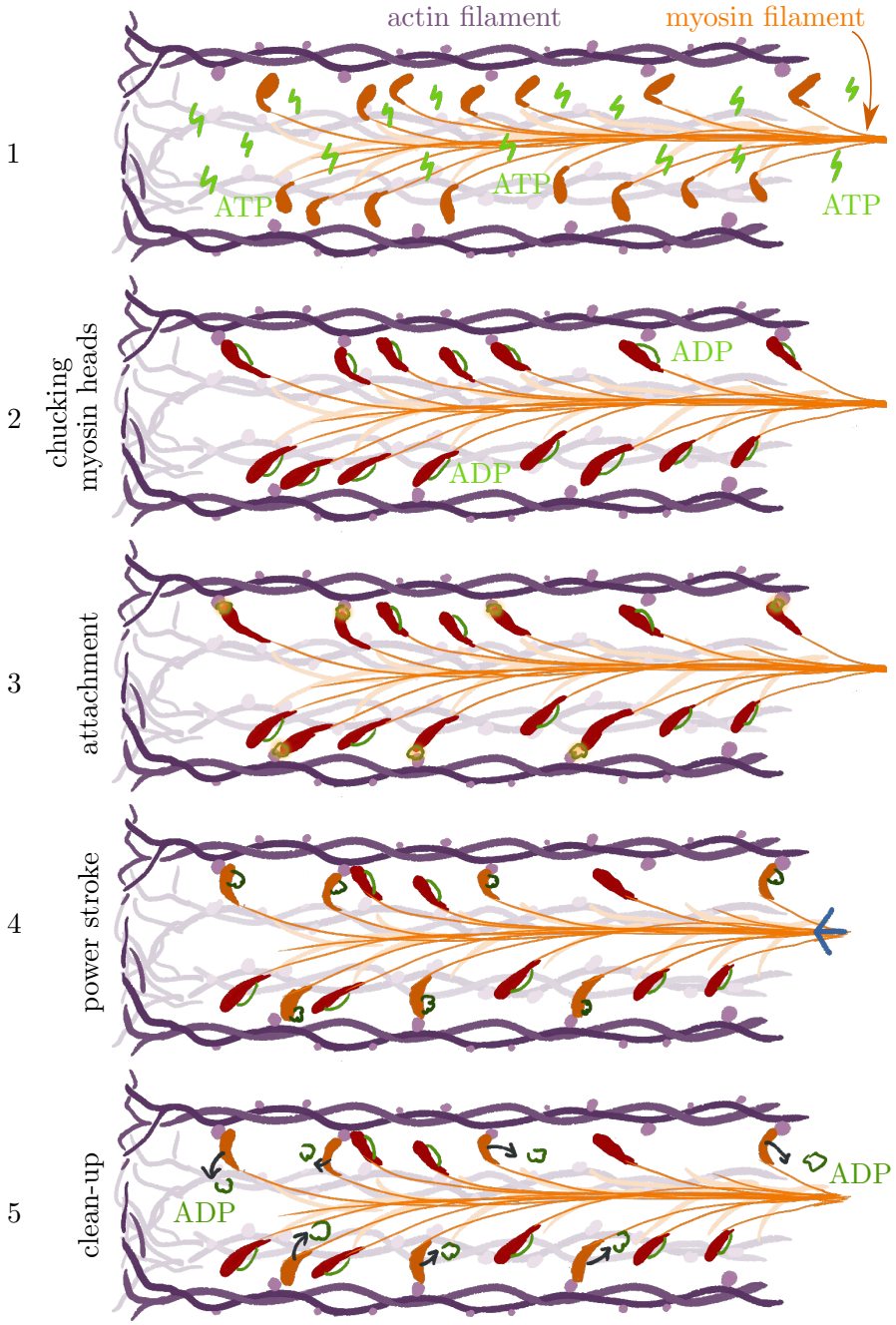

Figure 13. A very, very simplified sketch of the cross-bridge cycle.

2. Control of the Cross-Bridge Cycle

The cross-bridge cycle in skeletal muscle cells only takes place, if unblocked binding sites exist.

If no calcium ions are present next to the actin filaments, then the binding sites will be blocked by a troponin complex, which prevents chucked myosin heads to attach. This mechanism is used to control the number of cross-bridge cycles.

Compartment 2.1 (Sarcoplasma)**.** The fluid inside muscle cells is called Sarcoplasma. The actin filaments and myosin filaments are surrounded by the sarcoplasma.

Compartment 2.2 (Sarcoplasmic reticulum)**.** The sarcoplasmic reticulum stores calcium ions. In general, the calcium ion concentration inside the sarcoplasma is kept very low, such that a small increase of calcium diffuses rapidly throughout the cell. This allows calcium ions to act as a so called *second messenger*, which is used to deliver signals inside the cell to their recipient.

- **Electrical signaling:** Nerves and so called T-tubes allow controlled propagation of electrical signals throughout the muscle cell. Not every single muscle fiber is controlled individually, instead the nerves are attached to fiber bundles, which are controlled simultaneously.
- **Release of calcium ions:** If an electrical signal reaches a muscle cell, a complex cellular mechanism causes the release of calcium ion channels from the sarcoplasmic reticulum (SR) into the sarcoplasma, i.e. into the fluid compartment, which surrounds in particular the actin filaments.
  The spread of calcium ions is driven by diffusion, which is a fast process, if and only if the concentration in the sarcoplasma was initially very low.
- **Unblocking:** Two calcium ions can bind to one blocking troponin complex, which causes a change in the configuration of the troponin complex such that the binding sites are able to connect with chucked myosin heads. In this way the calcium ions initiate the cross-bridge cycling.
- **Clean-up:** Again, a crucial step is the return into the initial state. This step is highly energy consuming, since all calcium ions need to be pumped back into the sarcoplasmic reticulum.

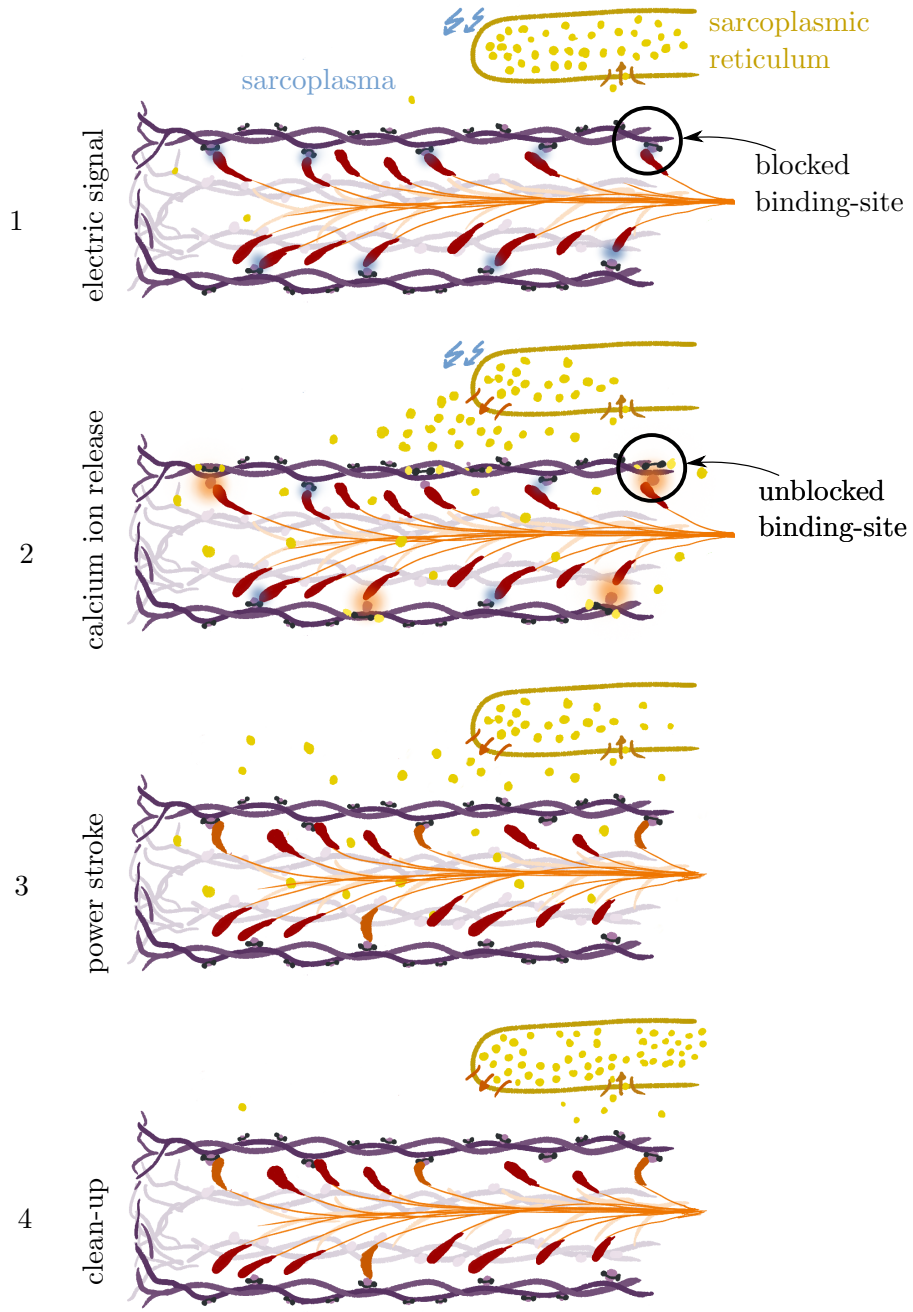

Figure 14. The cross-bridge cycle only takes place, if the calcium ions diffuse into the sarcoplasma and bind with the troponin complex at the binding-sites.

Remark 2.3 (The role of calcium dynamics in skeletal muscle cells)**.** Initially, this thesis was intended to focus around the role of calcium waves in skeletal muscle cells. But since nature does not follow a mathematicians wishes, wave propagation in skeletal muscle cells seems to be less essential than in other types of muscles [**DFKS16**, Section 7.3]. The propagation of calcium in skeletal muscles is mostly restricted to one dimensional muscle fibers. If the calcium ions are buffered inside the sarcoplasmic reticulum, they bind with other molecules, which prevents more complicated and fast dynamics of buffered calcium.

Remark 2.4 (Control in other muscle cells)**.** The control mechanisms in cardiac and smooth muscles differ a lot from the described control in skeletal muscle cells.

Cardiac muscles have a complex geometry, in which electrical signals and calcium ions propagate in complex patterns. This is essential for the function of our heart muscles. But like in skeletal muscle cells, the release of calcium ions unblocks the cross-bridge cycling.

In smooth muscle cells, the cross-bridge cycle takes place during the absence of calcium. But cross-bridges also stay attached by default after the power stroke.

3. Mathematical Models for Muscle Contraction

3.1. Hill's Model for Muscle Contraction. One of the first quantitative models for muscle contraction was due to Archibald Hill, who proposed to model a skeletal muscle as a combination of an contractible and a elastic element.

The dynamics of a muscle are determined by a force-velocity relation, which predicts the generated force of a muscle cell depending on the current contraction and the contraction velocity of the muscle.

The model fails to predict the reaction of a muscle to fast spontaneous contraction and other extreme events, but due to its simplicity, it is still very popular and useful. We will not go into details here and directly describe a more advanced model, which is based on physiological principles.

3.2. Huxley's Two State Model for Cross-Bridges. In this section we derive a model for the density of bound and unbound myosin heads. Before we derive the dynamics for these densities, we collect a few questions to answer why we are interested in the densities of attached cross-bridges. In fact, we are mostly interested in the moments of the cross-bridge density.

The first moments of the cross-bridge density.

Remark 2.5 (How strong is the generated force?)**.** If a myosin head is bound to an actin binding site, we assume it to act like a linear spring, which generates a force given by Hook's law

$$F_{\text{single}} = -\kappa \cdot (q - q_{\text{eq}}).$$

For simplicity we choose the equilibrium to be $q_{\text{eq}} := 0$.

Let $\rho_{\text{xb}}(q)$ denotes the density of bound myosin heads with displacement q. [2] We can compute the total force by summing up all individual contributions

$$F_{total} = -\kappa \int_{\mathbb{R}} q \cdot \rho_{\text{xb}}(q)\,\mathrm{d}q = -\kappa \cdot Q_1.$$

It is important to realize, that this quantity only depends on the first moment Q_1 of the density ρ_{xb}.

Remark 2.6 (How stiff are the connected filaments?)**.** If we change the relative position of the filaments instantaneously by a certain length h, the

[2] "xb" is a shortcut for cross-bridge.

displacement of each cross-bridge will also change by this quantity. We can compute the change of the total force as

$$F_{\text{new}} = -\kappa \int_{\mathbb{R}} (q+h) \cdot \rho_{\text{xb}}(q)\,\mathrm{d}q = F_{\text{old}} - hq\kappa \int_{\mathbb{R}} \rho_{\text{xb}}(q)\,\mathrm{d}q$$
$$= F_{\text{old}} - \kappa h Q_0.$$

Thus, the stiffness is given by

$$\text{Tension} = \kappa Q_0.$$

Again, the quantity of interest is just the zero-th moment Q_0 of the cross-bridge density ρ_{xb}.

Remark 2.7 (Energy of the cross-bridges)**.** The total energy of a single myosin head is

$$E_{\text{single}} = \frac{m}{2}\dot{q}_2 + \frac{1}{2}\kappa q^2,$$

where m denotes the mass of a myosin head.

Since all cross-bridges are attached to the same actin filament, their velocities are all equal. We denote the common velocity by v_f. Summation yields the total energy for a collection of cross-bridges

$$E_{\text{total}} = \frac{1}{2}\int_{\mathbb{R}} (m v_f^2 + \kappa q^2)\rho_{\text{xb}}(q)\,\mathrm{d}q.$$

The mass of a single myosin head m is negligibly small.

Time Dynamics of cross-bridge Densities.

We model the transition of an unbound myosin head at displacement q to a bound cross-bridge to occur with probability $f(q)$. The reverse transition probability is denoted by $g(q)$. In other words, the transition behaves like a chemical reaction

$$U \underset{g(q)}{\overset{f(q)}{\rightleftarrows}} B.$$

In fact, the transition probabilities can be derived by thermodynamic principle [**MZ91**].

Remark 2.8 (Modeling of calcium control)**.** The attachment of myosin heads to actin binding-sites is only possible in the presence of calcium ions.

To model this effect, it is common to use an activation function $r([\mathrm{Ca}^{2+}])$, which depends on the current calcium concentration. The modified transition probabilities are then given by

$$U \underset{r([\mathrm{Ca}^{2+}])g(q)}{\overset{r([\mathrm{Ca}^{2+}])f(q)}{\rightleftarrows}} B.$$

Remark 2.9 (Overlapping actin filaments)**.** For strong contraction of the sarcomeres, the actin filaments might overlap, which reduces the number of usable binding-sites. Conversely, a strong extension reduces the overlap of the actin filament with the myosin filaments, and therefore the number of reachable binding-sites also reduces. Hence, it is reasonable to let the transition probabilities also depend on the fiber stretch q_f, i.e.

$$U \underset{r([\mathrm{Ca}^{2+}])g(q;\, q_f)}{\overset{r([\mathrm{Ca}^{2+}])f(q;\, q_f)}{\rightleftarrows}} B.$$

Remark 2.10 (Lagrangian vs. Eulerian viewpoint)**.** For a given sliding velocity v_f the displacements of all myosin heads will be transported in the direction of v_f.

If we use the coordinates

$$\widetilde{q} := q_f + q,$$

a fixed coordinate $\widetilde{q}$ would correspond to the trajectory of an individual myosin head, which is the Lagrangian viewpoint.

But we will continue to use q as a primary variable, which corresponds to the Eulerian description.

In particular, we have to use the material derivative

$$\frac{\mathrm{D}\rho_{\mathrm{xb}}}{\mathrm{D}t} = \frac{\partial \rho_{\mathrm{xb}}}{\partial t} + v_f \frac{\partial \rho_{\mathrm{xb}}}{\partial q},$$

when we model the attachment and detachment of myosin heads as a reaction equation.

Model 2.11 (Two State Cross-Bridge Model)**.** For given filament sliding velocity v_f, length q_f and transition probabilities as in Remark 2.9, the densities of unbound myosin heads $\rho_{\mathrm{xb}}(q,t)$ and bound cross-bridges $\rho_{\mathrm{xb}}(q,t)$ are governed by the transport reaction equation

$$\frac{\mathrm{D}\rho_{\mathrm{xb}}}{\mathrm{D}t} = \frac{\partial \rho_{\mathrm{xb}}}{\partial t} + v_f \cdot \frac{\partial \rho_{\mathrm{xb}}}{\partial q} = f \cdot (1 - \rho_{\mathrm{xb}}) - g \cdot \rho_{\mathrm{xb}}. \tag{2.1}$$

The calcium dependency is included in the transition probability functions f and g.

An important and nontrivial challenge is to find appropriate transition probabilities. Since the model is just a rough approximation of the real cross-bridge cycles, we can not assume to derive these probabilities directly from biochemical principles.

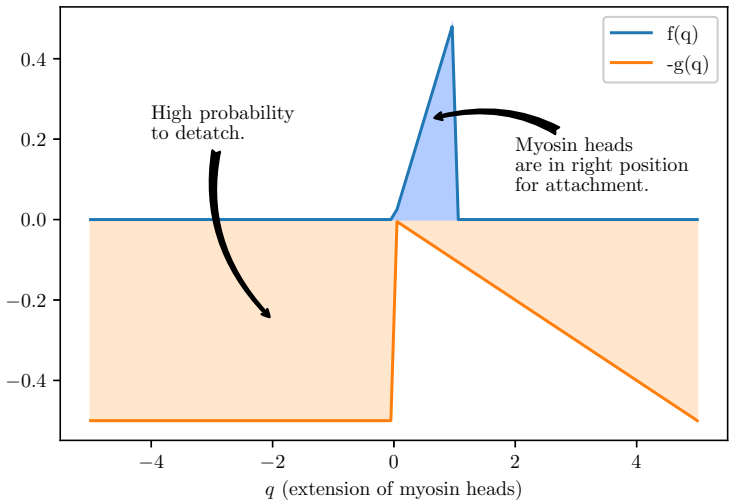

Figure 15. Simplified transition probabilities. The q-axis is nondimensional, such that $q = 1$ corresponds to the maximal extension of a myosin head.

Remark 2.12 (Simple transition probabilities)**.** Within this thesis, we will only consider transition probailities of the form

$$f(q) = \begin{cases} 0, & \text{for } q < 0, \\ f_1 \cdot q, & \text{for } 0 < q < 1, \\ 0, & \text{for } 1 < q, \end{cases} \tag{2.2}$$

and

$$q(q) = \begin{cases} g_2, & \text{for } q < 0, \\ g_1 \cdot q, & \text{for } q > 0. \end{cases} \tag{2.3}$$

Realistic values can be found in [**Zah81**, page 98], which are plotted in Figure 16.

Remark 2.13 (Energy consumption)**.** In Remark 2.7 we have already computed the total energy of all cross-bridges. We see that the creation of a cross-bridge increases the energy of the system and detachment of a cross-bridge decreases the energy of the system.

Example 2.14 (Quasi-steady states)**.** For a simple form of the transition probabilities, it is simple to compute the quasi-steady states of the two state model.

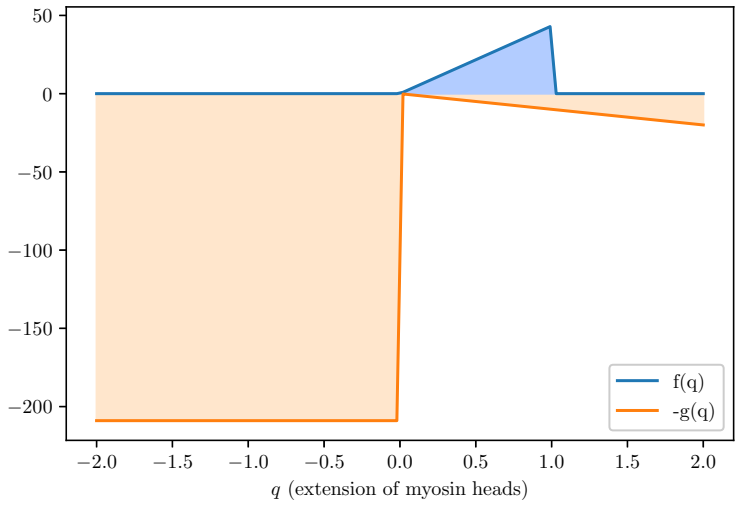

Figure 16. Transition probability function, taken from [**Zah81**, page 98].

Quasi-steady states are solutions of the two state model, with constant density function, i.e.

$$\frac{\partial \rho_{\mathrm{xb}}}{\partial t} = 0.$$

Nonetheless, the cross-bridge cycling does not stop in a quasi-steady state.

For a constant contraction velocity $v < 0$ and transition probabilities as in Remark 2.12, it is easy to compute the exact solution

$$\rho_{\mathrm{xb}}(q) = \begin{cases} F_1(1 - \mathrm{e}^{-\frac{\phi}{v}})\mathrm{e}^{\frac{q}{2}G_2\frac{\phi}{v}}, & \text{for } q < 0, \\ F_1\left(1 - \mathrm{e}^{\frac{\phi}{v}(q^2-1)}\right), & \text{for } 0 < q < 1, \\ 0, & \text{else,} \end{cases}$$

where we used the variables $\phi = \frac{h}{2}(f_1 + g_1)$, $F_1 = \frac{f_1}{f_1+g_1}$ and $G_2 = \frac{g_2}{f_1+g_2}$ [**KS09**].

Despite the many parameters, this solution is still intuitive, since it captures that attached cross-bridges will get transported in the contraction direction, which is the reason why the peak of the distribution is at $q = 0$. For negative displacement, the quasi-steady state density of cross-bridges decays exponentially, which is no surprise, since the detach probability function is a constant $g(q) = g_2$ for negative extensions $q < 0$.

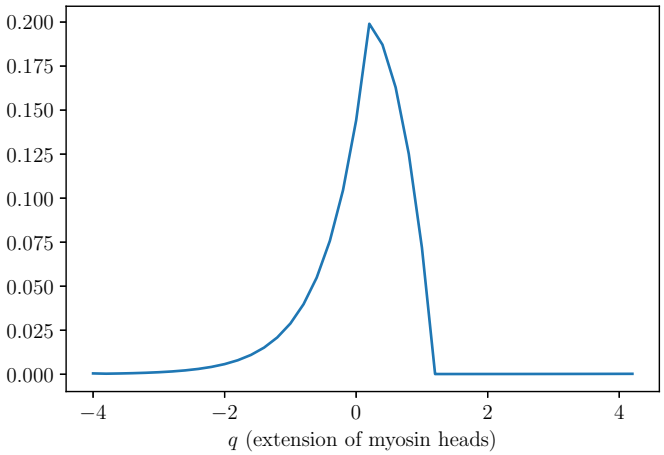

Figure 17. A typical quasi-steady state during a contraction of the muscle. Cross-bridges will still attach, shorten and detach, but without changing the distribution of cross-bridge extensions.

4. A Popular Method: The Distributed Moment Approximation

In the context of macro-scale simulations, the numerical solution of the transport equation Equation (2.1) in each point $X \in \mathcal{B}$ of the skeletal muscle would be computational demanding. A method developed in [**Zah81**] avoids this drawback and allows a reduction to a system of ODE.

The key motivation behind this approximation is the idea, that we are not interested in the actual densities, but just their moments.

We may assume that all densities are of the simple form of a scaled normal distribution with moments $Q_0(t), Q_1(t)$ and $Q_2(t)$. For simplicity we define $\sigma^2(t) = Q_2(t) - Q_1^2(t)$, moreover we only consider the bound density for a moment, which is now given by

$$\rho_{\mathrm{xb}}(q,t) = Q_0(t) \cdot \frac{1}{\sqrt{2\pi\sigma^2(t)}} \cdot \exp\left(-\frac{(q - Q_1(t))^2}{2\sigma^2(t)}\right).$$

We now let the moments depend on time and aim at finding their time dynamics. Inserting the scaled normal distribution into the two state model (Model 2.11) yields equations for the moments.

Model 2.15 (Distributed Moment Method)**.** The first three moments $\boldsymbol{Q} = (Q_0, Q_1, Q_2)^T$ of a normal distributed density μ_b are approximated as solutions of the differential equation

$$\begin{aligned}\dot{Q}_0 &= b_0 - F_0(\boldsymbol{Q}),\\ \dot{Q}_1 &= b_1 - F_1(\boldsymbol{Q}) - v_f Q_0,\\ \dot{Q}_2 &= b_2 - F_2(\boldsymbol{Q}) - 2v_f Q_1.\end{aligned}$$

The additional functions b_i and F_i are defined for as

$$\begin{aligned}b_k &= \int q^k f(q)\,\mathrm{d}q,\\ F_k &= \int q^k \left(f(q) - g(q)\right)\rho_{\mathrm{xb}}(q)\,\mathrm{d}q.\end{aligned}$$

It is important to notice, that the exact evaluation of F_k and b_k is possible, if f and g are piecewise polynomial functions, since then the result is a combination of polynomials and moments of the normal distribution. Explicit expressions can be found in the appendix of [**Zah81**].

Remark 2.16 (Non consistency of the distributed moment method)**.** If the transition probabilities f, g do not vanish, then the exact solutions will not stay normal distributed. An important case for not normal distributed solutions of the two state model are the quasi-steady states.

The inconsistency was already known during the development of this method, but its efficiency and the good conservative properties of moment methods are the reason, why this method is still very popular and useful. The dynamics which are generated by the model capture many essential features of the exact solutions. And since the parameters and the choice of the transition probabilities are already a rough approximation, it is reasonable to choose parameters, just in a way to optimize the solutions of the distributed moment method to be close to the real data.

Vice versa, parameters in publications using the distributed moment method are maybe not optimal parameters for a consistently approximated two state model.

In Figure 18 and Figure 19, the difference between the distributed moment method and a consistent upwind discretisation of the two state model are plotted. The transition probabilities are exactly as in Figure 16. The upwind solution converges against the exact solution and time integration for both models was done using the solver *lsoda* from the FORTRAN library *odepack* with sufficiently small time steps.

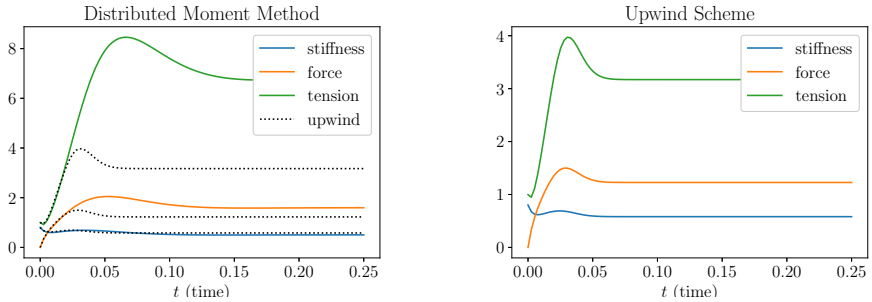

Figure 18. Simulation results for the first three moments of the two state model with constant extension velocity $v_f = 100$. Since the cross-bridges are transported again the contraction direction, the resulting force is larger, until an equilibrium of cross-bridge attachment and detachment is obtained.

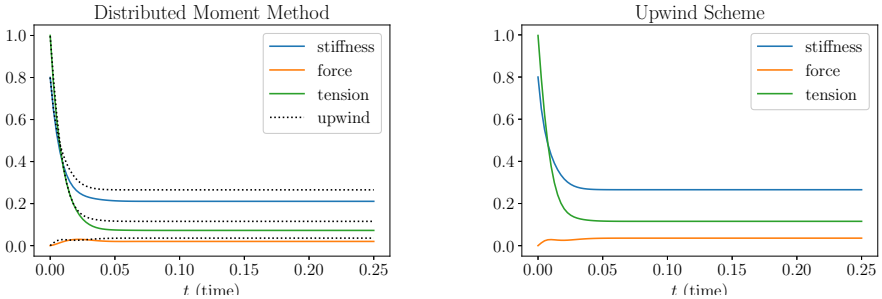

Figure 19. For a contraction with velocity $v = -100$, the quasi-steady state is reached faster. The equilibrium points of the distributed moment method and the exact system differ, since the quasi-steady states are not normal distributed.

Remark 2.17 (Many states models)**.** As usual in biological modelling, the reality is far more complex than computational models. Myosin heads are complex molecules and their dynamics is highly nonlinear. Besides biochemical models, also more complex cross-bridge models have been developed. These models extend the two state model by adding additional states like half strained or fully strained attached myosin heads or different states of the troponin complex [**HKR$^+$16**], [**HR14**], [**Zah97**].

Remark 2.18 (Non-axial models)**.** A typical characteristic of continuum mechanics of solids is the possibility of shear deformations. These deformations break various assumed symmetries of the cross-bridge model. An example is shown in Figure 20.

With a view on multi-scale models, an interesting extension to non-axial models has also been developed, for example in [**Zah96**]. The idea is to consider also shear deformations and their effect on filament arrangement,

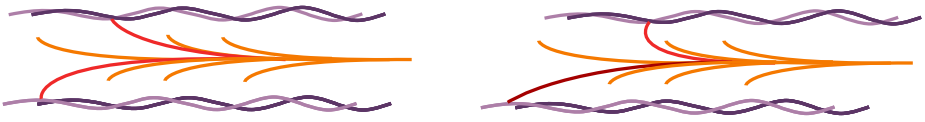

Figure 20. Shear deformations break the mirror symmetry of the parallel filaments. Shearing causes different changes of attached myosin head extensions, therefore a single contraction velocity has to be replaced by more complicated terms of the deformation rate tensor.

this leads to a more complicated expression for the material derivative. A simple example is sketched in Figure 20. The authors conclude, that non-contractable proteins may play a significant role in muscle mechanics by equilibrating unsymmetrical active stresses [**Zah96**].

Remark 2.19 (Maximal shortening velocity)**.** For some velocity the amount of newly attached myosin heads with positive displacement $x > 0$ equals the amount of those with negative displacement $x < 0$, hence no force is generated. This effect is seen in practice [**KS09**, Section 15.3].

5. Hyperelastic Models for Skeletal Muscle Tissue

The principle idea in most models, is a split of the stress into active and passive terms, i.e.

$$\boldsymbol{S} = \boldsymbol{S}_{\text{active}} + \boldsymbol{S}_{\text{passive}}.$$

Here it is useful to work with the second Piola-Kirchhoff stress tensor $\boldsymbol{S}(\boldsymbol{C}) = \boldsymbol{F}^{-T}\boldsymbol{P}(\boldsymbol{C}) : T^*\mathcal{B} \to T^*\mathcal{B}$, which is the pull-back of $\boldsymbol{P}$ onto material coordinates.

We will collect models for both parts of the stress. Since the action stress causes a contraction of the fibers, it is useful to define a model for muscle fibers, which is suited for hyperelasticity.

5.1. Geometry of Muscle Fibers.

Definition 2.20 (Line fields [**Lee13**, chapter 19] and fiber distributions)**.** A *line field on* $\mathcal{B}$ (or *distribution of rank* 1) is a rank-1 subbunde of $T\mathcal{B}$.

We will choose a normalized vectorfield

$$\boldsymbol{N}_f : \mathcal{B} \to T\mathcal{B}, \quad \text{with } \left\|\boldsymbol{N}_f\right\|^2_{T\mathcal{B}} = 1,$$

to define a line field $\operatorname{span}(\boldsymbol{N}_f) \subseteq T\mathcal{B}$, which describes the direction of the muscle fibers in the material space $\mathcal{B}$.

We will call $\boldsymbol{N}_f$ the *fiber distribution*.[3]

We denote the push-forward of vector field $\boldsymbol{N}_f$ into the spatial space by a lower case letter, i.e.

$$\boldsymbol{n}_f := \boldsymbol{F}\,\boldsymbol{N}_f : \mathcal{B} \to T\mathcal{S}.$$

(This vector field represents the spatial direction and the actual stretch of the fibers. It is not normalized.)

Remark 2.21 (Stretching of fibers)**.** We can use the deformation gradient $\boldsymbol{F}$ or the right Cauchy-Green tensor $\boldsymbol{C}$ to calculate the stretch in fiber direction. In the general case, with a Riemannian metric $\boldsymbol{G}$ on the material space $\mathcal{B}$ and $\boldsymbol{g}$ on the spatial space $\mathcal{S}$, the square of the stretching in fiber direction is given as

$$\left\|\boldsymbol{n}_f\right\|^2_{T\mathcal{S}} = \boldsymbol{g}(\boldsymbol{F}\,\boldsymbol{N}_f, \boldsymbol{F}\,\boldsymbol{N}_f) = \boldsymbol{G}(\boldsymbol{N}_f, \boldsymbol{F}^T\boldsymbol{F}\,\boldsymbol{N}_f).$$

The musical isomorphism $\flat$, which is defined via $\boldsymbol{N}_f^\flat := \boldsymbol{G}(\boldsymbol{N}_f, \cdot)$, suggests the following notation for the squared stretch in fiber direction

$$\boldsymbol{N}_f^\flat \otimes \boldsymbol{N}_f(\boldsymbol{C}) = \boldsymbol{G}(\boldsymbol{N}_f, \boldsymbol{C}\,\boldsymbol{N}_f).$$

This value is always positive and the stretch in fiber direction is well defined as

$$\sqrt{\boldsymbol{N}_f^\flat \otimes \boldsymbol{N}_f(\boldsymbol{C})}.$$

(A negative stretch is not possible, since the deformation has to preserve the orientation.)

In cartesian coordiantes, with trivial metric tensor $\boldsymbol{G} = \boldsymbol{I}$, we can use the simple formula

$$\sqrt{\boldsymbol{N}_f^T\boldsymbol{C}\,\boldsymbol{N}_f}.$$

Definition 2.22 (Fiber stretch and deformation rate)**.** We define the *fiber stretch* as

$$q_f := q_f(\boldsymbol{C}) := \sqrt{\boldsymbol{N}_f^\flat \otimes \boldsymbol{N}_f(\boldsymbol{C})},$$

we will often neglect the dependency on $\boldsymbol{C}$.

The *fiber deformation velocity* is defined as

$$v_f := \dot{q}_f = \frac{1}{2q_f}\boldsymbol{N}_f^T \otimes \boldsymbol{N}_f^T(\boldsymbol{F}^T\dot{\boldsymbol{F}} + \dot{\boldsymbol{F}}^T\boldsymbol{F}).$$

Sometimes the notation $I_4 := q_f^2$ is used, since I_4 is similar to an invariant of the deformation tensor.

[3] Strictly speaking, the distribution of rank 1 is given by $\operatorname{span}(\boldsymbol{N}_f) \subseteq T\mathcal{B}$ and $\boldsymbol{N}_f$ is only a global frame of the distribution. But the difference is not essential for us.

Remark 2.23 (A simple construction of fiber distributions)**.** With no data at hand, we can only guess a reasonable fiber distribution.

A common trick to generate a line field between two poles, is to use a gradient field of a harmonic potential u, which solves the Laplace equation

$$\begin{cases} \Delta u & = 0, \quad \text{in } \mathcal{B}, \\ u & = 1, \quad \text{on } \partial_{\text{top}}\mathcal{B}, \\ u & = 0, \quad \text{on } \partial_{\text{bottom}}\mathcal{B}, \\ \nabla u \cdot \boldsymbol{N} & = 0, \quad \text{on } \partial_N \mathcal{B}. \end{cases} \tag{2.4}$$

We then define the fiber distribution as the normalized gradient field of u, i.e.

$$\boldsymbol{N}_f := \frac{1}{\|\nabla u\|} \nabla u.$$

Within this thesis, we always use either a upward pointing fiber distribution or a choice like above to define the fiber distribution. But this choice may not even be topologically equivalent to real muscle fiber distributions.

5.2. Passive Material Laws. Various publications suggest the use of the Mooney-Rivlin material law from Remark 1.23 to model skeletal muscle tissue. We have used the parameters from [**HR14**, Table 2].

To model the influence of fibers to an Mooney-Rivlin material, anisotropic stress contributions are also used in skeletal muscle models, which can be found for example in [**HR14**, Section 2.1.1.].

5.3. Active Material Laws. The active stress term accounts for the contraction mechanism of the muscle. Its essential part is always a stress term, which acts tangential to the muscles fiber distribution.

The contraction strength should be independent from the current deformation of the muscle tissue. The term $\boldsymbol{n}_f = \boldsymbol{F}\,\boldsymbol{N}_f$ is not normalized in the spatial space and we need to scale the tensor $\boldsymbol{N}_f \otimes \boldsymbol{N}_f$ by the current fiber stretch q_f. This scaling leads to the correct stress terms.

Model 2.24 (Active contraction stress)**.** For a given scalar field

$$p_{\text{act}} : \mathcal{B} \to [0, 1]\,,$$

the contraction stress in fiber direction is modelled by the strain energy

$$W_{\text{active}}(\boldsymbol{C}) := p_{\text{act}} \sqrt{\boldsymbol{N}_f^\flat \otimes \boldsymbol{N}_f(\boldsymbol{C})}.$$

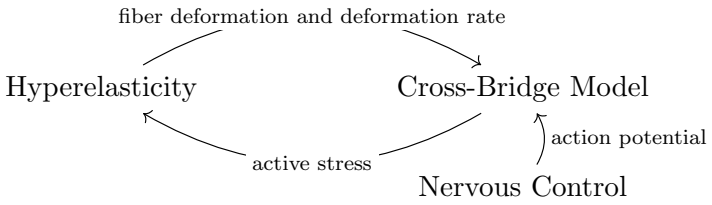

Figure 21. Interaction between the macroscopic model of hyperelasticity and the microscopic model.

The field p_{act} models the current contraction force. In case of a two state model, it would be the summation of the force generated by the myosin heads, i.e.

$$p_{\text{act}} = -\kappa \int_{\mathbb{R}} \mu_b(q) q \, \mathrm{d}q. \tag{2.5}$$

The corresponding active stress is given by

$$\boldsymbol{S}_{\text{active}}(\boldsymbol{C}) = \frac{p_{\text{act}}}{q_f(\boldsymbol{C})} \boldsymbol{N}_f^\flat \otimes \boldsymbol{N}_f.$$

More active stress terms are also reasonable and considered in recent publications. An interesting new level of detail was achieved in [**HKR**$^+$**17**], where the influence of small actin-titin strings is modeled as well. These strings are not purely elastic, but their attachment and length depends on the history of calcium ion concentration within the muscle.

5.4. (Quasi-)incompressibility of skeletal muscle tissue.
It is widely agreed, that skeletal muscle tissues are almost incompressible [**HR13**], [**SSP09**], [**BR08**], since a large portion of its volume consists of water (i.e. sacroplasma and extracellular matrix fluid). In most models we will consider the incompressibility to be already included in the passive material law.

5.5. Summary. In Figure 21 the interaction between the macro-scale model and the micro-scale model are visualized. The resulting model is stated in Model 2.25.

In most recent publications, the two state model is either simulated by the distributed moment (Model 2.15) [**BR08**] or the cross-bride model is used to derive relations between deformation, contraction velocity and generated forces [**HR13**].

Model 2.25 (Coupled model between hyperelasticity and two state model)**.** We model a skeletal muscle tissue as a hyperelastic body (Model 1.18)

$$\rho\ddot{\varphi} = \boldsymbol{b} + \operatorname{Div}(\boldsymbol{P}_{\text{passive}} + p\boldsymbol{G} + \boldsymbol{P}_{\text{active}}), \tag{2.6}$$

$$\det(\mathrm{D}\varphi)\ -1 - \frac{p}{\kappa}\ = 0, \tag{2.7}$$

(2.8)

with the Mooney-Rivlin material law from Remark 1.23 for the passive stress component and an additional (quasi-)incompressibility constraint g as in Model 1.38 or Equation (1.17).

On each material point $X \in \mathcal{B}$, the cross-bridge dynamics are modeled by

$$\frac{\partial \rho_{\text{xb}}}{\partial t} + \dot{q}_f \frac{\partial \rho_{\text{xb}}}{\partial q} = f(1 - \rho_{\text{xb}}) - g\rho_{xb}. \tag{2.9}$$

The transition probabilities f and g possibly depend on the fiber stretch q_f and the calcium ion concentration $[\mathrm{Ca}^{2+}]$.

With

$$\boldsymbol{P}_{\text{passive}} = \frac{\partial \mathcal{W}_{\text{passive}}}{\partial\, \mathrm{D}\varphi}, \quad \boldsymbol{P}_{\text{active}} = \frac{\partial \mathcal{W}_{\text{active}}}{\partial\, \mathrm{D}\varphi},$$

where the active strain energy is

$$\mathcal{W}_{\text{active}} := p_{\text{act}} q_f. \tag{2.10}$$

The activation p_{act} is defined by Equation (2.5).

Chapter 3

A Lagrangian Perspective on Cross-Bridge Theory

In this chapter, we present a field theoretic perspective on cross-bridge theory and identify an underlying Lagrangian system. The transport equation for the cross-bridge density will be derived as a Liouville equation of a constrained system.

However, attachment and detachment of cross-bridges breaks the Lagrangian structure.

My contributions: This chapter contains my own work. Up to my knowledge, the relation between cross-bridge theory and the Liouville equation from statistical mechanics was never presented in publications about skeletal muscle models before.

Point of Departure. We want to reconsider Model 2.25, but we only consider the case of vanishing attachment and detachment probabilities, i.e. $f = g = 0$. Therefore, no attachment and detachment can happen and the resulting system is purely Lagrangian.

In Model 2.25, coupling is achieved by the relations

$$\text{“Sliding velocity”} = \text{“Contraction rate in fiber direction”}$$

$$v = \frac{\mathrm{d}}{\mathrm{d}t}\sqrt{\boldsymbol{N}_f^\flat \otimes \boldsymbol{N}_f(\boldsymbol{C})} = \frac{\mathrm{d}}{\mathrm{d}t} q_f \tag{3.1}$$

and

$$W = W_{\text{iso}} + Q_1\sqrt{\boldsymbol{N}_f^\flat \otimes \boldsymbol{N}_f(\boldsymbol{C})} = W_{\text{iso}} + Q_1 I_4. \tag{3.2}$$

If we integrate Equation (3.1), we end up with

$$q^i = \sqrt{\boldsymbol{N}_f^\flat \otimes \boldsymbol{N}_f(\boldsymbol{C})} + \text{const}. \tag{3.3}$$

We will use Equation (3.3) to derive Equation (3.2) as a coupling term of a constrained Lagrangian system.

The value of 'const' is given by

$$q^i(X, t=0) - q_f(\boldsymbol{C}(X, t=0)),$$

but we do not introduce a new variable and use the same symbol for all myosin heads instead.

How to force a Lagrangian systems to follow a fixed path. To start gentle, we will consider a linear spring whose positions are constrained to follow a given path.

Model 3.1 (A trivial linear spring)**.** For a given path $q_{\text{constr}} : [0, T] \to \mathbb{R}$, we represent the dynamics of a single cross-bridge as a single linear spring.

The Lagrangian is given by

$$L = \frac{1}{2}m\dot{q}^2 - \frac{1}{2}\kappa q^2.$$

Additionally, we add the constraint

$$0 = g(q, t) := q_{\text{constr}}(t) - q.$$

Obviously, the constraint of Model 3.1 fully determines its dynamics, but we work out the role of the Lagrange multipliers in this case. In fact, exactly the same calculation will apply, when we replace q_{constr} by the fiber stretch of the skeletal muscle later.

The Euler-Lagrange equations for the Lagrangian $\widetilde{\mathcal{L}}(q, \dot{q}, \lambda) = \mathcal{L} - \lambda g(q, t)$ are given by

$$\begin{aligned} 0 &= \frac{\partial \mathcal{L}}{\partial q} - \lambda\frac{\partial g}{\partial q} - \frac{\mathrm{d}}{\mathrm{d}t}\frac{\partial \mathcal{L}}{\partial \dot{q}} \\ &= \frac{\partial \mathcal{L}}{\partial q} + \lambda - \frac{\mathrm{d}}{\mathrm{d}t}\frac{\partial \mathcal{L}}{\partial \dot{q}} \\ &= -\kappa q + \lambda - m\ddot{q} \end{aligned} \tag{3.4}$$

and

$$q = q_{\text{constr}}. \tag{3.5}$$

If we use the second derivative of the constraint from Equation (3.5),

$$\ddot{q} = \ddot{q}_{\text{constr}},$$

we can replace $\ddot{q}$ in the Equation (3.4) and get

$$\lambda = \kappa q + m\ddot{q}_{\text{constr}}. \tag{3.6}$$

Remark 3.2 (Lagrange multipliers for fixed path constraints)**.** The Lagrange multiplier λ simply cancels out the original force $F_{\text{unconstr}} = -\kappa q$ and replaces it by the acceleration of the fixed path $F_{\text{constr}} = m\ddot{q}_{\text{constr}}$. If we ignore units, we have

$$\lambda = -F_{\text{unconstr}} + F_{\text{constr}}.$$

Remark 3.3 (A field of trivial linear springs)**.** If we consider a field of fixed paths $q_{\text{constr}} : \mathcal{B} \times [0,T] \to \mathbb{R}$ and a field of linear springs $q : \mathcal{B} \times [0,T] \to \mathbb{R}$, the exact same calculation applies as well.

1. Coupling between Hyperelasticity and Cross-Bridge Theory

As in the derivation for the equations of a continuous rope in Section 5, we will first define a discrete model for a large, but finite, number of cross-bridges. From there, we can derive the usual continuous model.

Model 3.4 (Hyperelasticity and cross-bridges, discrete version)**.**
1. We use the usual model of hyperelasticity () with deformation field

$$\varphi : \mathcal{B} \times [0,T] \to \mathbb{R}^3$$

and the strain energy

$$\mathcal{W} = \mathcal{W}_{\text{passive}}.$$

2. We denote the centers of every individual sarcomere by

$$X_k \in \mathcal{B}, \quad \text{for all } k = 1, \dots, K.$$

At each center, a collection of N_a attached cross-bridges is modelled as a collection of linear springs with stiffness κ and mass m_{xb}. The motion is described by the trajectory

$$\boldsymbol{q}_k : [0,T] \to \mathbb{R}^{N_a}.$$

The Lagrangian is given as

$$L_k = \frac{m_{\text{xb}}}{2} \|\dot{\boldsymbol{q}}\|_2^2 - \frac{\kappa}{2} \|\boldsymbol{q}\|_2^2 .$$

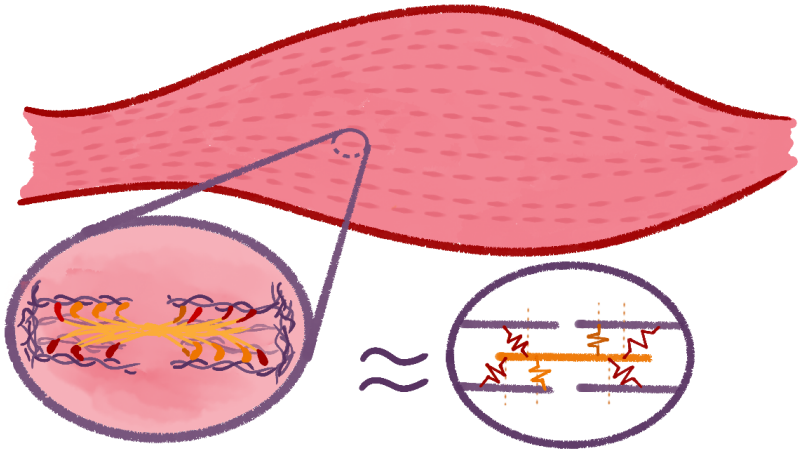

Figure 1. At each point X_k, we model one sarcomere as a collection of attached cross-bridges.

3. These two models are coupled via the constraints

$$g_{i,k}(\mathrm{D}\varphi, \dot{q}_k) = \sqrt{\boldsymbol{N}_f^\flat \otimes \boldsymbol{N}_f\,(\boldsymbol{C})}\Big|_{X_k} - q_k^i + \text{const.}$$

The constant depends only on the initial conditions, i.e. the initial extensions of the cross-bridges.

Model 3.5 (Hyperelasticity and cross-bridges, semi-continuous version)**.** We continue Model 3.4.

2b. We now assume that the sarcomere centers X_k are distributed with density

$$\rho_{\mathrm{sc}} : \mathcal{B} \to \mathbb{R}.$$

The configuration of the cross-bridge model will be represented by a field

$$\boldsymbol{q} : \mathcal{B} \times [0, T] \to \mathbb{R}^{N_a}$$

and the Lagrangian (density) is given as

$$\mathcal{L}_{\mathrm{xb}} = \rho_{\mathrm{sc}} \cdot \left(\frac{m_{\mathrm{xb}}}{2} \left\| \dot{q} \right\|_2^2 - \frac{\kappa}{2} \left\| q \right\|_2^2 \right).$$

3b. In the continuous formulation, we use the constraints

$$g_i(\mathrm{D}\varphi, q^i) = \sqrt{\boldsymbol{N}_f^\flat \otimes \boldsymbol{N}_f\,(\boldsymbol{C})} - q^i + \text{const.} \tag{3.7}$$

4. The augmented Lagrangian of the complete model is given as

$$\widetilde{\mathcal{L}} = \mathcal{L}_{\text{xb}} + \mathcal{L}_{\text{hyperelasticity}} + \sum_i \lambda^i g_i. \tag{3.8}$$

Remark 3.6 (Velocity constraint vs. position constraint)**.** In general, the constraints $g = 0$ and $\dot{g} = 0$ have different Lagrange multipliers and the relation is not always obvious. However, if $g(q)$ depends only on q, the Lagrange multipliers are related via $\lambda_g = \dot{\lambda}_{\dot{g}}$.

Initially, the derivation of the active stress term in the following lemma was based on the velocity constraint (3.1), which requires the use of the second order Euler-Lagrange equations, since the fiber contraction velocity v_f depends on a second order derivative of the configuration φ. But it turns out that the position constraints are easier and imply an almost trivial proof.

We are now able to compute the active stress as a coupling term. In fact, no difficult computations are needed, since the stress is just a term of the constrained Euler-Lagrange equations for fields.

Lemma 3.7 (Active stress as coupling term)**.** *The Euler-Lagrange equations for Model 3.5 are*

$$\rho\ddot{\varphi} = \boldsymbol{b} + \operatorname{Div}(\boldsymbol{P}_{\text{passive}} + \boldsymbol{P}_{\text{active}}), \tag{3.9}$$

$$m\ddot{\boldsymbol{q}} = -\kappa\boldsymbol{q} + \boldsymbol{\lambda} \quad \textit{and} \tag{3.10}$$

$$\boldsymbol{g} = 0, . \tag{3.11}$$

with

$$\boldsymbol{P}_{\text{passive}} = \frac{\partial \mathcal{W}_{\text{passive}}}{\partial \operatorname{D}\varphi}, \quad \boldsymbol{P}_{\text{active}} = \frac{\partial \mathcal{W}_{\text{active}}}{\partial \operatorname{D}\varphi},$$

where the active strain energy is given by

$$\mathcal{W}_{\text{active}} := \sum_i \lambda^i q_f. \tag{3.12}$$

Moreover, the Lagrange multipliers are explicitly given by

$$\lambda^i = \kappa q^i - m\frac{\mathrm{d}^2}{\mathrm{d}t^2} q_f. \tag{3.13}$$

Proof. 1. We use the constrained Euler-Lagrange equation (1.15) applied to the augmented Lagrangian

$$\mathcal{L} = \mathcal{L}_{\text{hyper}}(\varphi, \operatorname{D}\varphi, \dot{\varphi}) + \mathcal{L}_{\text{xb}}(\boldsymbol{q}, \dot{\boldsymbol{q}}) - \sum_i \lambda^i g_i(q^i, \operatorname{D}\varphi).$$

This directly implies (3.11), which is a result of variation of the Lagrange multipliers $\boldsymbol{\lambda}$, see (1.15b).

2. We also notice that (3.10) was already calculated in Model 3.1. Variation in q^i yields the equation

$$\frac{\partial \mathcal{L}_{\text{xb}}}{\partial q^i} - \lambda^i \frac{\partial g_i}{\partial q^i} - \frac{\mathrm{d}}{\mathrm{d}t}\frac{\partial \mathcal{L}_{\text{xb}}}{\partial \dot{q}^i} = 0.$$

The constraint g_i is of the form

$$g_i = -q^i + \underbrace{q_f + \text{const.}}_{\text{does not depend on } q^i}$$

Therefore, we get

$$\frac{\partial g_i}{\partial q^i} = -1,$$

which yields the additional term $+\boldsymbol{\lambda}$ in (3.10). The remaining terms are just the Equations of a linear spring.

3. In (3.9), only the term $\boldsymbol{P}_{\text{active}}$ is new compared to the equations of unconstrained hyperelastic motion. According to (1.15a) the coupling term is given by

$$-\sum_{i,j} \frac{\mathrm{d}}{\mathrm{d}X^i}\left(-\lambda^j \frac{\partial g_j}{\partial \,\mathrm{D}_i\varphi}\right).$$

Hence, the active stress is given by

$$\boldsymbol{P}_{\text{active}} = \sum_j \lambda^j \frac{\partial g_j}{\partial \,\mathrm{D}\varphi}.$$

Similar than before, we can ignore some terms of g_j, because

$$g_i = q_f - \underbrace{q^i + \text{const.}}_{\text{does not depend on } \mathrm{D}\varphi}$$

Therefore, we can replace g by q_f to compute the active stress, which yields

$$\boldsymbol{P}_{\text{active}} = \sum_j \lambda^i \frac{\partial q_f}{\partial \,\mathrm{D}\varphi} = \frac{\partial \mathcal{W}_{\text{active}}}{\partial \,\mathrm{D}\varphi}.$$

This completes the proof of the Equations (3.9), (3.10) and (3.11).

4. To get the explicit form of the Lagrange multiplier λ^i we repeat the computations leading to Equation (3.6).

The second derivative of the constraint $q_f - q^i + \text{const} = 0$ is

$$\ddot{q} = \frac{\mathrm{d}^2}{\mathrm{d}t^2} q_f.$$

Replacing $\ddot{q}$ in Equation (3.10) yields

$$\lambda^i = \kappa q^i + m \frac{\mathrm{d}^2}{\mathrm{d}t^2} q_f,$$

which is exactly Equation (3.13). □

Remark 3.8 (Relation to active stress in established models)**.** In the established models (Model 2.24), the active strain energy $\mathcal{W}_{\text{active}}$ is

$$\mathcal{W}_{\text{active}} = p_{\text{act}} q_f.$$

If we compare this choice with our result in (3.12), we see

$$p_{\text{act}} \stackrel{?}{=} \sum_i \lambda^i.$$

The explicit formula of the Lagrange multipliers (3.13) yields

$$\int_{\mathbb{R}} \kappa q \mu_b(q) \,\mathrm{d}q =: p_{\text{act}} \stackrel{?}{=} \sum_{i=1}^{N_a} \left(\kappa q^i + m \frac{\mathrm{d}^2}{\mathrm{d}t^2} q_f \right).$$

In the limit $N_a \to \infty$, we can identify

$$\int_{\mathbb{R}} \kappa q \mu_b(q) \,\mathrm{d}q \approx \sum_i \kappa q^i.$$

We will shortly prove a local statement for the limit case $m \to 0$. The mass m can be seen as a parameter of the system. If the complete system is well-posed, the solutions should depend continuously on the data.

Remark 3.9 (Active stress for vanishing cross-bridge mass)**.** The Euler-Lagrange equations for Model 3.5 with $m = 0$ are

$$\rho \ddot{\varphi} = \boldsymbol{b} + \operatorname{Div}(\boldsymbol{P}_{\text{passive}} + \boldsymbol{P}_{\text{active}}), \tag{3.14}$$

$$q^i = q_f + \text{const}, \tag{3.15}$$

$$\boldsymbol{g} = 0, \tag{3.16}$$

with

$$\boldsymbol{P}_{\text{passive}} = \frac{\partial \mathcal{W}_{\text{passive}}}{\partial \operatorname{D}\varphi}, \quad \boldsymbol{P}_{\text{active}} = \frac{\partial \mathcal{W}_{\text{active}}}{\partial \operatorname{D}\varphi},$$

where the active strain energy is given as

$$\mathcal{W}_{\text{active}} := \sum_i \lambda^i q_f. \tag{3.17}$$

Moreover, the Lagrange multipliers are explicitly given by

$$\lambda^i = \kappa q^i. \tag{3.18}$$

The second term $m \frac{\mathrm{d}^2}{\mathrm{d}t^2} q_f$ does not make a big difference between both models, since the mass of a single cross-bridge is negligibly small.

We want to remark that our derivation of $\mathcal{W}_{\text{active}}$ only requires the understanding of q_f as the fiber stretch, but not of the conceptually more complicated active stress tensor $\boldsymbol{P}_{\text{active}}$.

Why are tiny cross-bridges better? Before we formally set the cross-bridge mass to zero, we want to explore in which way less and heavier cross-bridges would lead to different muscle dynamics.

Remark 3.10 (The curse of dimensionality and cross-bridges)**.** Usually, the coupling between two oscillating systems can lead easily to highly chaotic dynamics, which is a consequence of complicated feedback between the systems.

This is not the case in muscle dynamics. The fundamental underlying reason is the ratio between stiffness and mass.

For a material with elasticity modulus E, cross-section A and equilibrium length L, the axial stiffness is given by $\kappa = E\frac{A}{L}$.

In Equation (3.13) we see that a small mass m of the myosin heads is preferable for our model, since one coupling term vanishes effectively.

If we look at the scaling behavior of κ and m we find

$$m \approx s^3 \quad \text{and} \quad \kappa = \frac{E \cdot A}{L_0} \approx s^1,$$

where s is a characteristic length scale of the system.

If we copy the mechanism of a muscle on a larger scale, we see that the mass would grow rapidly. This results in a more complicated coupling behavior between the myosin heads – the working bees of the muscle – and the large contracting solid.

2. The Liouville Equation for Cross-Bridges

Keeping track of each single cross-bridge is numerically unfavorable, because the dimension of our system increases with the number of cross-bridges. Therefore, we want to represent the state of our cross-bridges by a density function $\rho_{\text{xb}}(q)$ instead. The computational effort to store an approximation of $\rho_{\text{xb}}(q)$ does not depend on the number of cross-bridges, which allows us to simulate a large ensemble of cross-bridges.

To derive the evolution of a particle density, it is useful to swap into the Hamilton formalism.

Remark 3.11 (Hamilton mechanics and Liouville's equation)**.** The relation between the Lagrangian and the Hamiltonian formulation of classical mechanics is given by

$$\boldsymbol{p} := \frac{\partial L}{\partial \dot{\boldsymbol{q}}} \quad \text{and} \quad H(\boldsymbol{q}, \boldsymbol{p}) := p\dot{q} - L(\boldsymbol{q}, \dot{\boldsymbol{q}}).$$

The Liouville equation for this Hamiltonian is often denoted by

$$\dot{\rho} = -\{\rho, H\}.$$

It describes the evolution of an initial density $\rho(\boldsymbol{q}, \boldsymbol{p}, t = 0) = \rho_0(\boldsymbol{q}, \boldsymbol{p})$ along the flow of the Hamiltonian system. For a derivation of this equation, we refer to [**MR11**, Proposition 5.5.6.].

For our application, it is useful to recall the relation to the methods of characteristics.

In coordinates, Liouville's equations reads

$$\dot{\rho} + \sum_i \left(\frac{\partial \rho}{\partial q^i} \frac{\partial H}{\partial p_i} - \frac{\partial \rho}{\partial p_i} \frac{\partial H}{\partial q^i} \right) = 0. \tag{3.19}$$

This equation is a first order partial differential equation for

$$\rho : T^*\mathbb{R}^n \times [0, T] \to \mathbb{R} : (\boldsymbol{q}, \boldsymbol{p}, t) \mapsto \rho(\boldsymbol{q}, \boldsymbol{p}, t),$$

with initial conditions

$$\rho = \rho_0 \quad \text{at } t = 0.$$

In a reverse manner, we can show the physical meaning of Equation (3.19) by the *method of characteristics*. The characteristic curves $\boldsymbol{q}(t), \boldsymbol{p}(t)$ for Equation (3.19) are the solutions of the characteristic system

$$\dot{\boldsymbol{q}} = \frac{\partial H}{\partial \boldsymbol{p}}, \quad \text{and} \quad \dot{\boldsymbol{p}} = -\frac{\partial H}{\partial \boldsymbol{q}}.$$

These equations are exactly the equations of motion of Hamilton mechanics. Hence, the characteristic curves are exactly the trajectories of single particles of the Hamiltonian system.

The solution of Liouville's equation is characterised by

$$\rho(\boldsymbol{q}(t), \boldsymbol{q}(t), t) = \rho_0(\boldsymbol{q}(0), \boldsymbol{p}(0)).$$

Hence, the particle density at $(\boldsymbol{q}(0), \boldsymbol{p}(0))$ will be transported along the flow of the Hamiltonian system. This situation is sketched in Figure 2.

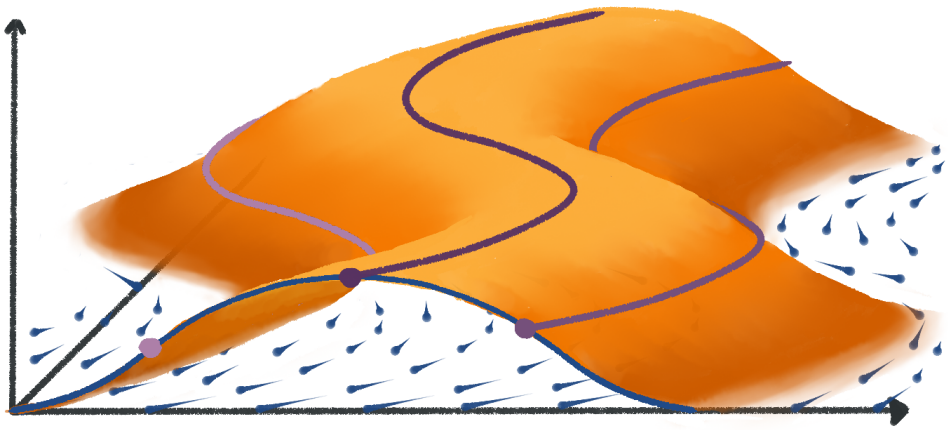

Figure 2. Each characteristic curve of the Liouville equation corresponds to the path of a single particle of the Lagrangian system.

Partial application of Liouville's equation. Our application is slightly different compared to the classical application of Liouville's equation. We do not want to transform the complete system into a Liouville equation, but only one part of it. The remaining system will still be subject to the Euler-Lagrange equations.

We consider the Lagrangian

$$\mathcal{L} = \mathcal{L}_{\text{hyper}}(j^1(\varphi)) + \mathcal{L}_{\text{xb}}(j^1(q)) - \sum_i \lambda^i g_i(\mathrm{D}\varphi, q)$$

We want to replace the state variable $\boldsymbol{q} \in \mathbb{R}^{N_a}$ for N_a cross-bridges by a density $\rho_{\text{xb}}(q)$ of cross-bridges. As we have seen previously, we are looking for a partial differential equation, whose characteristic curves are the equations of motion.

Due to the constraints, the equations of motion are trivial with respect to $\boldsymbol{q}$. To fit into our setting, we use the derivative of the constraints g_i as a starting point, i.e.

$$\dot{q}^i = \dot{q}_f.$$

The transport equation

$$\frac{\partial \rho_{\text{xb}}}{\partial t} + \dot{q}_f \frac{\partial \rho_{\text{xb}}}{\partial q} = 0$$

is therefore the evolution equation of ρ_{xb}.

This equation coincides with the two state model with vanishing transition probabilities $f = g = 0$.

We arrive at a conservative model, which will be the starting point for the development for numerical methods in Section 4.2.

Model 3.12 (Hyperelasticity and one state model)**.** The mixed Euler-Lagrange and Liouville equations for Model 3.5 are given by

$$\rho\ddot{\varphi} = \boldsymbol{b} + \mathrm{Div}(\boldsymbol{P}_{\mathrm{passive}} + \boldsymbol{P}_{\mathrm{active}}), \tag{3.20}$$

$$\frac{\partial \rho_{\mathrm{xb}}}{\partial t} + \dot{q}_f \frac{\partial \rho_{\mathrm{xb}}}{\partial q} = 0, \tag{3.21}$$

with

$$\boldsymbol{P}_{\mathrm{passive}} = \frac{\partial \mathcal{W}_{\mathrm{passive}}}{\partial \,\mathrm{D}\varphi}, \quad \boldsymbol{P}_{\mathrm{active}} = \frac{\partial \mathcal{W}_{\mathrm{active}}}{\partial \,\mathrm{D}\varphi},$$

where the active strain energy is

$$\mathcal{W}_{\mathrm{active}} := \int_{\mathbb{R}} \lambda(q)\rho_{\mathrm{xb}}(q)q_f(\mathrm{D}\varphi)\,\mathrm{d}q. \tag{3.22}$$

Moreover, the Lagrange multipliers are explicitly given by

$$\lambda(q) = \kappa q. \tag{3.23}$$

3. Averaging in Cross-Bridge Theories

In some sense, the use of smooth classical field theory is totally inadequate to model the densities of cross-bridges. Per se, the state of two neighboring sarcomeres can be totally different and will be different. But, sarcomeres in one region receive almost the same electrical signals and thus the controlling calcium ion concentration will be very similar.

Seen as a collection of systems which are exposed to similar external influences, we can locally view them as a statistical ensemble of physical systems, whose average can be represented by a smooth field of densities.

Regardless of the physical dynamics, we will not be able to simulate all single sarcomeres. Hence, we will use the assumptions that densities of cross-bridges do not vary much locally and can be approximated by a smooth field.

4. Non-conservative two state model

If we follow a single myosin-head throughout the cross-bridge cycle, we could model its dynamics as a complicated stochastic system.

But the resulting dynamics are far too complicated for the methods used in this chapter.

A fundamental problem is the almost binary state change between attached cross-bridges and unbound myosin heads. The number of myosin heads is finite, but the attachment of a cross-bridge corresponds to the instantaneous activation of a new constraint $\dot{q}^i = v_f$. Hence, we can not include the cross-bridge cycle as an external force if we model single myosin heads directly.

Another complication is the blocking of binding-sites by other myosin heads, which would require to model also a finite number of binding-sites and their state to determine the likelihood for the creation of a new cross-bridge.

The two state model (Model 2.11) is only a rough approximation of the real dynamics. As such it is possible that no easy underlying particle system exists which yields this model in the limit. At least, we were not able to find one.

Of course, the reasoning behind the two state model directly applies to the density ρ_{xb} in Remark 3.9. This just yields the classical Model 2.25.

Chapter 4

Numerical Methods for Nonlinear Hyperelasticity and Cross-Bridge Models

In this chapter we will summarize common numerical tools for static and dynamic hyperelasticity.

The finite element method (FEM) is a well established theory for continuum mechanical simulations, in particular for rubber-like, soft tissues. We will give a short introduction to the methods involved in the solution of the system of nonlinear partial differential equations in elasticity. A careful analysis of these numerical methods is beyond the scope of this thesis and we also ignore any kinds of uniqueness and existence problems.

For time integration, we used explicit methods with small time steps, since these methods are far less expensive and allow the use of small time steps. Unfortunately, we were not able to overcome all numerical challenges in the case of incompressible hyperelastic motion, where explicit methods become very unstable.

We will present numerical results of static contraction experiments and for the motion of a contracting solid. In the end, we will demonstrate an implementation of the complete model, where a two-state cross-bridge model is used to compute the active contraction stress of an hyperelastic solid.

We mainly used [**Wri08**] to learn about nonlinear finite elements and their application in elasticity. The main references for this chapter are [**Deu11**], [**AH09**] and [**BBF13**]. And for time integration we used [**Sim13**], [**MW01**] and [**HLW06**].

My contributions: All numerical experiments in this chapter where implemented by myself, using of the FEniCS framework. My contributions are the implementation of Model 2.25 as shown in Section 4.5 and the numerical experiments in Section 4.2 and Section 4.3.

1. Nonlinear Finite Elements for Static Hyperelasticity

We are interested to solve the *nonlinear* variational problem from Equation (1.14), where we seek to find a configuration $\varphi \in \mathcal{C}$, which satisfies

$$\underbrace{\mathrm{d}S(\varphi)[\eta]}_{=:\,\widetilde{a}(\varphi,\eta)} + \underbrace{F_{\boldsymbol{b}}[\eta] + F_{\tau}[\eta]}_{=:\,-\widetilde{\ell}[\eta]} = 0, \qquad \text{for all } \eta \in T_{\varphi}\mathcal{C}. \tag{4.1}$$

This equation is linear in the variation η, but nonlinear with respect to the solution candidate $\varphi \in \mathcal{C}$. Hence, we can define a nonlinar map

$$\widetilde{A} : \mathcal{C} \to T^*\mathcal{C} : \varphi \mapsto \widetilde{a}(\varphi, \cdot).$$

Now, the variational problem can also be formulated as a root-finding problem. For this purpose, we define

$$F : \mathcal{C} \to T^*\mathcal{C} : \varphi \mapsto \widetilde{A}(\varphi) - \widetilde{\ell}.$$

The solutions $\varphi \in \mathcal{C}$ of the variational problem are exactly the roots of F, i.e.

$$\widetilde{a}(\varphi, \eta) = \widetilde{\ell}[\eta], \qquad \text{for all } \eta \in T_{\varphi}\mathcal{C},$$

holds, if and only if

$$F(\varphi) = 0 \in T^*\mathcal{C}.$$

We require F to have a unique root x^*, or in other words, the variational problem should have a unique solution.

Remark 4.1 (Sobolev spaces)**.** As noted already, the space of smooth functions is too restrictive for applicable existence theorems. Moreover, most finite element bases are not smooth on the boundaries of the computational cells. As a consequence, the configuration spaces must contain weakly differentiable functions. The choice of the appropriate function spaces depends on the Lagrangian density $\mathcal{L}$, the domain $\mathcal{B}$ and the boundary conditions.

For linear elasticity, a reasonable choice would be

$$\mathcal{C} := \{\varphi \in H^1(\mathcal{B}, \mathbb{R}^d) \mid \mathrm{Tr}(\varphi) = \varphi_D \text{ on } \partial_D\mathcal{B}\},$$

where $\mathrm{Tr} : H^1(\mathcal{B}, \mathbb{R}^d) \to H^{\frac{1}{2}}(\partial_D \mathcal{B}, \mathbb{R}^d)$ is the trace functional of the Sobolev space $H^1(\mathcal{B}, \mathbb{R}^d)$ and $\varphi_D : \partial_D \mathcal{B} \to \mathbb{R}^d$ are the Dirichlet boundary conditions. We assume to have nice boundary conditions, in particular the set $\mathcal{C}$ should not be empty.

The space $\mathcal{C}$ is an affine linear subspace of the Hilbert space $H^1(\mathcal{B}, \mathbb{R}^d)$. After shifting the affine subspace $\mathcal{C}$, such that it contains the zero, we can identify $H^1(\mathcal{B}, \mathbb{R}^d) \cong \mathcal{C} \cong T_\varphi \mathcal{C} \cong T^*_\varphi \mathcal{C}$.

The use of Sobolev spaces changes the topology of our function space and therefore the notation of convergence, which influences for example also the notation of differentiability. We will commit the crime of ignoring these details and refer to the detailed treatment of functional analytic aspects of elasticity in [**MH83**, Chapter 6].

1.1. Newtons method in Banach spaces. To solve the root finding problem $F = 0$, we can use Newtons method, which generalises well to infinite dimensional spaces and provides an analytic tool to construct the solution.

If $F : \mathcal{C} \to T^*\mathcal{C}$ is Fréchet differentiable, we can linearise the root-finding problem

$$0 = F(\varphi + \xi) = F(\varphi) + \mathrm{D}F(\varphi)[\xi] + \mathcal{O}(\|\xi\|^2)$$

to determine a step $\xi \in T_\varphi \mathcal{C}$ towards the root of the function F.

In this context, Newton's method reads

$$\mathrm{D}F(\varphi^k)[\xi^k] = -F(\varphi^k), \quad \varphi^{k+1} := \varphi^k + \xi^k, \qquad \text{for all } k = 0, 1, \dots$$

Each step $\xi^k \in T_{\varphi^k} \mathcal{C}$ is the solution of an infinite dimensional linear problem

$$\mathrm{D}F(\varphi^k)[\xi^k] = -F(\varphi^k) \in T^*\mathcal{C}, \tag{4.2}$$

which is the linearisation of the nonlinear problem $F(\varphi) = 0$ around the point φ^k.

If F represents a nonlinear PDE, then each step requires the solution of the corresponding linearised PDE.

We assume that the Newton sequence is well defined and converges to a limit point $\varphi^* := \lim_k \varphi^k$. Of course, this may not be satisfied in the case of nonlinear elasticity, since physical strain energy densities $\mathcal{W}$ are not convex functions.

1.2. The Linearised Problem. To solve the linearised problem in Equation (4.2), we will use the finite element method, which is based on a Galerkin-projection of the weak formulation for a PDE.

The linearised problem is given by

$$\mathrm{D}F(\varphi^k)[\xi^k] + F(\varphi^k) = \mathrm{D}\widetilde{A}(\varphi^k)[\xi^k] + \widetilde{A}(\varphi^k) - \widetilde{\ell} = 0 \in T^*\mathcal{C},$$

where $\xi^k \in T_{\varphi^k}\mathcal{C}$ denotes a variation of φ^k.

If we insert $\widetilde{a}(\varphi, \cdot) = \widetilde{A}(\varphi)$, we get

$$\frac{\partial \widetilde{a}}{\partial \varphi}(\varphi^k, \cdot)[\xi^k] + \widetilde{A}(\varphi^k) - \widetilde{\ell} = 0,$$

where $\frac{\partial \widetilde{a}}{\partial \varphi}$ denotes the Fréchet derivative of $\widetilde{a}$ with respect to its first argument.

Hence, $\xi^k \in T_{\varphi^k}\mathcal{C}$ is characterized as the solution of the linear variational problem

$$a^k(\xi^k, \eta) = \ell^k[\eta], \quad \text{for all } \eta \in T\mathcal{C}, \tag{4.3}$$

with

$$a^k(\xi, \eta) := \frac{\partial \widetilde{a}}{\partial \varphi}(\varphi^k, \eta)[\xi] \quad \text{and} \quad \ell^k[\eta] := \ell + \widetilde{A}(\varphi^k).$$

Notice, that the variation $\xi := 0 \in T_{\varphi^k}\mathcal{C}$ does not correspond to a stress-free configuration of the solid! The typical equations of linear elasticity are only recovered, if the current configuration φ_k is stress-free.

1.3. The Galerkin Method for the Linearized Problem. For the linearized problem, we finally can use the finite element method, which has its theoretical foundation in the Galerkin-projection.

In this subsection, we follow [**AH09**, Section 9.1].

Let us denote the Hilbert space of variations as $V := T_{\varphi^k}\mathcal{C}$.

In the case of linear hyperelasticity, the existence of a unique solution for Equation (4.3) is well understood and follows for example from an application of the classical Lax-Milgram Lemma [**AH09**, Section 8.1].

In particular we know, that the bilinear form a^k is bounded

$$\left|a^k(\xi, \eta)\right| \leq M \left\|\xi\right\|_V \left\|\eta\right\|_V, \quad \text{for all } \xi, \eta \in V.$$

And as a consequence of Korn's inequality, it is also strongly elliptic

$$a^k(\eta, \eta) \geq c_0 \left\|\eta\right\|_V^2, \quad \text{for all } \eta \in V.$$

To get an associated finite dimensional approximation, the Galerkin method suggests to choose a finite dimensional subspace $V_N \subseteq V$. The projection of the variational equation onto V_N yields the finite dimensional problem

$$\xi_N^k \in V_N, \quad a^k(\xi_N^k, \eta) = \ell^k(\eta), \qquad \text{for all } v \in V_N. \tag{4.4}$$

Another application of the Lax-Milgram Lemma yields, that this system is also uniquely solvable.

For a basis $\{\phi_i\}_i$ of V_N the projected linear system can be rewritten as

$$\xi_N^k = \sum \gamma_i^k \phi_i, \quad A_N^k \cdot \boldsymbol{\gamma}^k = \boldsymbol{b}_N^k.$$

The coefficients of the *stiffness matrix* A are given by $A_{ij}^k = a^k(\phi_i, \phi_j)$ and the *load vector* is defined as $b_i^k = \ell^k(\phi_i)$.

The assembling of these matrices is one of the computational challenging tasks in the finite element methods. The dependency on the current configuration φ^k forces us to repeat the assembly step again and again in each iteration of the (exterior) Newton method.

If we choose an increasing sequence of sufficiently large finite dimensional subspaces

$$V_1 \subset V_2 \subset \cdots \subseteq V, \quad \text{with } \overline{\bigcup_{n \geq 1} V_N} = V,$$

the corresponding solutions ξ_N^k converges in the limit to the exact solution, i.e.

$$\xi^k = \lim_N \xi_N^k.$$

This analytical procedure is called the Galerkin method.

1.4. The Principle of Asymptotic Mesh Independence. In the previous section, we have discussed the solutions of the linearized problem. If we fix a particular finite dimensional test and trial space V_N, we can compute a Newton sequence φ_N^k, but this sequence does not solve the root finding problem $F = 0$, but a projected version of this problem, i.e. $F_N = 0$. As such it is also unclear if the resulting sequence has a similar convergence behaviour or if it gets sufficiently close.

The situation is summarized in the following diagram.

$$\begin{array}{ccc} F = 0 & \xrightarrow{\text{Newton}} & \varphi^k \\ \Big\downarrow{\scriptstyle \text{FEM}} & & {\scriptstyle ?}\Big\uparrow \\ F_N = 0 & \xrightarrow{\text{Newton}} & \varphi_N^k \end{array}$$

This section follows [**Deu11**, Chapter 8].

To analyze the situation, it is useful to rewrite Equation (4.4) again as a root finding problem. The Galerkin-projection in Equation (4.4) corresponds to a replacement of

$$F : \mathcal{C} \to T^*\mathcal{C}$$

by

$$F_N : V_N \to V_N^* : \varphi \mapsto F(\varphi)\big|_{V_N},$$

where $F(\varphi)\big|_{V_N} : V_N \to \mathbb{R}$ denotes the restriction of $F(\varphi) : T_\varphi\mathcal{C} \to \mathbb{R}$ to the space of test functions $V_N \subseteq T\mathcal{C}$.

The restriction of the domain of F corresponds to the choice of the trial space to be V_N and restricting $F(\varphi)$ fixes the test space to be V_N.

The first obvious question is, whether the roots converge in the limit. Let $\varphi_N^* := \lim_{k\to\infty} \varphi_N^k$ denote the limit point of Newtons method, applied to F_N. Then, we obviously want to know if these approximations also converge to φ^*, i.e.

$$\varphi_N^* \overset{?}{\to} \varphi^*, \quad \text{for } N \to \infty.$$

In practice, we are only able to compute φ_N^k for a large, but finite number N. Under technical assumptions, it is possible to prove that for sufficiently large N, a bound of the form

$$\limsup_{k\to\infty} \left\| \varphi_N^k - \varphi^k \right\| \leq \frac{1}{\omega}$$

holds. In this estimate, ω denotes a common affine covariant Lipschitz constant of the Newton schemes for F and F_N, related to the quadratic convergences, for details we refer to [**Deu11**, Theorem 8.2]. With stronger assumptions, is also possible to show the existence and uniqueness of the discrete solution point φ_N^* and the quadratic convergence of the Newton sequence φ_N^k [**Deu11**, Theorem 8.5].

If the sequences φ^k and φ_N^k show similar convergence behaviour for sufficiently large N, we speak of *asymptotic mesh independence*, since N usually corresponds to the resolution of the computational mesh.

In Figure 1, a simplified version of this situation is sketched. The branches can be considered to correspond to one discretization level N.

1.5. Newton Methods for Large Finite Dimensional Problems. The application of Newton methods to large systems requires some additional care in theory and implementation, since the direct solution of

$$\mathrm{D}F_N(\varphi_N^k)[\xi_N^k] = -F_N(\varphi_N^k)$$

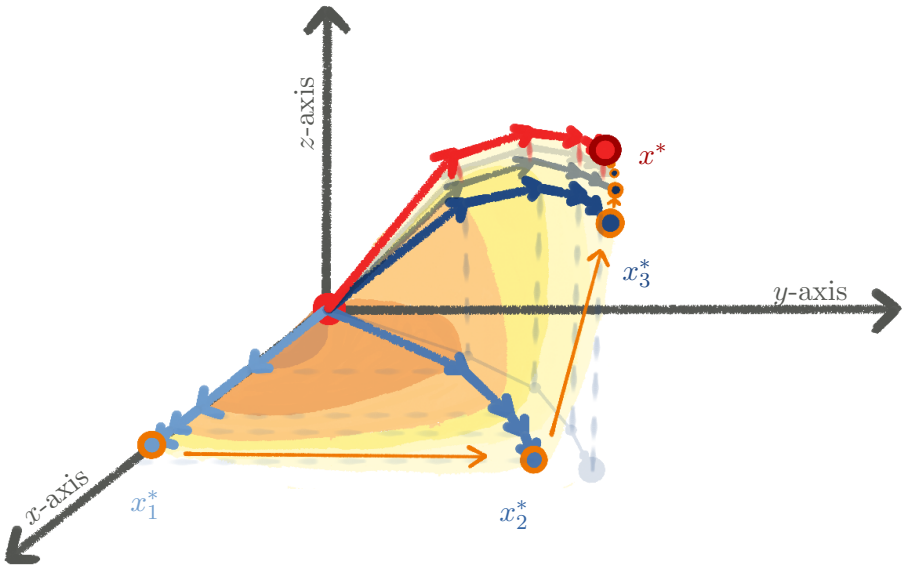

Figure 1. The blue dots represent Newton sequences φ_1^k, φ_2^k and φ_3^k, which are restricted to the x-axis, xy-plane and xyz-subspace. The red dots represent a Newton sequence x^k in an infinite dimensional space (of course, it is not possible to visualise infinite dimensions in this plot). [**Deu11**, Figure 8.1]

might be computationally infeasible.

To shorten the notation, we aim at solving

$$F(\boldsymbol{x}) = 0,$$

for $F : D \subseteq \mathbb{R}^n \to \mathbb{R}^n$, which is assumed to be sufficiently differentiable.

This section is also based on [**Deu11**].

There exist many modifications of Newton's method. We only summarize the relevant modifications for our application.

1.5.1. *Ordinary Newton method.* The well-known classical Newton method reads

$$\mathrm{D}F(\boldsymbol{x}^k)\Delta\boldsymbol{x}^k = -F(\boldsymbol{x}^k), \quad \boldsymbol{x}^{k+1} = \boldsymbol{x}^k + \Delta\boldsymbol{x}^k, \qquad \text{for all } k = 0, 1, \ldots.$$

Locally around a solution, the method is convergent of second order. The domain of convergence is not only a theoretical assumption. Depending on

the initial guess, the method may not converge at all or only to a local minimum.

1.5.2. *Simplified Newton method.* In high dimension, the computation of the Jacobian is time consuming. A common trick to overcome this bottleneck is to update the Jacobian only once in a while. For a theoretical description, we simply assume that only the initial Jacobian is computed, which yields the following method

$$\mathrm{D}F(\boldsymbol{x}^0)\Delta\boldsymbol{x}^k = -F(\boldsymbol{x}^k), \quad \boldsymbol{x}^{k+1} = \boldsymbol{x}^k + \Delta\boldsymbol{x}^k, \qquad \text{for all } k = 0, 1, \dots, K.$$

After K steps the point $\boldsymbol{x}^{K+1}$ can be used as a new initial point. This speeds up each single iteration, but both the number of iterations and the domain of convergence change.

1.5.3. *Inexact Newton methods.* If the solution of the linear system

$$\mathrm{D}F(\boldsymbol{x}^k)\Delta\boldsymbol{x}^k = -F(\boldsymbol{x}^k) \tag{4.5}$$

is carried out by an iterative method, we call the method *inexact*.

This yields an additional iteration in each step, for example

$$\boldsymbol{y}^k_{l+1} := \Phi^k(\boldsymbol{y}^k_l), \quad \text{for all } l = 0, 1, \dots$$

and

$$\Delta\boldsymbol{x}^k := \lim_l \boldsymbol{y}^k_l,$$

where Φ^k denotes some iterative method for the linear system in Equation (4.5).

The resulting method has two iterations. With *inner iteration* (of the variable l) we refer to the iterative solution of the linear system from Equation (4.5). The *outer iteration* (in the variable k) is the usual Newton iteration, carried out with the approximations of $\boldsymbol{y}^k_{L_k} \approx \Delta\boldsymbol{x}^k$, for some large L_k, which might depend on stopping criteria etc.

1.6. Summary.

(1) Find initial configuration φ_{init} and choose a finite dimensional test and trial space V_N.

(2) Outer Newton Iteration with respect to k:
   (a) Compute the linearisation of F around φ^k
   (b) Assembly of the stiffness matrix $\boldsymbol{A}$ and the load vector $\boldsymbol{b}$.
      (i) Iterative solution of the linear system $\boldsymbol{A}\boldsymbol{\xi}^k = \boldsymbol{b}$.
   (c) Set $\varphi^{k+1}_N := \varphi^k_N + \xi^k_n$.

1.7. Continuation Methods. The convergence of Newton's methods depends crucially on a good initial guess. Without a good initial guess, other strategies are needed to solve the problem numerically. For time stepping methods, the previous time step already provides a good initial guess. But for static hyperelasticity, the initial guess is usually just the stress free configuration of the body, which might be outside of the convergence range of Newton's method. We restrict our considerations to the static case.

Continuation methods provide a tool to overcome the lack of a good initial guess. For a mathematical treatment we refer to [**Deu11**, Chapter 5]. For a practical introduction and application in hyperelasticity, we recommend [**Wri08**, Chapter 5].

The idea is to replace the nonlinear problem

$$F(\varphi) = 0$$

by a perturbed problem,

$$F(\varphi; \lambda) = 0,$$

which depends on a new parameter $\lambda \in [0, 1]$. The dependency on λ should be regular enough, such that

$$\mathcal{N} := \{(\varphi, \lambda) \in \mathcal{C} \times [0, 1] \mid F(\varphi, \lambda) = 0\}$$

defines a smooth curve in $\mathcal{C} \times [0, 1]$. The perturbed problem should be chosen such that the original problem is obtained for $\lambda = 1$ and for $\lambda = 0$ a solution φ_0 of the perturbed problem should be available.

To solve the original problem, we start at $(\varphi_0, 0) \in \mathcal{N}$ and follow the curve $\mathcal{N}$ until we reach the desired solution $(\varphi_1, 1) \in \mathcal{N}$.

Remark 4.2 (A parametrization for static hyperelasticity)**.** For static hyperelasticity, we could define

$$F(\varphi; \lambda) := \mathrm{d}S(\varphi) + \lambda(F_{\boldsymbol{\tau}} + F_{\boldsymbol{b}}).$$

Additionally, it is also reasonable to replace the Dirichlet boundary conditions

$$\varphi = \varphi_0 + u_{\text{init}}, \quad \text{on } \partial_D \mathcal{B},$$

by

$$\varphi = \varphi_0 + \lambda u_{\text{init}}, \quad \text{on } \partial_D \mathcal{B}.$$

We want to note, that this is only one out of many possible choices!

Remark 4.3 (Parametrization for (quasi-)incompressible hyperelasticity)**.** If we also impose incompressibility, a parametrization as suggested in Remark 4.2 is often insufficient, since also for small λ no solutions can be found.

To fix this, it is helpful to use a relaxation like in Remark 1.39 where the problem

$$F(\varphi, p; \lambda) = \mathrm{d}\widetilde{S}(\varphi, p) + \lambda(F_{\boldsymbol{\tau}} + F_{\boldsymbol{b}}) = 0,$$

was relaxed via an additional term $\frac{p^2}{2\kappa}$, which yields

$$F(\varphi, p; \lambda, \kappa) := \mathrm{d}\widetilde{S}(\varphi, p) + \lambda(F_{\boldsymbol{\tau}} + F_{\boldsymbol{b}}) + \frac{p^2}{2\kappa} = 0.$$

For small parameters κ, the quadratic term p^2 dominates the problem and therefore the Newton methods will converge more likely.

But we need to update the two parameters $\lambda \to 0$ and $\kappa \to \infty$.

Method 4.4 (Natural parameter continuation)**.** If we start with $\lambda_0 = 0$ and an initial guess φ_0, such that

$$F(\varphi_0; \lambda_0) = 0$$

is satisfied, we could choose a next step $\lambda_1 > \lambda_0$ and try to find φ_1 with Newton's methods such that

$$F(\varphi_1; \lambda_1) = 0.$$

We can iterate this process until we reach $\lambda_k = 1$.

In our simulations, we used a constant maximal step size $h_{\max}$ and the update rule

$$\lambda_{k+1} = \lambda_k + \frac{1}{2^l} h.$$

Whenever the solution method fails, we increase $l' = l + 1$ and try again to solve the less perturbed system. If the previous solution step was successful, we decrease the value $l' = \max(l - 1, 1)$.

Method 4.5 (Heuristic parameter continuation for two parameters)**.** In the situation of two parameters λ and κ, a new update strategy must be used.

Since κ should attain large values, it is instructive to introduce another parameter $\gamma \in [0, 1]$ and set

$$\kappa(\gamma) = 10^{n_0 + \gamma(n_1 - n_0)},$$

where n_0 and n_1 are two exponents, such that $\kappa(0)$ yields a simple problem and $\kappa(1)$ is close to the incompressible case. We used for example $\kappa(0) = 10^4$ and $\kappa(1) \approx 10^7$, but this also depends on the scale of the problem.

For our application, it was sufficient to apply Method 4.4 recursively. If we fix a value $\overline{\lambda_1}$, we can consider

$$F(\varphi, p; \overline{\lambda_1}, \gamma) = 0$$

as a continuation problem with parameter γ. This problem can be solved with Method 4.4, which yields solutions φ_1 and p_1 satisfying

$$F(\varphi_1, p_1; \overline{\lambda_1}, \gamma = 1) = 0.$$

Therefore, we can solve $F(\varphi, p; \lambda)$, which allows us to apply Method 4.4 onto the parameter λ.

Remark 4.6 (Advanced continuation methods)**.** We want to remark, that we used the natural parameter continuation due to its simplicity. More advanced methods exist and are also used in elasticity. One approach would be, to solve in each continuation step the system $\widetilde{G} = 0$ for

$$\widetilde{G} : (\varphi, \lambda) \mapsto (F(\varphi; \lambda), G(\lambda; \lambda_0)),$$

where G is some chosen function, which encourages a step closer to the desired solution. In this way, both φ_1 and λ_1 are found simultaneously by an application of Newton's method.

We do not use such advanced methods for our simulations, due to the related complexity of their integration in FEniCS.

1.8. Mixed Finite Elements. If we simulate incompressible or quasi-incompressible materials, the Lagrange multiplier p becomes an additional unknown of the system and we need to choose a trail and test space for this new component of the solution.

Choosing the same type of finite elements for the discretization of the displacement φ and the pressure p is naive. For example, the mixed finite element $\mathcal{P}^1$-$\mathcal{P}^1$ fails to satisfy any inf-sup condition for the linearized problem and the discretization is not stable. More details about inf-sup conditions can be found in [**BBF13**, section 4.2.2].

The choice of stable finite elements is crucial in order to get a convergent method. A detailed treatment about mixed finite elements can be found in [**BBF13**].

For our numerical experiments, we simply used the Taylor-Hood pairing $\mathcal{P}^1$-$\mathcal{P}^0$ or $\mathcal{P}^2$-$\mathcal{P}^1$, which was for example also used in [**SSP09**].

Remark 4.7 (Finite elements for the pressure variable.)**.** The Lagrange multiplier is only unique up to an additive constant. Therefore we either need to define boundary conditions for the pressure or use finite elements which respect this procedure.

The appropriate space for the pressure variable without boundary conditions would be

$$p \in L^2(\mathcal{B}, \mathbb{R}) \,/_{\mathbb{R}},$$

where two pressure fields are identified with each other if they only differ by a constant. This can be achieved numerically, if we orthogonalize the finite element basis $(\phi_i)_{i=1,\dots,N}$ such that the new basis $(\widetilde{\phi}_i)_{i=1,\dots,N-1}$ is orthogonal to the constant function. For linear problems, this procedure in implemented in FEniCS.

2. FEniCS – A Magic Finite Element Framework

Mathematical treatments of Finite Element Methods usually forget to stress an important practical point: A Finite Element implementation is literally as strong as it weakest link. One wrong sign or one false index will skew up all results!

With this in mind, an automatic finite element framework like FEniCS is not just handy, it is essential to get simulations working within a limited time frame.

FEniCS makes great use of symbolic expressions. This allows to define simulations using a source code, which closely follows the mathematical formulation of the problem. Therefore, we do not need to find explicit formulas for the stress tensors from elasticity.

But, as a tool for spatial discretization, the framework still lacks high-level interfaces for the use of time integration methods, which is a big drawback if advanced time integration methods are required for the simulation of motion.

Example 4.8 (Static Hyperelasticity)**.** In this example we explain the principal steps required to solve a PDE using FEniCS. We left out technical details like the loading of mesh files or the definitions of boundary conditions.

After we have loaded the mesh file, a typical FEniCS simulation starts with the definition of the finite element spaces. This is shown in the code listing below. Various finite element types are available in the framework. In this example we used quadratic Lagrange elements for the displacement variable and linear Lagrange elements for the pressure. After the initialization of these elements, we can define the trial and test space V.

```
# Init finite elements spaces
element_u = VectorElement("CG", mesh.ufl_cell(), degree=2)
element_p = FiniteElement("CG", mesh.ufl_cell(), degree=1)

# Mixed finite element space
TH = element_u * element_p
```

```
# Create function space
V = FunctionSpace(mesh, TH)
```

In the next step, we prepare relevant constants and expressions for the model. The object `Expression` also allows to define general functions, which have to be valid C++ code, since all expressions will be compiled. This step is crucial for the fast assembly of the linear systems. The parameter `scale` in the definition of `p_act` and `B` can be used as a continuation parameter.

```
# Mooney-Rivlin parameters (in Pa)
c_10 = Constant(6.352e4);  c_01 = Constant(3.627e3)
rho = Constant(1.1e3)

# current muscle contraction
p_act = Expression("p_max*p_act*scale",
                   p_act=1., p_max=73e3, scale=0.,
                   degree=0)

# Define acting body force per unit volume
B = Expression(("scale*gravity", "0."),
               scale=0., gravity=9.81, element=element_u)

# Traction force on the boundary
tau  = Constant((100.0,  0.0, 0.))
```

The next lines of code are almost like mathematical statements. The function `u` represents the displacement field, it is related to the deformation field φ via, $\varphi = \mathrm{id} + u$. The last line defines two test functions η and q.

```
# Define test and trial functions
w = Function(V)  # most recently computed solution
(u, p) = split(w); p = variable(p)
(eta, q) = TestFunctions(V)
```

The next lines implement the Lagrangian $\mathcal{L}$ of the system and the fiber distribution N_f. In this example, the fibers are just aligned parallel to the z-axis.

An assumption, which is hidden between the lines, is that the mesh corresponds to the stress-free initial condition of the solid.

```
I = Identity(3)             # Identity tensor
F = variable(I + grad(u))   # Deformation gradient
C = F.T * F                 # Right Cauchy-Green tensor
J = det(C)**0.5

# Invariants
I_1 = tr(C)
I_2 = 0.5*((tr(C))**2 - (tr(C*C)))

# Fiber directions
N_f = as_vector([[0.0], [0.0], [1,0]])
I_4 = inner(a_0, C*a_0)

# Storage strain energy
W_iso = c_10*(I_1 - 3) + c_01*(I_2 - 3)
W_act = p_act*sqrt(I_4)

# Constraint
g = J-1

# Augmented Lagrange function
L = -W_iso - W_act - p*g

# Compute stress tensors
P = diff(W_iso+W_act, F)
G = diff(g, F)
```

In close analogy to Section 1, we can define a function `F` for the nonlinear problem. To define the weak form of our partial differential equation, we can use operators and the inner product. The symbolic tools from FEniCS will automatically translate this weak formulation into the unified finite element language, for which efficient assembly routines exists.

```
# Nonlinear weak formulation
F = ((inner(P + p*G ,grad(eta)) + inner(B,eta) + g*q)*dx
      - inner(tau,eta)*ds(1))
```

At this stage, we can already call a function to solve the nonlinear problem directly. For more control, we can also prepare the linearization. The function `derivative` computes the symbolic derivative of `F` at the point `w` in direction `xi`. In each step of the Newton iteration, we will solve for the trial function `xi`, which determines the next step of `w`.

```
# Prepare linearized problem (around w)
xi = fe.TrialFunction(V)
DF = derivative(DS, w, xi)
```

FEniCS allows to call various different solvers and methods for an inexact Newton iteration. We can also change the number of used quadrature points or set additional options. In this example, we only use the option to optimize the compiled C++ . In the last line of the code, we can plot the resulting solution. This is one of the main advantages of a high-level interface for FEniCS, since we can investigate the computed solutions directly.

```
# Init nonlinear solver
ffc_options = {"optimize": True}
problem = NonlinearVariationalProblem(
                        F, w, bcs_u + bcs_p,
                        J=DF,
                        form_compiler_parameters=ffc_options)

solver = fe.NonlinearVariationalSolver(problem)
solver.solve()

# Plot solution
plot(w.sub(0), mode='displacement')
```

Remark 4.9 (Efficiency of FEniCS)**.** For complex simulations, efficiency is almost as important as a readable source code. For this reason, most finite element codes are written in FORTRAN, C++ or other hardware efficient languages. Just like FEniCS itself. The python interface is really just an interface to call powerful C++ routines underneath. Giving an overview of all sub-projects and ideas is quite complex. For further details, we refer to the official FEniCS book [**LMW12**].

To highlight another aspect of the magic behind FEniCS, it is worth noting, that FEniCS is build on top of the idea of a unified finite element language (UFL). One important part of the FEniCS project is the generation of efficient C++ code for fast numerical assembling. This generated C++ code is highly optimized. For example, at first all weak forms will generate some code which follows roughly their implementation in python. But then, an optimization of this code will take place to collect duplicated computations and spare out unused variables and computations.

Having this in mind, it is instructive to focus on readable python code instead of optimizing already on this level.

3. Numerical Results for Static Hyperelasticity with Constraints

To demonstrate the methods discussed in previous sections, we simulate how a two dimensional muscle lifts a weight. Of course, the simulation results are unrelated to real weightlifting, since the strength of our arms is a result of a multi-body system of bones (rigid bodies), skeletal muscles and other connective tissues. The computational mesh for the muscle is shown in Figure 2.

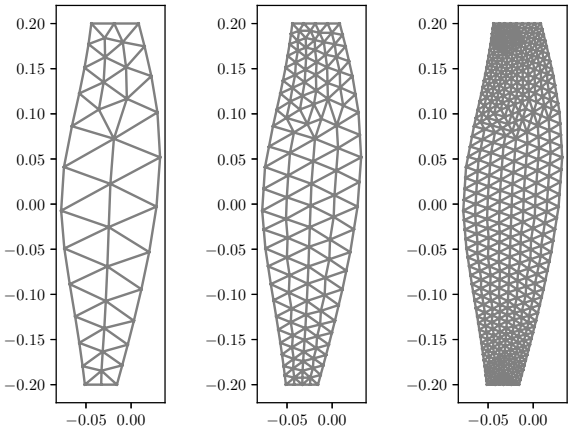

Figure 2. The original mesh on the left and two uniformly refined versions. The numerically experiments in this section where performed with the second mesh.

The plots in Figure 3 are generated with a slightly modified version of the source code from Example 4.8. In two dimensions the use of continuation methods is only necessary for large increments of the continuation parameter `scale`.

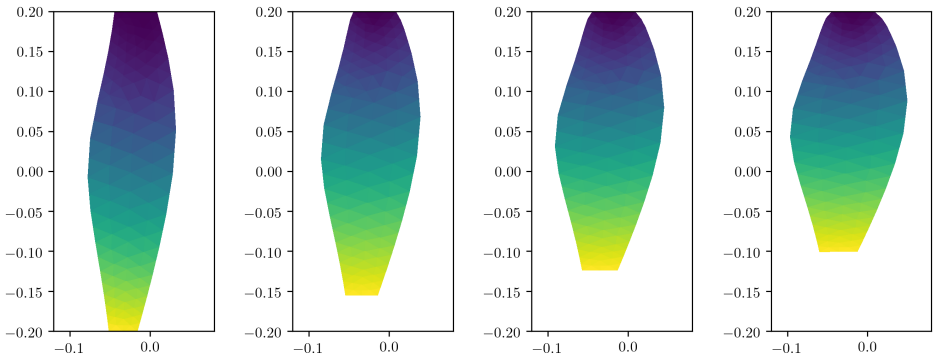

Figure 3. Different muscles activations with uniform sarcomere density. The plots were created with continuation parameters `scale=0, 0.4, 0.8, 1.2` and a strict incompressibility constraint. The continuation parameter in this example corresponds to different muscle activations.

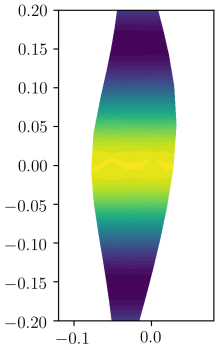

Figure 4. Plot for an example density ρ_{sc} of sarcomeres. At the end of the muscle, the density is lower. The chosen density is not realistic, but it models an increase of supportive tissue in areas which are close to the tendon.

3.1. Static Hyperelasticity with non-uniform sarcomere density. To show the flexibility of the numerical implementation with FEniCS, we demonstrate a small variation, which is the first step towards a real multi-scale model. A similar approach is also used in [**RSS17**].

Following the notation from Model 3.5, we use a non-uniform density ρ_{sc} of sarcomeres. This approach is used to model a higher percentage of surrounding tissue at the end and the beginning of the skeletal muscle.

The choice of the density ρ_{sc} is shown in Figure 4. Numerical simulations for different contraction strengths are shown in Figure 5.

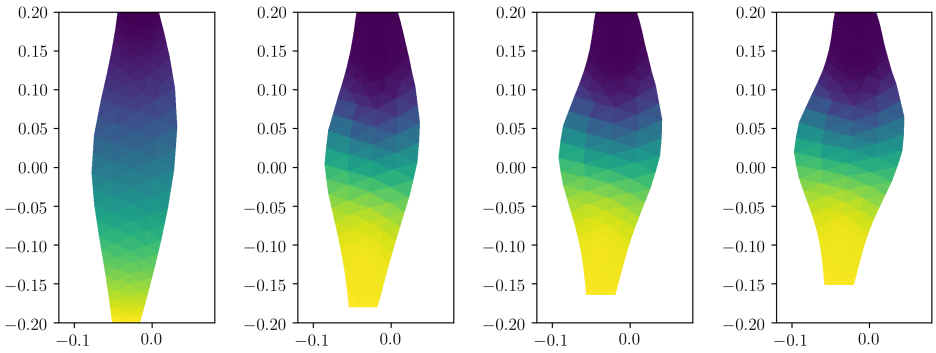

Figure 5. The repeated experiment from Figure 5, but with non-uniform sacromere density as in Figure 4. As expected, the deformed body now contracts more in the center, which is at least intuitively closer to the behavior of real skeletal muscles.

4. Time Integration Methods

In this section, we compare two numerical methods for the cross-bridge transport equation, we discuss a numerical experiment with explicit integration schemes for incompressible hyperelasticity and finally, we shortly demonstrate an implementation for a coupled model of a hyperelastic solid and the cross-bridge model.

For this section we used [**Wri08**] and [**Sim13**].

4.1. Numerical Methods for Cross-Bridge Models. To focus on coupling effects between a cross-bridge model and the muscle tissue, we replace the equations of hyperelasticity for the muscle tissue in Model 3.12 by an equation for a simple linear spring. The resulting model is summarized in Model 4.10.

Model 4.10 (Linear spring and two state model)**.** We consider the mixed Euler-Lagrange and Liouville equations

$$m_f \ddot{q}_f = -\kappa_f q_f + p_{\text{act}}, \tag{4.6}$$

$$\frac{\partial \rho_{\text{xb}}}{\partial t} + \dot{q}_f \frac{\partial \rho_{\text{xb}}}{\partial q} = f(1 - \rho_{\text{xb}}) - g\rho_{\text{xb}}. \tag{4.7}$$

If the transition probabilities vanish, $f = g = 0$, we get the corresponding one state model.

The activation is given by

$$p_{\text{act}} := \int_{\mathbb{R}} q\kappa\rho_{\text{xb}}(q)\,\mathrm{d}q. \tag{4.8}$$

Remark 4.11 (Clash of different numerical methods)**.** An interesting feature of Model 4.10 is the mix between two very different systems with special numerical methods for each of them.

The Liouville equation (4.7) is, due to the constraints, a one dimensional conservation law. For these kinds of equations, special finite volume methods or finite difference methods exits. We will use the upwind method for our numerical experiments.

On the other hand, the Hamiltonian system (4.6) inhibits a special geometric structure for which symplectic and variational time integration methods are advantageous.

We will shortly define some classical numerical methods, which are applicable for Model 4.10.

Method 4.12 (Upwind scheme and Strang splitting)**.** We use the notation

$$\rho_i^j := \rho_{\mathrm{xb}}(q_i, t_j),$$

where $q_i = \Delta q \cdot i$ represent an equidistant grid in space and $t_j = \Delta t \cdot j$ are equidistant time steps.

The upwind method is given by

$$\rho_i^{j+1} := \Phi_{\mathrm{up}}^{\Delta t}(\boldsymbol{\rho}^j) := \rho_i^j + \frac{\Delta t}{2\Delta q}\Big(v_f(\rho_{i-1}^j - 2\rho_i^j + \rho_{i+1}^j) \tag{4.9}$$

$$+ \left|v_f\right|(\rho_{i+1}^j - \rho_{i-1}^j)\Big). \tag{4.10}$$

This method is a conservative, first order accurate scheme for the transport equation. Its stability condition is given by the *CFL-condition*

$$\left|\frac{v_f \Delta t}{\Delta x}\right| < 1.$$

We will use zero Dirichlet boundary conditions for the transport equation. However, in the following experiments, we will see that this choice is simple, but not perfect for our application.

For the two state model, we need to simulate the source terms as well. The most simple choice is an explicit Euler scheme

$$\Phi_{\mathrm{src}}^{\Delta t}(\boldsymbol{\rho}^j) := \rho_i^j + \Delta t\left(f(q_i)(1-\rho_i^j) - g(q_i)\rho_i^j\right)$$

To combine the two integrators, we use a simple splitting scheme

$$\boldsymbol{\rho}^{j+1} := \Phi_{\mathrm{src}}^{\Delta t/2} \circ \Phi_{\mathrm{up}}^{\Delta t} \circ \Phi_{\mathrm{src}}^{\Delta t/2}(\boldsymbol{\rho}^j). \tag{4.11}$$

Method 4.13 (The method of moving frames)**.** As noted in Remark 2.10, the transport equations correspond to a Lagrangian viewpoint. Despite the fact that we also use the Lagrangian viewpoint for the simulation of the hyperelastic solid, there is no reason not to use the Eulerian viewpoint for the two state model.

If we apply the coordinate transformation

$$\widetilde{q} := q + q_f,$$

the two state model transforms into

$$\frac{\mathrm{D}\widetilde{\rho_{\mathrm{xb}}}}{\mathrm{D}t} = f(1-\widetilde{\rho_{\mathrm{xb}}}) - g\widetilde{\rho_{\mathrm{xb}}}.$$

Evaluated at a discrete grid $\widetilde{q_i}$, we get a set of ordinary differential equations

$$\frac{\partial \widetilde{\rho}_i}{\partial t}(t) = f(\widetilde{q_i} - q_f(t))(1-\widetilde{\rho}_i(t)) - g(\widetilde{q_i} - q_f(t))\widetilde{\rho}_i(t).$$

We will use the explicit Euler method to integrate these equations.

Method 4.14 (Symplectic Euler scheme)**.** Again, we will use the notations

$$q_f^j := q_f(t_j) \quad \text{and} \quad v_f^j := v_f(t_j).$$

Applied to Equation (4.6), the symplectic Euler scheme reads

$$\begin{aligned} v_f^{j+1} &:= v_f^j + \Delta t(-\lambda q_f^j + p_{\text{act}}^j), \\ q_f^{j+1} &:= q_f^j + \Delta t v_f^{j+1}. \end{aligned}$$

If we know the discrete density $\boldsymbol{\rho}^j$, we can compute p_{act}^j with the discrete version of Equation (4.8).

The symplectic Euler method is well-suited for the simulation of linear springs, since it preserves the total energy of the physical system asymptotically.

We will combine Method 4.14 with Method 4.12 and with Method 4.13. Simulation results are presented in the next two subsections.

4.2. Numerical experiments with the one state model. For vanishing transition probabilities, $f = g = 0$, the moving frame method is almost optimal, since the density remains constant from the Eulerian viewpoint. The upwind scheme cannot take advantage from vanishing transition probabilities, a simulation result can be seen in Figure 6.

In Figure 7 we can directly see why the upwind scheme loses energy. If the extension of the fiber q_f is large, all corss-bridges are getting closer to the boundary of the numerical grid.

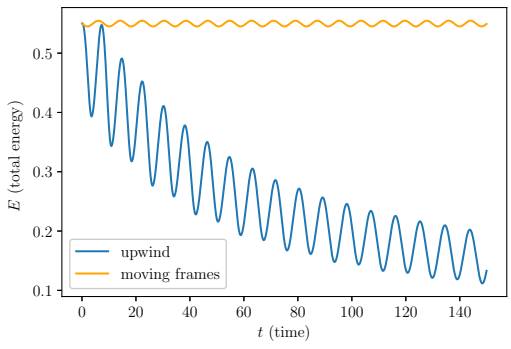

Figure 6. The total energy of Model 4.10 for both methods. The upwind methods fails to preserve the energy.

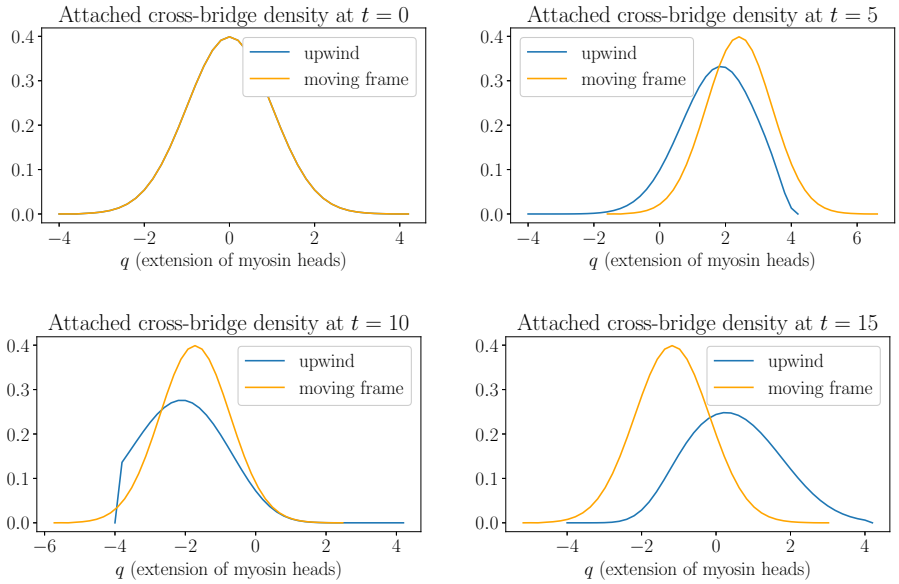

Figure 7. Density evolution in the conservative case $f = g = 0$. In the moving frame approach, the 'frame' follows the exterior Hamiltonian system. At $t = 10$ we can see how the frame of the upwind method represent the exact density.

The comparison is of course a bit unfair, since the moving frame approach is an exact solution for the conservation law, and hence the numerical properties of the symplectic time integration dominate the simulation result.

4.3. Numerical experiments for the non-conservative case. In the previous section, the moving frame method was clearly advantageous, compared to the upwind scheme. Surprisingly, the moving frame approach suffers badly from instabilities if the transition probabilities f, g are not zero.

We have use transition probabilities like in Remark 2.12. Attachment of cross-bridges is always related to an energy flux

$$E_{\text{attachment}} = \int \kappa q f(q)(1 - \rho_{\text{xb}}(q)\,\mathrm{d}q$$

and detachment causes an energy flux

$$E_{\text{detachment}} = \int \kappa q g(q)\rho_{\text{xb}}(q)\,\mathrm{d}q.$$

In this way we can measure the energy, which is totally consumed by the system. The resulting numerical simulations are shown in Figure 8 and Figure 9.

The numerical experiments clearly show high oscillations in the solution of the moving frame method.

This is due to the negative terms in the right hand side of Equation (4.7), i.e.

$$\frac{\partial \rho_{\mathrm{xb}}}{\partial t} + \dot{q}_f \frac{\partial \rho_{\mathrm{xb}}}{\partial q} = f \cdot (1 - \rho_{\mathrm{xb}}) - g \cdot \rho_{\mathrm{xb}}.$$

This system is similar to the test equation for stiffness, $\dot{y} = -\lambda y$. The explicit Euler method is not a stiff integration method and leads to highly oscillating solutions. If we change the transition probabilities, such that the right hand side only contains positive coefficients, then the oscillations also disappear.

The numerical diffusion of the upwind method smears out these fast oscillations and shock waves.

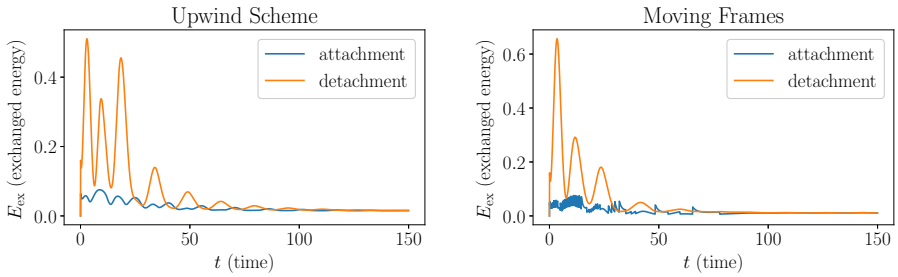

Figure 8. Energy increase and decrease due to attachment and detachment of cross-bridges. The moving frame methods creates highly oscillating solutions. Due to numerical diffusion, the upwind scheme does not suffer from this illness.

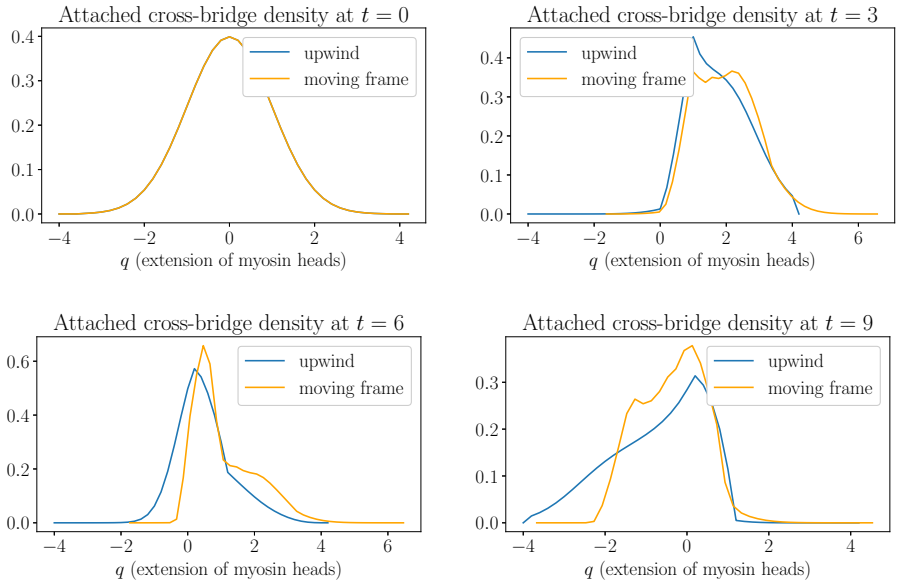

Figure 9. Density evolution in the non-conservative case. Shocks propagate in the solution of the moving frame approach, which leads to numerical instabilities. The numerical diffusion of the upwind scheme prevents these instabilities.

4.4. Experiments with explicit time integration methods. The most interesting phenomena of cross-bridge models are visible for fast events. A simulation with high resolution in time would be interesting to investigate the effect of the detailed cross-bridge model on the hyperelatic solid.

We tried to apply different explicit time integration schemes for differential-algebraic equations to incompressible and quasi-incompressible materials. The application of different explicit schemes to incompressible materials was never successful. An example is shown in Figure 10 and Figure 11.

For quasi-incompressible materials, time integration was possible with very small time steps. For incompressible materials, the time integration always failed, since very fast oscillations became dominant.

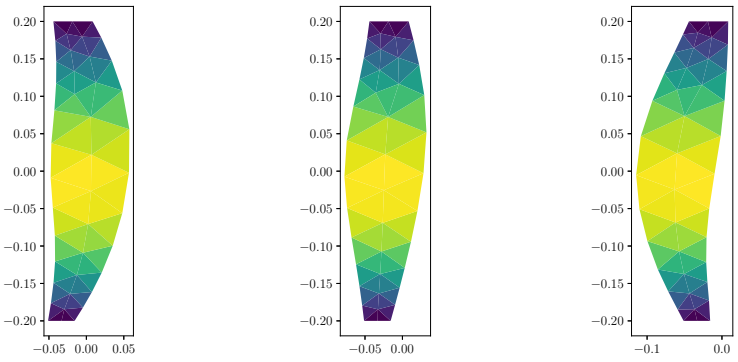

Figure 10. On the left: Initial position for the benchmark problem. In the center: Stress-free configuration of the body. On the right: Deformation after 5000 time steps with steps size $\Delta t = 10^{-4}$ for the quasi-incompressible material.

4.5. Implementation of the complete model. In the last section of this thesis, we want to present a proof-of-concept implementation of a quasi-compressible hyperelastic solid, with dynamically coupled two-state models like in Model 2.25.

Warning: The numerical results in this section are no reliable!

Due to time limitations during the creation of this work, we where not able to perform a serious convergence analysis for the numerical results of this section. The implementation shows at least, that a simulation is computationally possible.

Method 4.15 (Numerical methods for the complete model)**.** For spatial discretization, we used a $\mathcal{P}^2$-$\mathcal{P}^1$ Taylor-Hood pairing of finite elements for displacement and pressure.

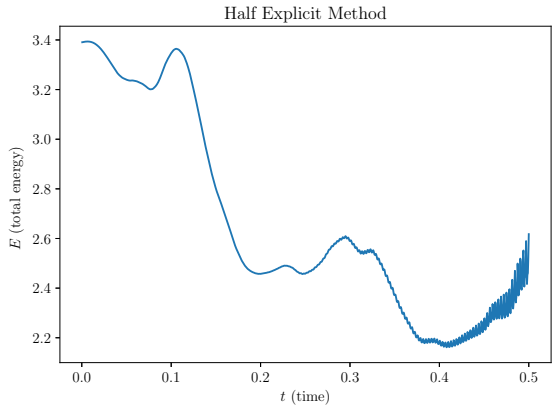

Figure 11. Even for very small time steps, the half explicit method yields a highly oscillating solutionf when applied for the simulation of an incompressible material.

At each quadrature point, the cross-bridge density $\rho_{\mathrm{xb}}(q)$ was discretized with respect to q by 20 cells. Therefore a 20 dimensional Lagrange element of degree 2 was used.

We used the half-explicit time integrator from [**Sim13**, Section 7.1.2.] for the time integration of the quasi-incompressible hyperelastic solid. The integration was only sucessful for small time steps. For the plots we used the step size $\Delta t = 10^{-5}$.

The two-state model was discretized by an upwind scheme with Strang splitting (Method 4.12).

The upwind method was chosen, since the results from Section 4.3 showed, that the upwind method is more stable than the moving frame method

The results presented in Figure 12 and Figure 13 where performed with the same material parameters as in Example 4.8 and bulk modulus $\kappa = 10^6$.

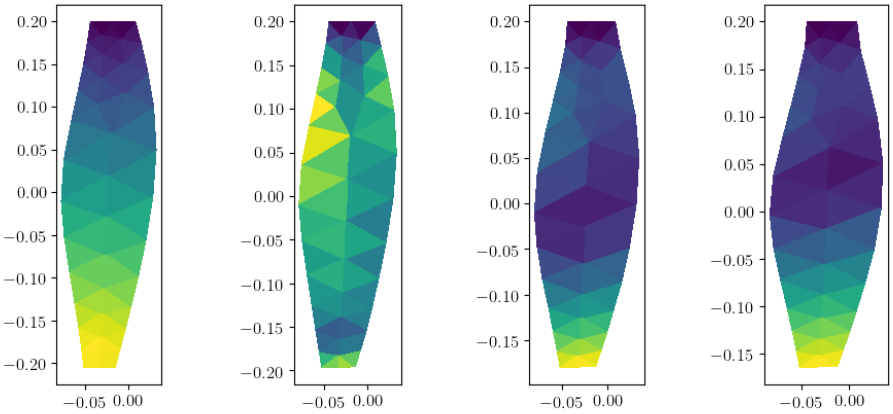

Figure 12. Deformation of the contracted skeletal muscle. At the beginning, lose bottom part of the muscle contracts most. After a while, the muscle reaches an equilibrium. For the simulations, 3000 time steps where used. We plotted the steps 300, 1205, 2111 and 2866.

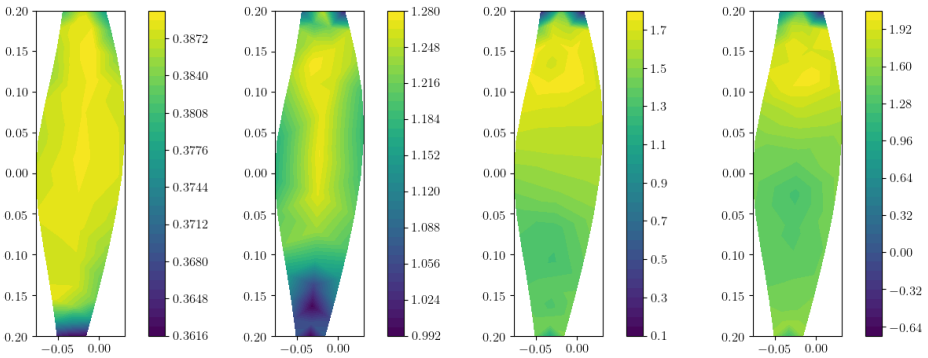

Figure 13. The color indicates the contraction force, generated by the two state model. The last plot shows the equilibrium of the system.

Conclusion

If this thesis was a movie, it would have an open ending. After one-hundred pages of theory, pictures and models, a stable and fast numerical simulation method is still missing. No happy end, yet.

On the theoretical side, we have presented a derivation for the conservative part from the cross-bridge model. This could be a foundation for the development of variational integrators for the complete system.

In the conservative case, the partial Liouville equation with constraints coincides with the transport equations for cross-bridges. This opens a door to new numerical questions: How can we treat a mixture of a Lagrangian system and a constrained Liouville equation numerically? Can we develop symplectic or variational integrators for these systems?

For the non-conservative case, we have identified a stiff behavior of the cross-bridge model and discovered that the upwind method is a dissipative, but more stable, numerical scheme for cross-bridges.

Acknowledgments

There is an old story about an Māori tribal chief, who was asked what the most important thing in life is and he replied: "People, People, People!"

The work on this master's thesis was partially supported by the German Academic Exchange Service (DAAD), which funded me a three month visit to James Sneyd and his research group at the University of Auckland, New Zealand. It was a great joy to join the research group of James, Elías, Ielyaas and Natân. I was delighted to learn a lot from them about physiology, applied math and research in general. It was fascinating to see how a great research group can have fun and be crazy, but without losing any focus and efficiency.

This thesis was supervised by Prof. Bernd Simeon, who encouraged me to follow my mathematical hobbies without any restrictions. The outcome might be a bit too close to the textbooks of Jerrold E. Marsden and the numerics are still unfinished, but during the creation of this thesis, I had time to develop my understanding about the mathematical foundations of physics, elasticity and physiology. I enjoyed the mathematical freedom and the direct and uncomplicated supervision.

I also want to thank Dr. Michael Gfrerer for his perfect book recommendations and his many practical advises.

Computational mathematics depends crucially on software development tools. Without these tools, various open source projects and great documentations, far more time would be necessary to develop, run and debug simulations. Therefore I feel constrained to thank for the great work of countless people of the open source community. One of those is of course the Wikipedia project,

which is always a first address for quick overviews and explainations. I used Python and several libraries from the NumPY initiative, namely FEniCS, numpy, scipy, sympy and matplotlib for all simulations in this thesis. In addition Paraview was used for visualization and the IDEs PyCharm and Spyder helped to manage my projects.

Moreover, I have to thank Todd Clark Brelje for his permission to use images from the virtual laboratory of physiology.

The most important support are of course my friends. They all helped me in the last few days to fix as much errors as possible. I would like to mention Julia Amman, Tim Bergner, Johannes Blühdorn, Christoph Hertrich, Jonathan Jahnke, Maximilian Mertin and Chetana Viswanath.

All errors in this thesis fall into my own responsibility. Especially, since all correctors had only very limited time to work trough this text.

Appendix A

Differential Calculus on Banach Spaces

We recall basic definition for differentiation of nonlinear maps between Banach spaces.

Definition A.1 (Gâteaux- and Fréchet-differentiable, [**Wer18**, Definition III.5.1])**.** Let X and Y be normed vector spaces, $U \subseteq X$ open and $f : U \to Y$ be a map.

(i) f is called *Gâteaux-differentiable* at $x_0 \in U$, if a continuous linear operator $T : X \to Y$ exists, with

$$\lim_{h \to 0} \frac{f(x_0 + hv) - f(x_0)}{h} = Tv, \qquad \text{for all } v \in X. \tag{A.1}$$

(ii) f is called *Fréchet-differentiable* at $x_0 \in U$, if the convergence in Equation A.1 is uniform with respect to $v \in X$ with $\|v\|_X \leq 1$.

(iii) f is called Gâteaux- resp. Fréchet-differentiable on U, if f is Gâteaux- resp. Fréchet-differentiable at all points $x_0 \in U$.
The operator T obtained as a limit in Equation A.1 depends on x_0 and is denoted by

$$\mathrm{D}f(x_0) : X \to Y.$$

We call

$$\mathrm{D}f : U \to L(X, Y)$$

the Gâteaux- resp. Fréchet-differential of f.

Remark A.2 (Nonlinear spaces)**.** The spaces X and Y can also be replaced by Banach manifolds. In this case, the Fréchet-differential is a map

$$\mathrm{D}f(x_0) : T_{x_0}X \to T_{f(x_0)}Y$$

and we call

$$\mathrm{D}f : TX \to TY$$

the differential of f. In the linear case, the isomorphism $T_{x_0}X \cong X$ is used.

Remark A.3 (Notation of directional derivatives)**.** We will use the syntax

$$\mathrm{D}f(x_0)[v] := \big(\mathrm{D}f(x_0)\big)\,(v).$$

To clearly separate points $x_0 \in X$ and directions $v \in T_{x_0}X \cong X$.

Sometimes we insert a vector field $v : X \to TX$ as directions and omit the points, i.e.

$$\mathrm{D}f[v] : X \to \mathbb{R} : x \mapsto \mathrm{D}f(x)[v(x)].$$

Theorem A.4 (Stationary Points)**.** *Let $U \subseteq B$ be an open set, $f : U \to \mathbb{R}$ Gâteaux-differentiable and let $x_0 \in B$ be a local extremal point, then* $\mathrm{D}f(x_0) = 0$.

Appendix B

Tools from Differential Geometry

1. Tangent Vectors as Velocities

Remark B.1 (Tangent Vectors)**.** Let $\mathcal{M}$ be a smooth manifold and $p \in \mathcal{M}$ a point and choose a local chart $h : U \to \mathbb{R}^m$, where $U \subseteq \mathcal{M}$ is an open set containing the point p.

We say that two smooth curves

$$\gamma_1, \gamma_2 : (-\varepsilon, \varepsilon) \to \mathcal{M}$$

have *first order contact at* $(0, p)$, if they hit the point p at the same time $t = 0$, i.e.

$$\gamma_1(0) = \gamma_2(0) = p$$

and if the velocity at $t = 0$ coincides in local coordinates, i.e.

$$\mathrm{D}(h \circ \gamma_1)(0) = \mathrm{D}(h \circ \gamma_1)(0).$$

A *tangent vector* $\eta \in T\mathcal{M}$ is an equivalence class of curves which have all first order contact at $(0, p)$.

2. Tensors and Two-Point Tensors

The deformation gradient $\boldsymbol{F} = \mathrm{D}\varphi : T\mathcal{B} \to T\mathcal{S}$ is one of the central objects in the study of elasticity. A clear language is useful in order to talk about tensors in elasticity. Like the deformation tensor, many tensors in elasticity

are not defined over only material or spatial spaces, but over both spaces at the same time. Therefore, we will shortly recall a few basics about two-point tensors from [**MH83**, section 1.4].

Using this language, we can define the divergence, contraction and double contraction of tensors.

Two-point tensors are objects with $p+q+l+m$ indices, therefore this section is a bit technical and it can be quite confusing.

Remark B.2 (Jumping over "$\to$")**.** A map

$$\widetilde{T} : V \to V.$$

defines an associated $\left(\begin{smallmatrix}1\\1\end{smallmatrix}\right)$-type tensor

$$T : V^* \times V \to \mathbb{R} : (\alpha, v) \mapsto \alpha(\widetilde{T}v).$$

Or, with the concept of tensor product spaces, we can say

$$T \in \left(V^* \times V\right)^* \cong V \otimes V^*. \tag{B.1}$$

An application of $V = V^{**}$ also allows us to apply the same trick for maps like

$$\widetilde{T} : V^* \to V^*,$$

in order to construct a corresponding map

$$T : V^* \times V^{**} \cong V^* \times V \to \mathbb{R}.$$

Remark B.3 (The type of a multilinear map)**.** For a general multi-linear map T, we can always find an associated map of the from

$$T : (V^*)^p \times V^q \to \mathbb{R}.$$

Hence

$$T \in (V)^{\otimes p} \otimes (V^*)^{\otimes q}.$$

Elements of this space are called *tensors of type* $\left(\begin{smallmatrix}p\\q\end{smallmatrix}\right)$.

Definition B.4 (Two-point tensor and tensor fields)**.** A *two-point tensor* of type $\left(\begin{smallmatrix}p & l\\ q & m\end{smallmatrix}\right)$ at $X \in \mathcal{B}$ over a mapping $\varphi : \mathcal{B} \to \mathcal{S}$ is a multilinear mapping

$$T : (T^*_X\mathcal{B})^p \times (T_X\mathcal{B})^q \times (T^*_x\mathcal{S})^l \times (T_x\mathcal{S})^m \to \mathbb{R},$$

where $x = \varphi(X)$.

A *two-point tensor field* T smoothly assigns a two-point tensor $T(X)$ to each material point $X \in \mathcal{B}$.

Using terminology from differential geometry we notate this as a section or a tensor field

$$T : \mathcal{B} \to (T\mathcal{B})^p \otimes (T^*\mathcal{B})^q \otimes (T\mathcal{S})^l \otimes (T^*\mathcal{S})^m.$$

Note that we have taken the dual spaces, like in Equation B.1.

Remark B.5 (The deformation gradient as a two-point tensor field)**.** In a similar fashion to Remark B.2, we can transform the deformation gradient

$$\mathrm{D}\varphi(X) : T_X\mathcal{B} \to T_x\mathcal{S}, \quad \text{with } x = \varphi(X),$$

into

$$\boldsymbol{F}(X) : T_X\mathcal{B} \times T_x^*\mathcal{S} \to \mathbb{R} : (\alpha, W) \mapsto \alpha(\mathrm{D}\varphi(X)[W]).$$

Hence the deformation gradient is a two-point tensor of type $\left(\begin{smallmatrix} 0 & 1 \\ 1 & 0 \end{smallmatrix}\right)$ and we can say it is a section

$$\boldsymbol{F} : \mathcal{B} \to T^*\mathcal{B} \otimes T\mathcal{S}. \tag{B.2}$$

Remark B.6 (The first Piola-Kirchhoff stress tensor)**.** For a strain energy $W(\mathrm{D}\varphi)$ the first Piola-Kirchhoff stress tensor is given as

$$\boldsymbol{P} = \frac{\partial W}{\partial\, \mathrm{D}\varphi}.$$

In view of Equation B.2 we can interpret the strain energy as a map

$$W : T^*\mathcal{B} \otimes T\mathcal{S} \to \mathbb{R}$$

and the first Piola-Kirchhoff stress tensor is the best linear approximation of this map (cp. Definition A.1), therefore

$$\boldsymbol{P}(\boldsymbol{F}) = \frac{\partial W}{\partial\, \mathrm{D}\varphi}(\mathrm{D}\varphi) : T^*\mathcal{B} \otimes T\mathcal{S} \to \mathbb{R}.$$

Jumping over the "$\to$" one last time yields a section

$$\boldsymbol{P}(\boldsymbol{F}) : \mathcal{B} \to T\mathcal{B} \otimes T^*\mathcal{S}.$$

Therefore it is a two-point tensor of type $\left(\begin{smallmatrix} 1 & 0 \\ 0 & 1 \end{smallmatrix}\right)$, which is exactly the opposite of the deformation tensor.

This is perfect, since we can insert a deformation tensor point-wise to get a real number. This will be applied in the calculus of variations, where we can interpret the gradient of a variation as a deformation tensor $\mathrm{D}\eta \in T\mathcal{B} \otimes T^*\mathcal{S}$ and define a map

$$\boldsymbol{P}(\boldsymbol{F})[\mathrm{D}\eta] : \mathcal{B} \to \mathbb{R} : X \mapsto \big(\boldsymbol{P}(\boldsymbol{F})\big)(X)[\mathrm{D}\eta(X)].$$

Bibliography

[AH09] Kendall E. Atkinson and Weimin Han, *Theoretical numerical analysis: A functional analysis framework*, 3rd ed ed., Texts in applied mathematics, no. 39, Springer, Dordrecht ; New York, 2009 (en).

[AJL+14] Bruce Alberts, Alexander Johnson, Julian Lewis, David Morgan, Martin Raff, Keith Roberts, and Peter Walter, *Molecular Biology of the Cell, Sixth Edition*, Garland Science, November 2014 (en).

[BBF13] Daniele Boffi, Franco Brezzi, and Michel Fortin, *Mixed Finite Element Methods and Applications*, Springer Series in Computational Mathematics, vol. 44, Springer Berlin Heidelberg, Berlin, Heidelberg, 2013 (en).

[BR08] Markus Böl and Stefanie Reese, *Micromechanical modelling of skeletal muscles based on the finite element method*, Computer Methods in Biomechanics and Biomedical Engineering **11** (2008), no. 5, 489–504 (en).

[CH17] Vicente Cortés and Alexander S. Haupt, *Mathematical Methods of Classical Physics*, SpringerBriefs in Physics, Springer International Publishing, Cham, 2017.

[Cia94] Philippe G. Ciarlet, *Three-Dimensional Elasticity*, Elsevier, February 1994 (en).

[Deu11] Peter Deuflhard, *Newton Methods for Nonlinear Problems*, Springer Series in Computational Mathematics, vol. 35, Springer Berlin Heidelberg, Berlin, Heidelberg, 2011.

[DFKS16] Geneviève Dupont, Martin Falcke, Vivien Kirk, and James Sneyd, *Models of Calcium Signalling*, Interdisciplinary Applied Mathematics, vol. 43, Springer International Publishing, Cham, 2016 (en).

[EEMnLRR96] Arturo Echeverría-Enríquez, Miguel C. Muñoz Lecanda, and Narciso Román-Roy, *Geometry of Lagrangian First-order Classical Field Theories*, Fortschritte der Physik/Progress of Physics **44** (1996), no. 3, 235–280 (en).

[GH06] Arthur C. Guyton and John Edward Hall, *Textbook of Medical Physiology*, Elsevier España, 2006 (es).

[Her00] Walter Herzog, *Skeletal Muscle Mechanics: From Mechanisms to Function*, John Wiley & Sons, October 2000 (en).

[HKR+16] Thomas Heidlauf, Thomas Klotz, Christian Rode, Ekin Altan, Christian Bleiler, Tobias Siebert, and Oliver Röhrle, *A multi-scale continuum model of skeletal muscle mechanics predicting force enhancement based on actin–titin interaction*, Biomechanics and Modeling in Mechanobiology **15** (2016), no. 6, 1423–1437 (en).

[HKR+17] Thomas Heidlauf, Thomas Klotz, Christian Rode, Tobias Siebert, and Oliver Röhrle, *A continuum-mechanical skeletal muscle model including actin-titin interaction predicts stable contractions on the descending limb of the force-length relation*, PLoS computational biology **13** (2017), no. 10, e1005773 (eng).

[HLW06] E. Hairer, Christian Lubich, and Gerhard Wanner, *Geometric numerical integration: Structure-preserving algorithms for ordinary differential equations*, 2nd ed ed., Springer series in computational mathematics, no. 31, Springer, Berlin ; New York, 2006 (en), OCLC: ocm69223213.

[How01] Jonathon Howard, *Mechanics of motor proteins and the cytoskeleton*, nachdr. ed., Sinauer, Sunderland, Mass, 2001 (eng), OCLC: 247917499.

[HR13] Thomas Heidlauf and Oliver Röhrle, *Modeling the Chemoelectromechanical Behavior of Skeletal Muscle Using the Parallel Open-Source Software Library OpenCMISS*, Computational and Mathematical Methods in Medicine **2013** (2013).

[HR14] ———, *A multiscale chemo-electro-mechanical skeletal muscle model to analyze muscle contraction and force generation for different muscle fiber arrangements*, Frontiers in Physiology **5** (2014) (English).

[IL03] Thomas Andrew Ivey and J. M. Landsberg, *Cartan for Beginners: Differential Geometry Via Moving Frames and Exterior Differential Systems*, American Mathematical Society, 2003 (en).

[KS09] James P. Keener and James Sneyd, *Mathematical physiology*, 2nd ed ed., Interdisciplinary applied mathematics, no. 8, Springer, New York, NY, 2009 (en), OCLC: ocn298595247.

[Lee13] John Lee, *Introduction to smooth manifolds*, 2. ed. ed., Springer, New York, 2013.

[LMW12] Anders Logg, Kent-Andre Mardal, and Garth Wells (eds.), *Automated Solution of Differential Equations by the Finite Element Method*, Lecture Notes in Computational Science and Engineering, vol. 84, Springer Berlin Heidelberg, Berlin, Heidelberg, 2012 (en).

[MH83] Jerrold E. Marsden and Thomas J. R. Hughes, *Mathematical Foundations of Elasticity*, Prentice-Hall, 1983 (en).

[MR11] Jerrold E Marsden and Tudor S Raţiu, *Introduction to mechanics and symmetry: A basic exposition of classical mechanical systems*, Springer, New York; London, 2011 (en), OCLC: 926993049.

[MW01] J. E. Marsden and M. West, *Discrete mechanics and variational integrators*, Acta Numerica 2001 **10** (2001), 357–514 (en).

[MZ91] S. P. Ma and G. I. Zahalak, *A distribution-moment model of energetics in skeletal muscle*, Journal of Biomechanics **24** (1991), no. 1, 21–35 (eng).

[RAS16] S. Rossi, N. Abboud, and G. Scovazzi, *Implicit finite incompressible elastodynamics with linear finite elements: A stabilized method in rate form*, Computer Methods in Applied Mechanics and Engineering **311** (2016), 208–249 (en).

[RSS17] O. Röhrle, M. Sprenger, and S. Schmitt, *A two-muscle, continuum-mechanical forward simulation of the upper limb*, Biomechanics and Modeling in Mechanobiology **16** (2017), no. 3, 743–762 (eng).

[Sim13] Bernd Simeon, *Computational Flexible Multibody Dynamics*, Springer Berlin Heidelberg, Berlin, Heidelberg, 2013 (en).

[SSP09] Bernd Simeon, Radu Serban, and Linda R. Petzold, *A model of macroscale deformation and microvibration in skeletal muscle tissue*, ESAIM: Mathematical Modelling and Numerical Analysis **43** (2009), no. 4, 805–823 (en).

[Tho98] Silvanus Phillips Thompson, *Calculus made easy being a very-simplest introduction to those beautiful methods of reckoning which are generally called by the terrifying names of the differential calculus and the integral calculus*, newly rev., updated, expanded, and annotated for its 1998 ed ed., St. Martin's Press, 1998.

[TN04] Clifford Truesdell and Walter Noll, *The Non-Linear Field Theories of Mechanics*, Springer Berlin Heidelberg, Berlin, Heidelberg, 2004 (en).

[Wer18] Dirk Werner, *Funktionalanalysis*, Springer-Lehrbuch, Springer Berlin Heidelberg, Berlin, Heidelberg, 2018.

[Wri08] P. Wriggers, *Nonlinear finite element methods*, Springer, Berlin, 2008 (en), OCLC: ocn236120878.

[Zah81] George Ireneus Zahalak, *A distribution-moment approximation for kinetic theories of muscular contraction*, Mathematical Biosciences **55** (1981), no. 1-2, 89–114 (en).

[Zah96] George I. Zahalak, *Non-axial Muscle Stress and Stiffness*, Journal of Theoretical Biology **182** (1996), no. 1, 59–84 (en).

[Zah97] G. I. Zahalak, *A Re-examination of Calcium Activation in the Huxley Cross-Bridge Model*, Journal of Biomechanical Engineering **119** (1997), no. 1, 20 (en).

Selbstständigkeitserklärung

Hiermit erkläre ich, dass ich die Masterarbeit selbst verfasst habe und keine anderen als die angegebenen Quellen als Hilfsmittel benutzt und sämtliche Zitate kenntlich gemacht habe.

Kaiserslautern, 15. Oktober 2018
Steffen Plunder